The PHILOSOPHICAL MAGAZINE

FIRST PUBLISHED IN 1798

2 Eighth Series No. 14 February 1957

A Journal of Theoretical Experimental and Applied Physics

PRICE £1 0s. 0d.
Annual Subscription £10 10s. 0d. payable in advance

ALERE FLAMMAM.
Printed and Published by
TAYLOR & FRANCIS LTD.
RED LION COURT, FLEET STREET, LONDON, E.C.4

The Specific Heat of Liquid Helium †

By R. W. Hill and O. V. Lounasmaa ‡
Clarendon Laboratory, Oxford

[Received November 27, 1956]

Abstract

New measurements of the specific heat of liquid helium between 1·80 and 5·05°K are presented, and some of their consequences for the helium vapour pressure scale of temperature discussed.

§ 1. Introduction

The work to be reported here forms part of an investigation of the entropy diagram of helium in the range 2 to 20°K and 0 to 100 atmospheres pressure. It is presented in advance of the main work because of its bearing on the helium vapour pressure scale of temperature, a subject of considerable current interest. In determining the diagram, entropy differences only are measured, and before absolute values can be given it is necessary to know the value at any one point. For our purposes, the most convenient reference point would be the liquid in equilibrium with the vapour at a chosen temperature, but the entropy is not known with sufficient accuracy. It was for this reason that new measurements of the specific heat were undertaken.

Below the λ-point, the most recent data are those of Kramers *et al.* (1952) between 0·20 and 1·85°K, and those of Hercus and Wilks (1954) from 1·10 to 2·05°K. In the immediate vicinity of the λ-point the best data are those of Keesom and Keesom (1935), while at higher temperatures there exist no more recent measurements than those of Keesom and Clusius (1932). Two difficulties arise : first, while the values of Kramers *et al.* and Keesom and Keesom fit smoothly together, those of Hercus and Wilks conflict with both ; second, the results of Keesom and Clusius show a considerable scatter, and are said to be uncertain to 3%.

A new determination of the specific heat above the λ-point was evidently desirable, and could conveniently be undertaken in our apparatus. Measurements below the λ-point were not foreseen when the apparatus was designed, and presented some difficulty. However, the nature of the disagreement between the results of Kramers *et al.* and those of Hercus and Wilks strongly suggests the presence of an undetected systematic error in one of them. A few points in a limited temperature range should then suffice to determine where the error lies. This was, in fact, as much as could be done without redesigning the apparatus.

† Communicated by Dr. K. Mendelssohn, F.R.S.
‡ On leave from Turku University, Finland.

§ 2. Experimental

The colorimeter was made of copper and was filled as far as possible with fine copper wire, leaving a volume of 21·3 cm^3 for the helium. A filling tube of german silver, 0·3 mm internal diameter, was used ; it ran directly from the calorimeter to a valve at room temperature, thereby keeping the dead volume of the system very small. The calorimeter was suspended inside a vacuum jacket immersed in liquid helium at its normal boiling point. Exchange gas was used to cool the calorimeter to liquid hydrogen temperatures and was then removed, and further cooling obtained by condensing liquid helium into a separate compartment of the calorimeter itself. By pumping this helium away, temperatures lower than that of the bath could be achieved down to a limit imposed by the size of the vessel. With large helium samples this limit was a little above the λ-point, in accordance with the use for which the system was designed. When it was later decided to carry out measurements of the specific heat below the λ-point, it was found that 1·8°K could be reached with a reasonable size of sample, and this was considered to be adequate for our purpose.

The particular virtue of this method of cooling is that exchange gas is used only at comparatively high temperatures where it is easily removed. Good thermal insulation is therefore obtained, and the temperature drifts encountered were only a few millidegrees per minute at worst. The small correction for these drifts is easily made as thermal equilibrium is established in about 10 seconds. As the critical point is approached the equilibrium time increases, but does not exceed one minute.

The thermometer used was a carbon composition radio resistor (47 ohm, $\frac{1}{4}$ watt, L.A.B.). For use below 4·2°K it was calibrated during every experiment against the helium vapour pressure on the scale designated by $T_{55\mathrm{E}}$ (Clement *et al.* 1955). No change of calibration could be detected during an experiment, and changes between experiments were small. This constancy was particularly valuable at high temperatures, where the thermometer was calibrated by using the calorimeter as the bulb of a constant volume gas thermometer. Calibrations of this type could not be carried out during a specific heat experiment, and adequate correction for changes is possible only if they are sufficiently small.

§ 3. Results

The saturation specific heat C_s cannot be measured with a calorimeter completely full of liquid, and an important correction must be applied for the heat supplied for evaporating liquid and heating the vapour. This correction can be obtained by elementary thermodynamics, yet the derivation does not appear to have been given in the literature of liquid helium.

Let S_t be the entropy of n moles of liquid and vapour in equilibrium, then $S_t = n_l S_l + n_v S_v$ where n_l and n_v are the number of moles of liquid and vapour respectively, and S_l and S_v are the molar entropies. Also

let V_l and V_v be the molar volumes and V the actual calorimeter volume. Then $S_t=n_lS_l+(n-n_l)(S_l+L/T)$ where L is the latent heat at temperature T. Using the relations $(n-n_l)V_v+n_lV_l=V$ and $L/T=(V_v-V_l)dp/dT$ we have $S_t=nS_l+(V-nV_l)dp/dT$, so that

$$C_s=TdS_l/dT=[C_t-Td/dT\{(V-nV_l)dp/dT\}]/n.$$

In this expression the total specific heat C_t must, of course, be corrected for the heat capacity of the calorimeter.

Below the λ-point the vapour correction is generally small, but it becomes important at higher temperatures where it can be positive or negative, depending on the value of n in relation to V. Some examples of this are given in table 1 ; here, as elsewhere, gram units are preferred

Table 1

T°K	n	Δ	C_t	C_s
2·055	0·477	+0·30	12·26	6·27
2·063	0·745	+0·03	19·16	6·43
3·94	0·466	+0·97	8·16	3·85
3·96	0·581	+0·03	9·16	3·92
3·95	0·646	−0·47	9·49	3·86
4·90	0·466	−4·36	12·26	8·91
4·92	0·527	−6·68	13·35	9·50

$\Delta=Td/dT\{(V-nV_l)dp/dT\}$ (Δ and C_t in joules deg^{-1} ; C_s in joules deg^{-1} gm^{-1})

to molar ones so as to conform to the general usage. The experimental results are shown in fig. 1 ; no distinction is made between points obtained with different values of n, but the scatter does not exceed 1%. The values of Keesom and Clusius, recalculated to the T_{55E} temperature scale, are included for comparison, and may be seen to scatter fairly evenly about the present ones. It is evident, however, that they are not accurate to 3% near the normal boiling point. Values obtained below the λ-point are also shown in fig. 2, where the larger scale affords easy comparison with those of Kramers *et al.* and Keesom and Keesom, represented by the solid line, and those of Hercus and Wilks, represented by the dotted line. All results are in terms of T_{55E}. It is obvious that our few points confirm the Leiden values ; therefore, although it is still not clear how the discrepancy between the two sets of results has arisen, we have taken the Leiden values to be the correct ones.

The accuracy of the results above the λ-point is limited primarily by the accuracy with which the sensitivity of the thermometer could be determined ; this is about 0·5%, and the specific heat values are considered to be accurate to 1% or better. Below the λ-point the thermal insulation is less satisfactory, due to the helium film in the filling tube. This is probably the reason for the greater scatter in the experimental results.

Fig. 1

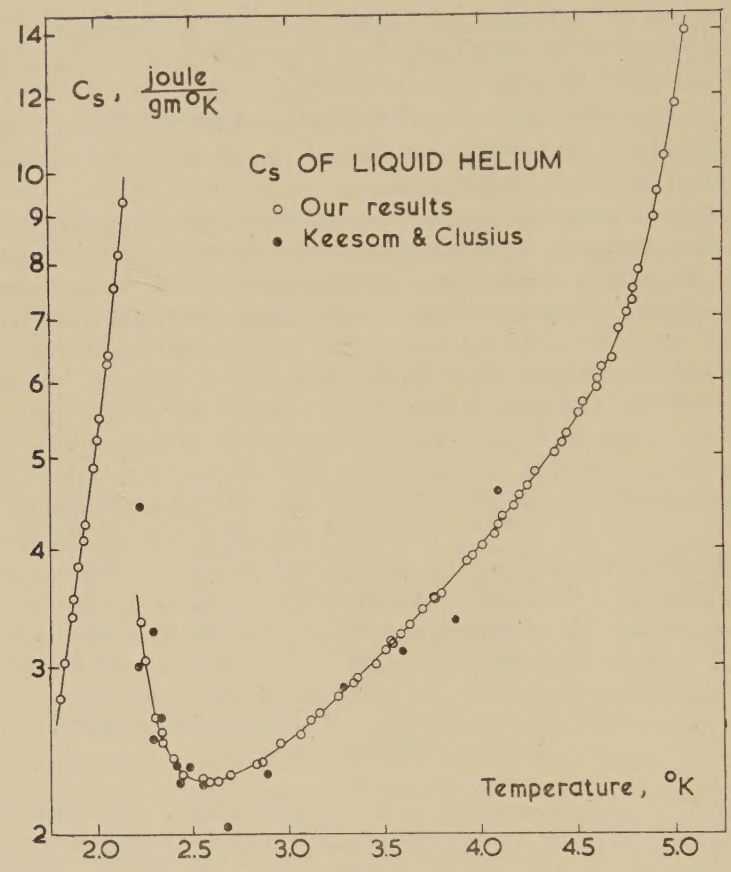
C_s, joule/gm°K
C_s OF LIQUID HELIUM
Our results
Keesom & Clusius
Temperature, °K
14
12
10
9
8
7
6
5
4
3
2
2.0
2.5
3.0
3.5
4.0
4.5
5.0

Fig. 2

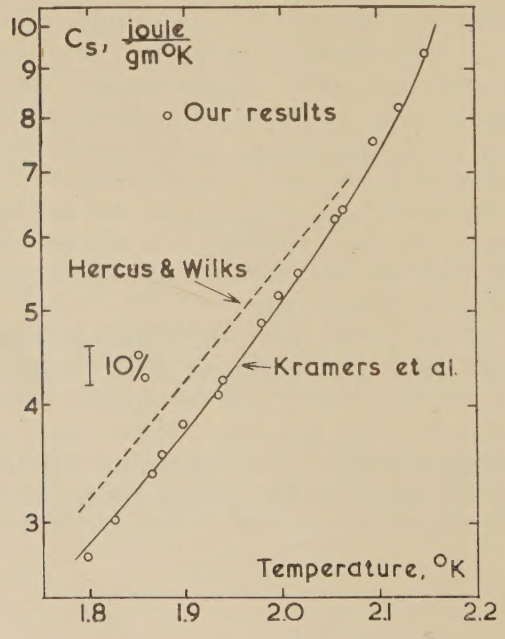
C_s, joule/gm°K
Our results
Hercus & Wilks
10%
Kramers et al.
Temperature, °K
10
9
8
7
6
5
4
3
1.8
1.9
2.0
2.1
2.2

In calculating the entropy values, the value of 0·535 joules deg^{-1} gm^{-1} at 1·80°K (Kramers *et al.*) has been taken as a starting point. Thereafter, the present results were used exclusively. Entropy and smoothed specific heat values are given in table 2.

Table 2. The Specific Heat and Entropy of Liquid Helium under its Saturation Vapour Pressure

T°K	C_s	S	T°K	C_s	S
1·80	2·81	0·535	3·40	2·97	2·71
1·85	3·26	0·619	3·50	3·11	2·80
1·90	3·79	0·715	3·60	3·26	2·89
1·95	4·39	0·820	3·70	3·42	2·97
2·00	5·18	0·940	3·80	3·60	3·06
2·05	6·16	1·08	3·90	3·78	3·16
2·10	7·51	1·24	4·00	3·99	3·26
2·15	9·35	1·44	4·10	4·23	3·36
2·1735	12·6	1·56	4·20	4·48	3·46
2·20	3·98	1·61	4·30	4·78	3·57
2·25	3·04	1·68	4·40	5·11	3·68
2·30	2·64	1·74	4·50	5·50	3·81
2·35	2·47	1·80	4·55	5·72	3·87
2·40	2·38	1·85	4·60	5·94	3·93
2·50	2·28	1·93	4·65	6·22	3·99
2·60	2·27	2·02	4·70	6·57	4·06
2·70	2·29	2·11	4·75	7·04	4·14
2·80	2·34	2·19	4·80	7·53	4·22
2·90	2·41	2·28	4·85	8·22	4·30
3·00	2·49	2·36	4·90	9·03	4·39
3·10	2·58	2·45	4·95	10·1	4·49
3·20	2·69	2·53	5·00	11·5	4·60
3·30	2·83	2·62	5·05	13·5	4·72

The unit for C_s and S is joules deg^{-1} gm^{-1}

§ 4. Discussion

At the present time, physicists are faced with two helium vapour pressure temperature scales, one of which, proposed by van Dijk and Durieux (1955), is based on the thermodynamic equation relating the vapour pressure to the thermal properties of the liquid and vapour phases. This scale has recently been criticised by Keller (1956), whose article contains a full account of the methods by which the two scales have been formulated. The basis of Keller's criticism is that the van Dijk scale is uncertain within rather wide limits because of uncertainties in the relevant thermal properties. In particular, the conflict between the Kramers and the Hercus and Wilks specific heats leads to doubts about the value of L_0, the latent heat at absolute zero. Again, the possible choice of values for the liquid specific heat above the λ-point, within the range of the Keesom and Clusius data, leads to uncertainties

which are much greater than the supposed difference between the scales. Keller therefore concludes that the apparent close agreement of the two scales is to some extent fortuitous.

The present data should help to reduce these uncertainties in two ways. Firstly, the confirmation of the specific heats of Kramers *et al.* would appear to justify van Dijk's neglect of the Hercus and Wilks data when estimating L_0. Secondly, the increased accuracy in the specific heat above the λ-point materially reduces the uncertainty in the 3–4°K range. The full consequences of our data for this part of the van Dijk scale will not be evident until a full recalculation can be carried out, but, since the uncertainty here is almost directly proportional to the uncertainty in the liquid entropy (Keller), it seems that at least a threefold increase in precision should be obtained.

Acknowledgments

The authors are indebted (R.W.H.) to the University of Oxford for the award of an I.C.I. Fellowship, and (O.V.L). to the Suomen Kulttuurirahasto and the British Council for scholarships.

References

Clement, J. R., Logan, J. K., and Gaffney, J., 1955, *Phys. Rev.*, **100**, 743.
Hercus, G., and Wilks, J., 1954, *Phil. Mag.*, **45**, 1163.
Keesom, W., and Clusius, K., 1932, *Leiden Comm.*, 219e.
Keesom, W., and Keesom, A., 1935, *Physica*, **2**, 557.
Keller, W. E., 1956, *Nature, Lond.*, **178**, 883.
Kramers, H., Wasscher, J., and Gorter, C., 1952, *Physica*, **18**, 329.
van Dijk, H., and Durieux, M., 1955, *Proc. 4th Intern. Conf. on Low Temperature Physics*, Paris.

^{8}Li Emission from Heavy Element Disintegrations Produced by 5·7 BeV Protons†

By S. J. Goldsack, W. O. Lock and B. A. Munir ‡
Department of Physics, Univetsity of Birmingham

[Received August 24, 1956]

Summary

A stack of Ilford G5 emulsions exposed to the 5·7 BeV proton beam of the Berkeley Bevatron has been searched for disintegrations of silver and bromine nuclei with ejected ^{8}Li fragments, and 91 examples found. The experimental results can be explained qualitatively by assuming that most of the fragments from stars with 12 or more black prongs are ejected as part of the evaporation process but a few of the fragments from the smaller stars (less than 12 black prongs) are ejected during the initial stages of the collision.

§ 1. Introduction

A previous paper from this laboratory (Munir 1956) has given data on the ejection of ^{8}Li fragments from nuclear disintegrations produced in G5 emulsions by 950 MeV protons. Through the kindness of Professor E. J. Lofgren at Berkeley, California, a stack of G5 emulsions was exposed for us to the 5·7 BeV proton beam of the Bevatron. These emulsions were searched for stars with ejected ^{8}Li fragments as in the work at 950 MeV. The high background in the emulsions, and the difficulty of establishing a reliable criterion to distinguish between light and heavy element disintegrations, led us to confine our attention to definite heavy element disintegrations.

§ 2. Experimental Procedure and Results

Ilford G5 emulsions, 400 μ and 600 μ thick were used. The primary proton beam was in the plane of the emulsion and parallel to one edge of the plates. The emulsions were searched under a $\times 10$ objective and $\times 15$ eyepieces. Each star with more than 5 black prongs and with a minimum track in the beam direction was examined under a $\times 45$ oil objective. All black prongs were followed either to their ends in the emulsion or to the point at which they left the plates. The precautions were in general the same as those observed previously (Munir 1956). All the ' hammer tracks ' found were assumed to be due to ^{8}Li nuclei stopping in the emulsion.

† Communicated by P. B. Moon, F.R.S.
‡ Now at the American University of Beirut, Lebanon.

In all, 7700 stars with 5 or more black prongs were examined and 91 examples of ^{8}Li emission found. Of the parent stars, 90 had 6 or more black prongs and must therefore correspond to heavy element disintegrations ; the remaining parent star had 5 black prongs but a total of 14 prongs and must represent a heavy element disintegration. A few of the 7700 stars examined had only a small number of associated grey prongs in addition to 5 or 6 black prongs and may, of course, correspond to light element disintegrations. Thus the figures for the frequency of ^{8}Li emission are probably lower limits.

It should also be pointed out that in this paper we are dealing with a slightly biased selection of heavy element disintegrations, for our method of searching the emulsions would miss a heavy element disintegration consisting of a very small number of prongs. Such interactions could only be found by seaching along the tracks of the primary protons. On the other hand, at a primary energy of 5·7 Bev the number of small heavy element stars will clearly be rather low. Thus the bias is probably not serious.

Fig. 1

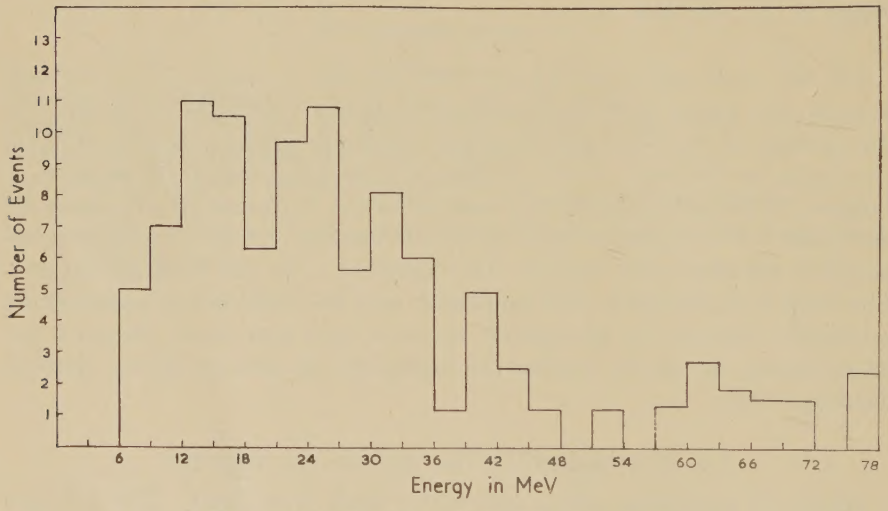

Energy distribution of the ^{8}Li fragments.

The energy distribution of ^{8}Li fragments is shown in fig. 1. It has a cut-off at 6 Mev. This value may be taken to be the height of the potential barrier facing a ^{8}Li nucleus in a silver or bromine nucleus when excited by the impact of a 5·7 Bev proton. The most energetic fragment recorded had an energy of 78 Mev. The distribution has been corrected in the usual way for loss of fragments leaving the emulsion before coming to rest.

The angular distribution of the fragments is plotted in intervals of equal solid angle in fig. 2. There are 55 fragments (observed number) in the forward direction (angle to primary direction less than 90°) and 36 in the backward direction.

The disintegrations with ejected ^{8}Li fragments have been divided into groups with different numbers of prongs and the frequency of emission of ^{8}Li fragments calculated for each group. These frequencies together with other relevant data are given in the table ; they have been corrected for loss due to fragments leaving the emulsion before coming to rest. The frequencies are plotted as a function of the mean excitation energy in fig. 3 ; the full line is that calculated by LeCouteur (private communication) on the basis of evaporation theory.

Fig. 2

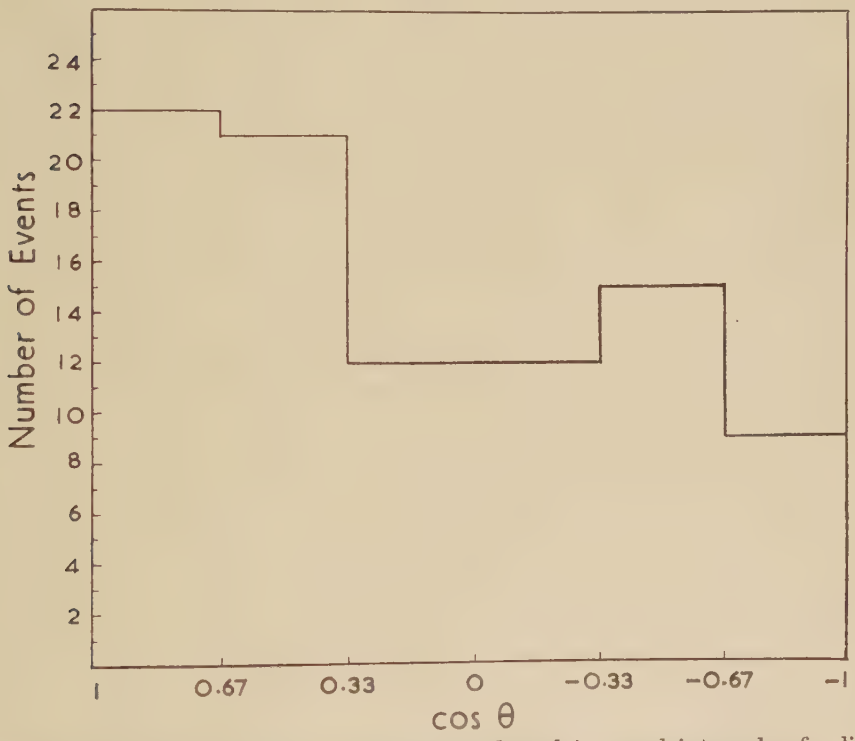

Angular distribution of the ^{8}Li fragments, plotted in equal intervals of solid angle, and measured with respect to the direction of the incident proton.

No. of Black Prongs	Mean Prong No.		No. of stars	No. of Fragments		Frequency	Excitation Energy (Mev)
	Total	Black		Obs.	Corrected		
5–8	14·6	7·1	3780	19	22·4	0·0059 ± 0·0012	260
9–11	19·2	10·1	1976	33	36·9	0·0186 ± 0·004	370
12–14	21·8	13·1	1269	21	23·5	0·0185 ± 0·004	490
15–20	25·6	17·2	656	17	18·0	0·0275 ± 0·007	630
23	31	23	21	1	1·2	—	—
Mean Value	20·2	10·3	7702	91	102	0·013 ± 0·001	380

§ 3. Discussion

Figure 1 shows that most of the fragments have energies between 6 and (say) 40 MeV but that there is a pronounced high energy tail. Suppose now that we separate the data into two groups depending on the number of black prongs in the parent star. Figures 4(*a*) and 4(*b*) are plots of the energy distributions, of the fragments from stars with less than 12 black prongs (' small ' stars) and with 12 or more black prongs (' large ' stars)

Fig. 3

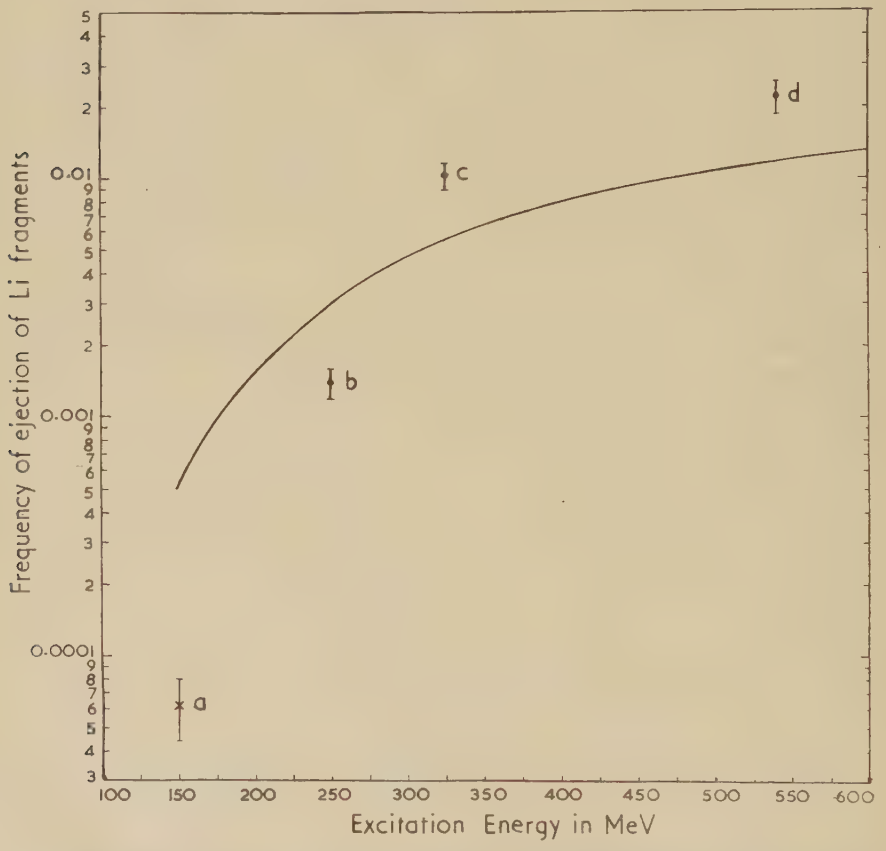

Frequency of ejection of the ^{8}Li fragments plotted as a function of the excitation energy of the parent stars ; the solid line is that calculated on the basis of evaporation theory (LeCouteur, private communication).

respectively. The mean excitation energy for each of these groups is 300 MeV and 550 MeV respectively ; there are 52 observed events in the first group and 39 in the second.

If the ^{8}Li fragments are ejected during the ' evaporation process ' then their energy spectrum $N(E)dE$ should be of the well-known form

$$N(E)dE = \frac{E-V}{T^2} \exp \frac{-(E-V)}{T} dE$$

where T is the nuclear temperature and V the potential barrier. In the present instance we may take $V=6$ MEV (see § 2) then $T=4{\cdot}3$ MEV for $U=300$ MEV and $7{\cdot}8$ MEV for $U=550$ MEV (see Lock *et al.* 1955). The energy spectra for these two excitation energies have been calculated using the above formula and plotted as full lines in figs. 4(*a*) and 4(*b*), normalized to the number of ^{8}Li fragments in each plot. The curve in fig. 4(*b*)

Fig. 4

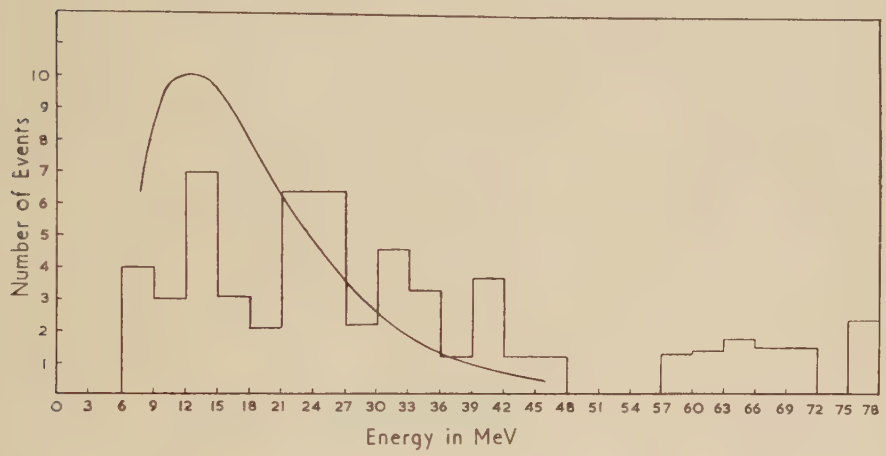

(*a*)

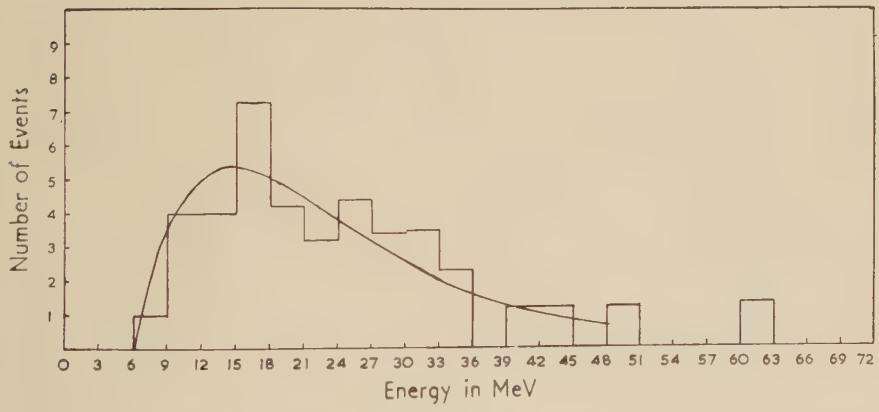

(*b*)

(*a*) Energy distribution of the ^{8}Li fragments ejected from stars with less than 12 black prongs. (*b*) Energy distribution of the ^{8}Li fragments ejected from stars with 12 or more black prongs.

(large stars) fits well with the experimental data but this is not the case for the small stars (fig. 4(*a*)) in which there is a definite preponderance of high energy fragments. As a tentative hypothesis we may assume that

Fig. 5

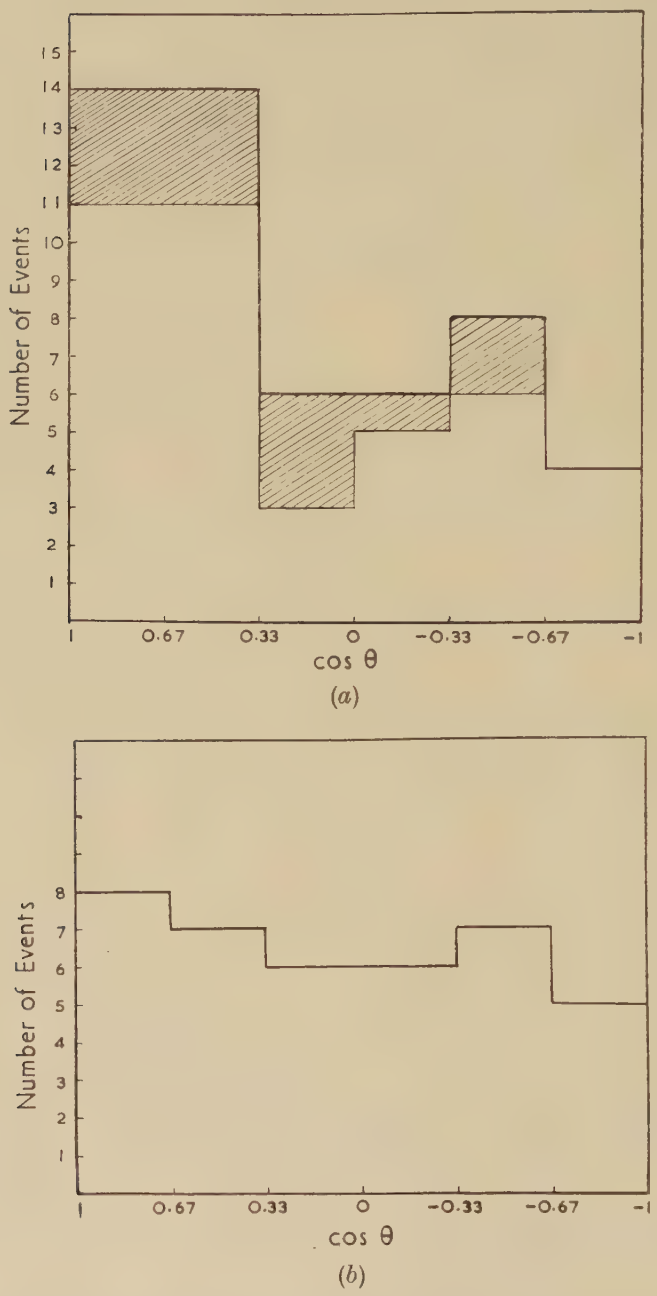

(*a*) Angular distribution of the ^{8}Li fragments ejected from stars with less than 12 black prongs ; the shaded area corresponds to those fragments with more than 36 Mev kinetic energy. (*b*) Angular distribution of the ^{8}Li fragments ejected from stars with 12 or more black prongs.

the fragments from the large stars are ejected as part of the evaporation process; this is, in fact, borne out by their angular distribution, shown in fig. 5(*b*), which is essentially isotropic, as it should be for an evaporation process. On the other hand, a substantial fraction of the fragments from the small stars have energies in excess of those predicted by the evaporation theory. Further, their angular distribution (fig. 5(*a*)) is markedly anisotropic. This strongly suggests that fragments are also being ejected during the initial nucleon–meson cascade in the struck nucleus; such fragments would be ejected in the forward direction and would have relatively high energies. To be more specific we suppose that the 12 fragments (observed number) in fig. 4(*a*) with energy more than 36 Mev arise from the cascade process. These 12 events are shown shaded in fig. 5(*a*); their forward to backward ratio is 9 : 3. The forward to backward ratio of the remaining 40 events is $25 : 15 = 1{\cdot}7 \pm 0{\cdot}6$ compared with $34 : 18 = 1{\cdot}9 \pm 0{\cdot}6$ for all 52 events. The value of $1{\cdot}7 \pm 0{\cdot}6$ is not in disagreement with a value of unity for this ratio; we have made no correction for centre of mass motion which may be appreciable in some cases.

Frequency of Ejection of ^{8}Li *Fragments*

(*a*) At 5·7 Bev

Figure 2 shows that the observed frequencies of emission at 5·7 Bev (points c and d) of the ^{8}Li fragments are higher by a factor of about two than those predicted by LeCouteur on the evaporation theory. This discrepancy remains if one considers only the fragments emitted from the 'large' stars which, as shown above, are otherwise consistent with the evaporation hypothesis.

On the other hand, we may compare the relative frequencies of emission as predicted by LeCouteur for 300 and 550 Mev excitation energy ('small' and 'large' stars). If we suppose that all the 42·7 fragments from the 1950 'large' stars of 550 Mev excitation energy are evaporation particles, then from the 5750 'small' stars of 300 Mev mean excitation energy one should expect 49·4 'evaporated' ^{8}Li fragments. The corrected number of observed fragments with energy less than 36 Mev is 42·1. Thus the remaining 17·2 events of higher energy probably arise from some other cause such as the 'cascade' hypothesis which we have discussed above.

We may perhaps regard the 'small' stars as those in which the primary proton makes an edge collision with the struck nucleus of silver or bromine. Thus the resulting disintegration is rather small and any aggregate of nucleons, such as a ^{8}Li fragment, which by some means may acquire some tens of Mev, has a good chance of escaping from the nucleus without making a collision. On the other hand, the 'large' stars may represent those cases in which the primary proton makes a head-on collision with a nucleus. Any nuclear fragment accelerated in the initial nucleon meson cascade now has a much smaller chance of escaping intact from the disintegrating nucleus. We may expect ^{8}Li fragments to arise largely, or perhaps entirely, from the 'evaporation' stage of the disintegration. The

discrepancy between the observed and predicted frequencies of emission of the fragments may be overcome in a further refinement of the theory or it may arise through an underestimate of the excitation energy involved.

(*b*) *Comparison with Frequencies of Ejection at Other Energies*

Point a on fig. 3 is the frequency of ejection of ^{8}Li fragments at 340 MEV. This was calculated from the results of Wright (1950) for the cross section of ^{8}Li ejection from silver and bromine nuclei combined with the inelastic scattering cross sections for these nuclei at 305 MEV determined by Millburn *et al.* (1954). Point b corresponds to the results of Munir (1956) at 950 MEV.

Both points a and b are well below the theoretical curve given by LeCouteur, which is in contrast to the situation at 5·7 BEV which we have discussed in § 2. The origin of the discrepancy between the experimental data and the predictions of LeCouteur, based on the evaporation theory, is not clear.

§ 4. CONCLUSIONS

^{8}Li fragments are ejected from the nuclear disintegrations of silver and bromine produced by 5·7 BEV protons with a much greater frequency than that expected on the basis of the usual evaporation theory. The results are consistent (expect for the absolute frequency of emission) with the assumption that the fragments from the stars with 12 or more black prongs arise almost entirely from the evaporation process, while those from the stars with less than 12 black prongs are partly ' evaporation particles ' and partly ' cascade ' particles. The exact mechanism which gives rise to the high energy (36–70 MEV) forward moving fragments remains to be elucidated.

ACKNOWLEDGMENTS

We wish to express our thanks to the many members of the Radiation Laboratory at Berkeley, California, who helped to make the exposure of the plates possible ; to Dr. K. J. LeCouteur for communicating to us the results of his calculations on the frequency of emission of ^{8}Li fragments as a function of excitation energy ; and to Miss D. Latham, Mrs. E. R. Lock, Mrs. P. V. March and Miss M. T. Parkes for their assistance with the scanning.

REFERENCES

LOCK, W. O., MARCH, P. V., and MCKEAGUE, R., 1955, *Proc. Roy. Soc.* A, **231,** 368.

MILLBURN, G. P., BIRNBAUM, W., CRANDALL, W. E., and SCHECTER, L., 1954, *Phys. Rev.*, **95,** 1268.

MUNIR, B. A., 1956, *Phil. Mag.*, **1,** 355.

WRIGHT, S. C., 1950, *Phys. Rev.*, **79,** 838.

The Low Energy End of the Cosmic Ray Spectrum of Alpha-Particles †

By P. H. Fowler and C. J. Waddington
H. H. Wills Physical Laboratory, Bristol, England
and
P. S. Freier, J. Naugle and E. P. Ney
University of Minnesota, Minneapolis, Minnesota

[Received August 12, 1956]

Abstract

An experiment has been carried out at Saskatoon, Canada, at a nominal geomagnetic latitude of 60·5°N, which shows the form of the low energy end of the cosmic ray alpha particle spectrum independent of the earth's magnetic field. The differential spectrum shows a maximum at about 300 Mev per nucleon. The number of particles on the low energy side of the maximum is too great to be accounted for by secondary production, and it is believed that this spectrum represents the differential spectrum of primary alpha particles outside the earth's magnetic field. A re-analysis of previous experiments at a lower geomagnetic latitude, 55°N, in the American continent, gives a spectrum very similar to the one obtained in Saskatoon. As a consequence of this it appears that the cut-off energies experienced by cosmic ray particles over the American continent are probably lower than those predicted by geomagnetic theory.

PART I

§ 1. Introduction

Because of the uncertainty introduced in attempts to infer the primary spectrum of cosmic rays from latitude measurements, it was felt that a direct experiment to determine the energy spectrum of the various components should be undertaken. Consequently, a series of balloon flights was carried out at Saskatoon, Canada, in the summer of 1954. This period was a time of minimum solar activity. The flight from which all of the information has been obtained so far was flown on the 18th June 1954, during the daylight hours. The experiment consisted of exposing a stack of 83, $3\frac{1}{2}$ in. by $9\frac{1}{2}$ in. 500-micron thick emulsions to cosmic rays at high geomagnetic latitude. The latitude of Saskatoon, Canada, was chosen in the following way. On the basis of then-current balloon techniques, and with the payload determined for this flight, the minimum pressure which was felt to be practical was 10 g cm^{-2}. This pressure determines a range cut-off imposed by the air above for all

† Communicated by the Authors.

components of the primaries, and if one is to study energy spectra in the absence of geomagnetic effects, the air cut-off for the lowest Z component to be studied must be equal to or greater than the energy cut-off imposed by the magnetic field at the latitude at which the experiment is to be carried out. The residual pressure which could be reached in the balloon experiment thereby specified an equivalent geomagnetic latitude for alpha-particles of 60·5°N. In view of the results which follow, it appears that Saskatoon may be at an even higher latitude than 60·5°N.

The detecting emulsion block was mounted in a frame which could be rotated by a small motor activated by a pressure device. The emulsion stack was enclosed in a pressurized spherical aluminium gondola. The instrumentation for the flight included an aneroid device which activated the motor which turned the photographic emulsion stack through 180° about a horizontal axis after the balloon had reached ceiling. The same signal which turned over the emulsion stack also opened the balloon appendix in order to insure as high an altitude in the flight as possible. In addition to this turnover switch, there was a ballasting servo system which 'followed up' as the balloon rose and set itself to ballast if the balloon descended as much as one millibar below its maximum ceiling altitude. There was also a 'down-camera' for photographing the ground and determining the trajectory, as well as a telemetering system utilizing a temperature controlled bellows which transmitted the pressure measured during flight. In addition, a camera photographed a Wallace and Tierman pressure gauge to give an independent record of the altitude of the flight.

All of the methods of pressure determination in the flight agreed to within 0·5 of a millibar, and the mean pressure at which the plates were exposed in their upright position at altitude was $10{\cdot}8 \pm 0{\cdot}6$ g/cm^2. Because the plates were in one position during ascent and were turned over at ceiling, one can separate those particles for which the direction of motion is known into a group that came in at ceiling altitude, and a group which came in during ascent.

Figure 1 shows the time–altitude curve for this flight. It can be seen from this curve that the period during which the plates were in their upright position represents a very constant level region of the flight.

Because of the importance of the determination of the charge of particles passing through the stack, a photometric device was developed to measure the ionization over a wide range of energy loss. The profile of the track is displayed on an oscilloscope and measurements of the track can be made with various slit widths. This measurement gives the equivalent obscuration of the track as compared with that which would have been produced by a wire of the width indicated in microns. Figure 2 shows the way in which this densitometer measurement varies with dE/dx, and for convenience the energy loss for charged particles at different speeds is also indicated in this graph. This figure shows the general characteristics of the G-5 emulsion in that the obscuration between about 20 and 100

Fig. 1

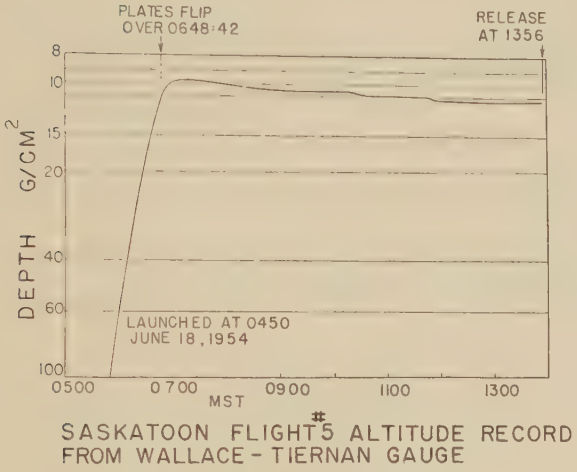

Time altitude curve for the flight of June 18, 1954.

Fig. 2

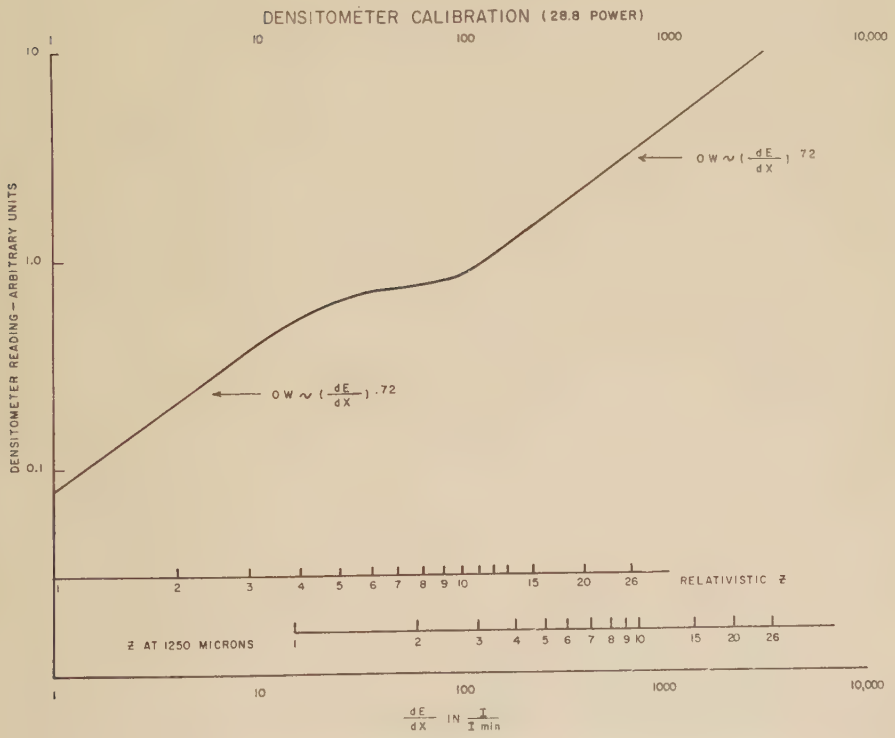

Variation of the equivalent width of emulsion tracks as a function of rate of energy loss.

times minimum ionization varies very little. It is desirable, then, to make ionization measurement with the densitometer in regions of the track where this plateau is not important. This condition is satisfied for the Saskatoon alpha-particles.

§ 2. Alpha-Particles at Saskatoon

The plates were scanned under $\times 360$ for particles which satisfied the following criteria :

1. Ionization greater than 3·5 minimum.
2. Projected length in each emulsion greater than 8 mm.
3. Zenith angle less than 45°.

Two regions of the stack were scanned. One entire vertical side was scanned for all particles which satisfied the above criteria and which entered the stack from the outside. The other region scanned was a line parallel to and 1 cm below the top surface of the stack. All particles crossing this line which satisfied the above criteria and which entered from the top of the stack were recorded. The total scan yielded 190

Fig. 3

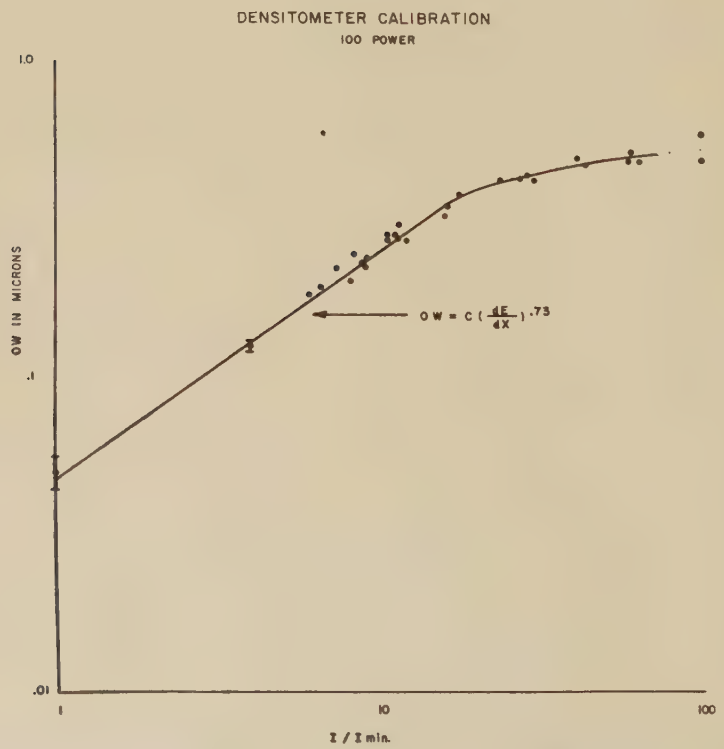

Densitometer calibration in the region from 1 to 100 times minimum ionization.

alpha-particles, plus four fast heavier nuclei, and approximately 1500 contamination particles, mostly slow protons.

Figure 3 shows a densitometer calibration appropriate for the alpha-particle scan. Measurements were made under a linear magnification of 100 times. All the tracks found were scattered by the Fowler coordinate method with 500 micron cells, and 20 of the slow alphas were followed until they ended.

Figure 4 shows the resolution between protons and alpha-particles obtained by plotting the densitometer measurements versus the scattering parameter obtained without noise elimination ('raw' scattering). The lines are the theoretical lines based on a scattering constant of 26 and the

Fig. 4

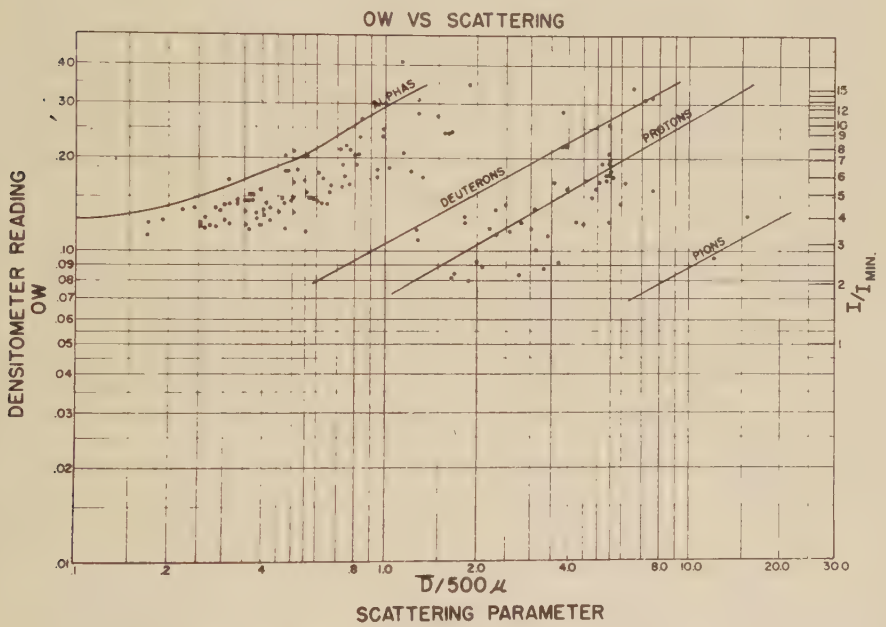

Plot of densitometer measurement of equivalent width versus 'raw' scattering in units of the average second difference in 500 micron cells. Note that the α-particles do not fall on the theoretical curve because of noise in the scattering.

known densitometer calibration. There are approximately 15 second differences on each track and an equal number of densitometer readings were taken throughout the emulsion, from the air surface to the glass surface, to average out the depth variation of this measurement.

To investigate the errors in the ionization determinations measurements were made on the track of a fast particle which passed through 60 emulsions. Using the dependence of width upon ionization the expected standard deviation of the energy determinations of alpha-particles from the ionization measurements was found to be 20% in the energy interval

100 to 400 Mev per nucleon, and of the order of 30% between 400 and 500 Mev per nucleon. Particles of energy less than 100 Mev per nucleon almost invariably ended in the stack and their energy was determined accurately by their range. Table 1 shows the pertinent values with

Table 1. Comparison of Predicted and Actual Energies for Alphas

Track number	Energy from range (Mev/nucleon)	Energy predicted from ionization measurement (Mev/nucleon)	Energy predicted from scattering (Mev/nucleon)	% Error in energy of column 3	% Error in energy of column 4
13	190	200	130	+5	−31
17	137	120	102	−12	−25
33	195	200	160	+3	−18
51	138	145	105	+6	−24
115	128	155	166	+27	+30
131	190	190	82	0	−45
241	120	137	60	+14	−50
310	135	140	100	+4	−26
346	61	77	82	+26	+35
380	106	120	94	+13	−11
212	19	19	27	0	+42
277	220	205	165	−7	−25
299	240	225	120	−6	−50
324	210	202	140	−4	−80
331	87	74	83	−15	−5
409	79	84	44	+6	−44
222	140	180	100	+29	−29
311	48	67	30	+40	−38
351	305	320	180	+5	−41
417	118	103	135	−13	+15
			average	11	33

respect to those followed particles which ended in the emulsions and for which the energy could be determined precisely. The mean error on the energy determined from the raw scattering measurements on these slow particles was about 33%. This value was approximately that expected from the number of available cells. The mean error in energy determined from the ionization measurements for these particles was only 11%, somewhat better than the estimate based on the fluctuations observed on the fast tracks. The estimate derived from the ionization was used for the determination of the energy in all cases in which the particle did not end. The scattering measurements were merely used in conjunction with those of ionization in order to allow identification of the particles (see fig. 4).

The flux values obtained must be corrected for the absorption of the alpha-particles in the air above the plates and for secondary alpha-particles produced in the air. The method of correction is described in the Appendix.

Table 2. Differential and Integral Fluxes

Number of alphas	Energy MEV/nucleon	Energy interval MEV	Flux at top of atmosphere uncorrected for secondaries Particles/m^2 ster sec MEV	% Correction	Flux at top of atmosphere corrected for production of secondaries. Particles/m^2 ster sec MEV
20	130	13	$0{\cdot}14 \pm 0{\cdot}04$	14	$0{\cdot}12 \pm 0{\cdot}04$
40	139	30	$0{\cdot}21 \pm 0{\cdot}03$	14	$0{\cdot}18 \pm 0{\cdot}03$
9	165	65	$0{\cdot}18 \pm 0{\cdot}06$	14	$0{\cdot}15 \pm 0{\cdot}06$
25	250	100	$0{\cdot}40 \pm 0{\cdot}08$	7	$0{\cdot}37 \pm 0{\cdot}08$
27	350	100	$0{\cdot}45 \pm 0{\cdot}09$	7	$0{\cdot}42 \pm 0{\cdot}09$
15	450	100	$0{\cdot}32 \pm 0{\cdot}08$	7	$0{\cdot}30 \pm 0{\cdot}08$
			Flux at top of atmosphere uncorrected for secondaries Particles/m^2 ster sec		Flux at top of atmosphere corrected for production of secondaries Particles/m^2 ster sec
190	135		310 ± 20	7	290 ± 20
181	200		300 ± 20	7	280 ± 20
156	300		255 ± 20	7	235 ± 20
114	500		190 ± 20	7	170 ± 20

Table 2 gives the differential and integral fluxes together with the magnitude of the correction for secondary alpha-particles produced in the air above the plates. The fluxes were measured under an average of 12 g/cm^2 of air. The energy listed in the table is the energy of the alpha-particles at the top of the atmosphere.

Fig. 5

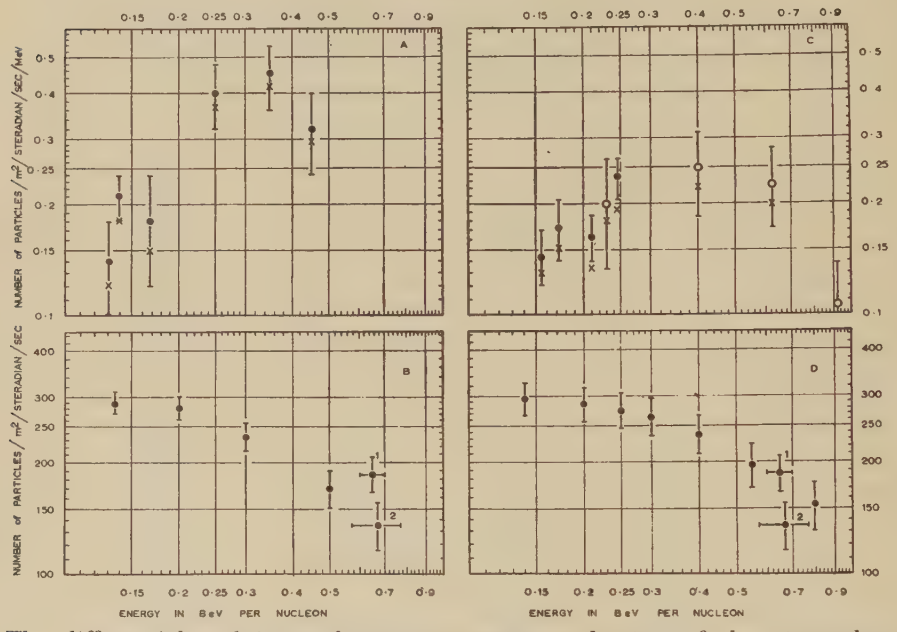

The differential and integral energy spectra at the top of the atmosphere observed over Saskatoon and Minnesota.

(*a*) The differential energy spectrum over Saskatoon. The crosses show the effects of the correction for the secondary production of alpha-particles.
(*b*) The integral energy spectrum over Saskatoon. Also shown are the results of Waddington (1956 b) over Southern England (1) and those of Linsley (1955) over America (2).
(*c*) The differential energy spectrum over Minnesota. The open circles show the results obtained by Waddington (1954) in this stack, while the closed circles are those obtained in the present analysis. The crosses have the same significance as on (*a*).
(*d*) The integral energy spectrum over Minnesota from the data of Waddington (1954) and the present analysis.

Figure 5(*a*) shows the differential energy spectrum determined from the densitometer energy measurements with the energy of the alpha-particles corrected to the top of the atmosphere. The flux corrected for secondary production of alphas is also shown. This spectrum shows a definite maximum at 300 Mev per nucleon, but also indicates the presence of primary alpha-particles with energies down to the average air cut-off

value of 124 MEV per nucleon. The flux of alpha-particles between 100–300 MEV per nucleon is of the order of 10 times too high to be explained by fragmentation of heavier particles, and cannot be ascribed to inelastic collisions of primary alpha-particles, or to alpha-particles from other nuclear disintegrations. The presence of this maximum would give rise to a 'knee' in the integral spectrum at an equivalent geomagnetic latitude of 57° 58°, but, as noted above, the 'knee' is not due to a sharp cut-off but is due instead to a maximum in the alpha-particle differential energy spectrum. Figure 5 (*b*) is an integral energy spectrum of the alpha-particles. The data plotted are those determinations in which the energy was determined directly.

PART II

§ 3. INTRODUCTION

Recent experiments have shown that the cut-off energies of cosmic ray particles cannot be calculated in the conventional manner from geomagnetic theory. In particular the experiments of Simpson *et al.* (1956) and Waddington (1956 b), first reported at the Mexico Conference, have shown respectively that the geomagnetic equator does not coincide with the positions of minimum cosmic ray intensity, and that the cut-off energies observed over England are considerably higher than those predicted by geomagnetic theory.

As a result it is clearly desirable that direct experimental determination of the true cut-off energies should be made at a number of points on the earth's surface. Such determination are particularly important over the American continent since the majority of cosmic ray investigations have been made there.

For this reason we have re-examined the experimental data on the multiply charged particles obtained by Dainton, Fowler and Kent (1952), in a stack of glass-backed emulsions flown on October 5, 1950 at Minneapolis; nominal geomagnetic latitude 55 N. This stack was flown at a mean altitude of 96 000 feet, and the mean amount of matter above the emulsions was 14 g/cm^2. As a result the alpha-particle air cut-off energy was 130 MEV per nucleon. The time latitude curve is shown in fig. 6.

At this geomagnetic latitude and longitude the cut-off energy for multiply charged particles incident vertically should, assuming a central dipole field, be 300 MEV per nucleon. If instead an eccentric dipole field displaced towards 154°E is assumed, Jory (1956), then the cut-off energy should be 350 MEV per nucleon. At these high latitudes the dependence of the cut-off energy on the zenith angle should not result in an appreciable spread in the experimentally observed cut-off energy.

In the above experiment it was noted that an appreciable proportion of the observed particles appeared to have entered the atmosphere with energies less than the expected cut-off value. The significance of the presence of the slow particles was not fully appreciated, and they were not analysed in detail. However, for the reasons outlined above, we have

now made a more careful and critical analysis of the low energy alpha-particles observed in this experiment, and find evidence that suggests that the cut-off energy over Minnesota was equal to or less than the air cut-off energy of 130 Mev per nucleon.

Fig. 6

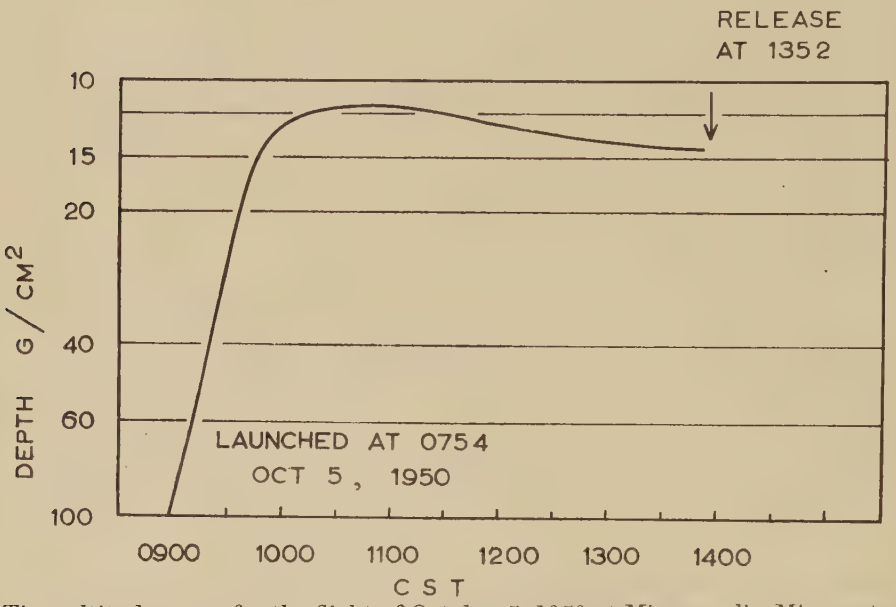

Time altitude curve for the flight of October 5, 1950 at Minneapolis, Minnesota.

§ 4. Re-Analysis

In the investigation of Dainton *et al.* the emulsions were scanned for tracks which were more than 6 mm long and which had a δ-ray density (N_δ) greater than that of a relativistic Lithium nucleus (1 per 100 μ). The variation of the scattering parameter, $\bar{\alpha}$, with the δ-ray density for the relevant tracks is shown in fig. 7. There was an appreciable scanning bias against tracks having δ-ray densities near the minimum value, and as a result we have only considered the slower alpha-particles, with higher δ-ray densities. The particles accepted were those which when entering the emulsions had an estimated residual range of less than 32 mm. These residual ranges were estimated (for those particles that did not come to rest) by determining the residual range corresponding to the measured values of $\bar{\alpha}$ and N_δ by referring to the position of the corresponding point on fig. 7, and then allowing for the distance between the centre of the measured segment and the point of entry. This procedure represents a convenient approximation to a more rigorous estimate of the range.

The scattering parameters were obtained from a noise elimination procedure between 400 and 200 micron cells, and were all greater than

about $0{\cdot}070°/100\,\mu$. It seems reasonable to assume that these values cannot have been seriously affected by any forms of distortion. That the above estimates of the residual ranges are not seriously affected by systematic errors, is shown, both by the close agreement between values calculated in this manner with those observed directly on particles ending in, and by the fact that 34 particles were observed to end as compared with the 31 that were expected to do so.

Fig. 7

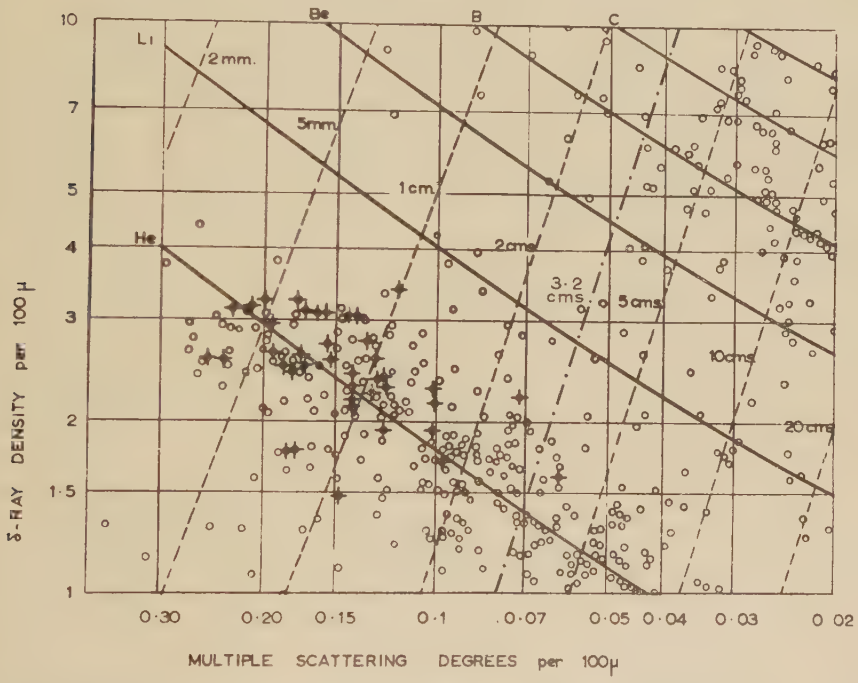

The variation of the δ-ray, density, N_δ with the scattering parameter, $\bar{\alpha}$. Those He-nuclei which end in the emulsion are shown by crosses.

Altogether 196 alpha-particles with estimated residual ranges of less than 3·2 cm of emulsion were found in this stack. In order to obtain values on the differential energy spectrum from this data, we defined certain groups of tracks in terms of their geometry, and thus in terms of the mean amount of matter they had traversed before being detected. Such a division enabled the fluxes to be calculated of those particles which entered the top of the atmosphere within a certain defined range of energy. In all four such groups were defined containing 162 of the alpha-particles. The details of the four groups are shown in table 3. In this table the successive columns show :—

(i) the group number ;
(ii) the number of alpha-particles in the group ;
(iii) the effective collecting area in m^2 steradian sec ;

Table 3

(i) Class	(ii) Number of alphas	(iii) Effective collecting area m^2/ster/sec	(iv) Mean amount of matter traversed g g/cm^2		(v) Mean Residual Δg g/cm^2	(vi) Mean energy E Mev/ nucleon	(vii) Spread in mean energy ΔE Mev	(viii) Flux at top of atmosphere uncorrected for secondaries Particles/m^2/ster/sec/Mev
			(air+glass)	(emulsion)				
I	38	10·8	14·6	2·3	0·58	155	35	$0·145 \pm 0·024$
II	26	7·2	18·3	2·3	1·31	172	33	$0·17 \pm 0·034$
III	46	17·6	27·3	2·3	3·92	210	31	$0·16 \pm 0·024$
IV	52	20·3	38·2	2·3	6·00	248	27	$0·23 \pm 0·032$

	(ix) Percentage correction due to fragmentations	(x) Percentage correction due to 'stripping'	(xi) Flux at top of atmosphere corrected for production of secondaries Particles/m^2/ster/sec/Mev
I	9	2	$0·13 \pm 0·02$
II	10	2	$0·15 \pm 0·03$
III	17	2	$0·13 \pm 0·02$
IV	16	2	$0·19 \pm 0·02$

(iv) the mean amount of matter through which the particles have passed before entry into the emulsion g ;

(v) the mean residual of the individual amounts of overlying matter Δg ;

(vi) the mean energy at the top of the atmosphere E, calculated from g ;

(vii) the spread in energy ΔE, due to the spread in the residual ranges accepted, 6–32 mm ;

(viii) the flux at the top of the atmosphere corrected only for absorption, in particles/m²/ster/sec/Mev ;

(ix) and (x) the percentage corrections due to fragmentation of heavier particles and due to the stripping of alpha-particles, Appendix (*a*) and (*b*) ;

(xi) the fully corrected flux at the top of the atmosphere.

In order to extrapolate the observed fluxes to the top of the atmosphere we have taken a mean free path of alpha-particles for absorption in air of 45 g/cm², Bradt and Peters (1950), Webber and McDonald (1955). The effect of the secondary production of alpha-particles has been considered separately, and the derivations of the corrections are shown in the Appendix. The corrected differential flux values derived in this analysis are shown in fig. 5 (*c*) together with those derived by Waddington (1954, 1956 b) in the same emulsions. Also shown in this fig. 5 (*d*), is the integral spectrum obtained in these emulsions from this analysis and from the data of Waddington, for comparison with that obtained at Saskatoon. Waddington's data was obtained from a scan made for alpha-particles of all energies and is directly comparable with the scan made for alpha-particles at Saskatoon.

It should be noted that although the differential spectrum obtained over Minnesota does not appear to rise to a pronounced maximum similar to that observed over Saskatoon, the two distributions are not significantly different.

§ 5. Conclusions

From these results we conclude that :

(1) The differential energy spectra of alpha-particles at Minneapolis in 1950 and at Saskatoon in 1954 were closely similar down to the lowest observable energies, in spite of the fact that they were obtained at very different geomagnetic latitude. In both experiments the spectra show a maximum at about 300 Mev per nucleon and then fall gradually to about 130 Mev per nucleon. Therefore, since Saskatoon is considerably nearer the north magnetic pole than Minneapolis, the cut-off energy over Minneapolis must have been less than 130 Mev per nucleon.

(2) Because of the similarity of these two spectra, it appears that the spectra must represent the distribution in energy of the cosmic ray alpha-particles before they arrive in the vicinity of the earth, as suggested by Ney at Mexico.

(3) This reduced cut-off energy implies that the latitude from which the cut-off energy should be calculated, the ' cosmic ray ' latitude, was at Minnesota, at least three degrees greater than the geomagnetic latitude,

(4) Any rise in the total ionization count greater than a few percent observed north of the cosmic ray latitude of Minnesota, must imply that the cosmic ray protons have a different rigidity spectrum to that of the alpha-particles.

(5) The present results are in disagreement with those of Ellis *et al.* (1954) who conclude that their data indicates a sharp cut-off for alpha-particles at an energy of 280 Mev per nucleon.

(6) It seems unsatisfactory to postulate that the spectrum in the low energy region is cut-off sharply by a magnetic field in space, and then the cut-off is ' smeared ' by traversal of matter. Since calculations show that the residual atmosphere and packing above the emulsions in these experiments was not able to produce any appreciable number of low energy particles, it would be necessary to invoke a large amount of absorber in space to smear out a sharp cut-off sufficiently to give the observed spectra.

APPENDIX

Corrections for Helium Nuclei Produced by Secondary Processes

There appear to be three processes by which an appreciable number of secondary helium nuclei could be produced.

(*a*) The production of secondary alpha-particles by the fragmentation of multiply charged particles in the matter above the emulsions.

In order to estimate the number of alpha-particles produced in this manner we have two assumptions. Firstly, that in an interaction which results in the fragmentation of an incident multiply charged particle the velocity of the fragments will be the same as that of the primary particle. Secondly, that the mean free paths and fragmentation probabilities are independent of energy. Both these assumptions appear to be reasonable.

If we consider a detector placed y g/cm^2 from the top of the atmosphere, then the number of secondary alpha-particles I, arriving at that detector from a layer of the atmosphere of thickness dx and distance x from the top of the atmosphere, due to the interactions of a parallel beam of multiply charged particles with charge Z, is given by :

$$dI = J(Z, R)\frac{P_{Z\alpha}}{\Lambda_Z}\exp(-x/\lambda_Z).\exp -(y-x)/\lambda_\alpha . dx \quad . \quad . \quad . \quad (1)$$

where $P_{Z\alpha}$ is the mean number of alpha-particles produced by a particle of charge Z in an interaction ; λ_Z and λ_α are the *absorption* mean free paths of the heavy particle and the alpha-particle respectively ; Λ_Z is the *interaction* mean free path of the heavy particle ; and $J\ (Z, R)$ is the number of particles of charge Z with a residual range, at the top of the atmosphere, betweeen R and $R + \Delta R$. Her R and $R + \Delta R$ are residual ranges such that the alpha-particles which result from interactions at a depth x arrive at the emulsions (depth y) with residual ranges of 6 and 32 mm respectively.

ΔR is therefore independent of both x and y for a given charge, and is equal to (32—6) . $2/Z$ mm of emulsion.

At high energies, where R is effectively independent of x, eqn. (1) may be integrated over all x to give the usual relation :

$$I = J(Z, R)\frac{\lambda_Z P_{Z\alpha}}{\Lambda_Z}\frac{\lambda_\alpha}{\lambda_\alpha - \lambda_Z}\left[\exp(-y/\lambda_\alpha) - \exp(-y/\lambda_Z)\right]. \quad . \quad . \quad (2)$$

At low energies $J(Z, R)$ is a complicated function of x, and it is convenient to integrate eqn. (1) numerically. In order to find the appropriate values of $J(Z, R)$ we have constructed from the differential energy spectrum of the alpha-particles shown in fig. 5, the differential range spectrum at the top of the atmosphere for the various charge components considered. We have assumed that the spectra of all these particles have the same variation with energy per nucleon.

Fig. 8

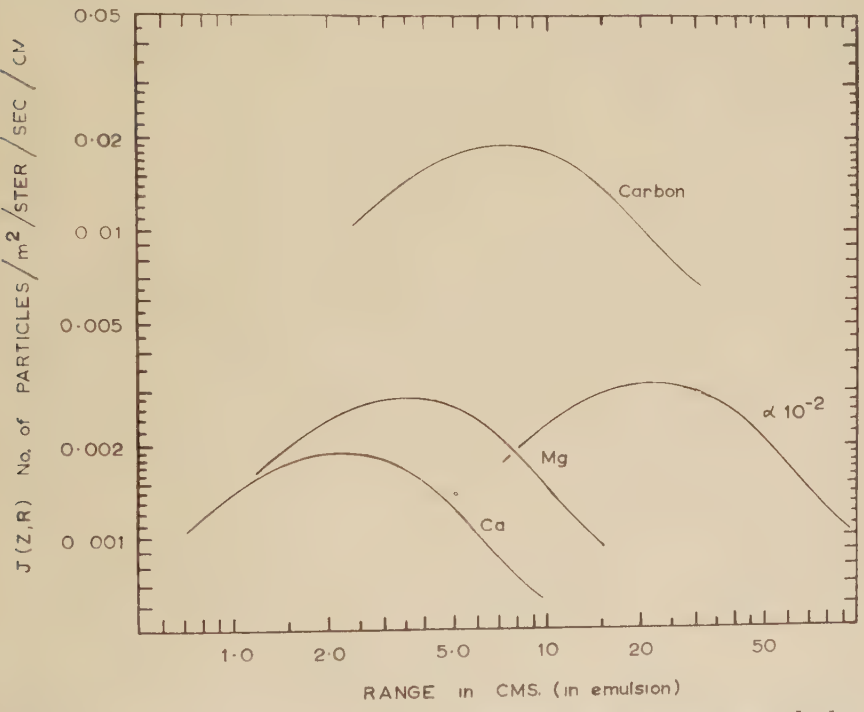

Differential range spectra for groups of particles with charges centred about carbon, magnesium, calcium, and, reduced by 10^2, helium.

These differential range spectra are shown in fig. 8 for groups of particles whose charges are centred about those of carbon, magnesium and calcium, and whose fluxes (at Minnesota) were taken as 20, 3 and 2 particles/m²/ster/sec respectively. The curve shown for the alpha-particles corresponds to 320 alpha-particles/m²/ster/sec.

The results of these corrections are shown in table 3. It can be seen that the corrections are all less than 20%. As a result it has not been considered necessary to modify the curves shown in fig. 8 for the effects of secondary production.

(*b*) The production of He^3 particles in stripping collisions of He^4-nuclei.

We have made a similar calculation to the one above to estimate the correction that will have to be applied for this process. In making this calculation we have assumed that 10% of all interactions in air will be of the He^4 stripping to He^3 type. This figure is based on an observed figure of $6{\cdot}3\%(\frac{19}{303})$ in emulsion, obtained from the combined data of Appa Rao *et al.* (1956) and Waddington (1956 a).

In this calculation the value of ΔR will have changed, since instead of accepting a He^4-nucleus with residual range between 6 and 32 mm, a He^3-nucleus will be accepted if its residual range lies beween 6 and 36 mm. Such He^3-nuclei will be produced by a He^4-nuclei with a ΔR of 40 mm.

Using the alpha-particle curve given in fig. 8 we find that the correction due to this stripping process amounts to about 2% in each of the groups defined in this experiment.

(*c*) The production of slow helium nuclei by singly and doubly charged nuclei in interactions.

It has been shown by Yasin (1955) that helium nuclei with energies greater than 80 Mev (not evaporation particles) emitted from disintegrations initiated by singly or doubly charged particles are predominantly He^3-nuclei. This conclusion is supported by inspecting the relative numbers of He^3- and He^4-nuclei—identified from their residual ranges—observed in emulsions exposed to the K^+ beam of the Bevatron. It is therefore theoretically possible to distinguish the He-nuclei produced in this manner from those of primary cosmic ray origin, which are presumably mostly He^4-nuclei. However, in specific cases it is rarely possible to distinguish between He^3- and He^4-nuclei ending in emulsions, and it was therefore necessary to calculate the rate of production of these He-nuclei from other experimental data.

We have used the results of Sorensen (1952) and of Dahanayake *et al.* (unpublished, but see Dahanayake *et al.* 1955). Sorensen considered He-nuclei with residual ranges greater than 0·7 mm emitted from stars found in emulsions exposed at 68 000 feet ; while Dahanayake *et al.* took a sample of those particles with residual ranges greater than 2 mm emitted from stars having two or more shower particles ($n_s \geqslant 2$) found in emulsions exposed at 85 000 feet. The energy distributions of the observed He-nuclei in the two experiments have been shown by Yasin (1955) to be closely similar, and to follow the relation :

$$N(E)dE = \frac{\text{const.}}{E^{1\cdot7}}\, dE. \qquad \ldots\ldots\ldots \quad (3)$$

Dahanayake *et al.* observed 90 He-nuclei, of which 32 had residual ranges greater than 6 mm, emitted from 4742 stars having $n_s \geqslant 2$. When a

correction was made for the geometrical selection used, it was found that about 150 He-nuclei with residual ranges greater than 6 mm had been emitted from these stars. In the emulsions used in the present experiment the density of stars with $n_s \geqslant 2$ was 73 stars per cm^3 of emulsion. Thus the production rate, for this type of star only, was 2·3 He-nuclei per cm^3 of emulsion.

Unfortunately, it is not possible to find the total production rate of He-nuclei from Sorensen's results, since the total number of stars examined was not specified. Hence we have had to use the production rate derived from the results of Dahanayake *et al.* and correct for the production of He-nuclei by stars with $n_s < 2$. To make this correction we have examined the observed star distributions in the emulsions used by Sorensen, as given by Camerini *et al.* (1952), and that in the emulsions used in the present experiment. We find that they are not appreciably different. From Sorensen's data it appears that for each star with $n_s \geqslant 2$ that emits a He-nucleus there are 2·8 with $n_s < 2$. Thus the total production rate in these emulsions of He-nuclei with residual ranges greater than 6 mm is 8·7 He-nuclei per cm^3 of emulsion.

In order to obtain an estimate of the total production rate in air from that in emulsion we have considered the numbers of black and grey prongs N_h emitted from the helium producing stars. In emulsion the elements carbon, nitrogen and oxygen (CNO) make up 25% of the total geometrical cross section, but only 15% of the total interaction cross section (Lock *et al.* 1955, for 950 Mev protons). From the data of Camerini *et al.* 75% of all stars have $N_h \leqslant 7$, and so simulate stars in light elements†. Thus, using the experimentally observed interaction cross section, only one-fifth of those stars with $N_h \leqslant 7$ are produced in light elements. Sorensen's data shows that only 30% of the He-nuclei come from stars with $N_h \leqslant 7$. Therefore, assuming that in small stars light and heavy nuceli are equally capable of producing He-nuclei, the production from CNO in emulsion was 0·52 He-nuclei per cm^3 of emulsion, or, 0·75 He-nuclei per g of CNO, since CNO have a density of 0·7 g/cm^3 of emulsion.

In work involving emulsions, there is generally a scanning bias against the detection of stars with small N_h. But, since Sorensen's results show that the efficiency of production of He-nuclei falls off sharply as N_h decreases, and, since a star with a 6 mm He-nucleus is less likely to be missed than a typical small N_h star, we have assumed that for these purposes the effects of any scanning loss of small stars may be neglected.

In calculating the production rate in CNO, we have assumed that in small stars light nuclei are equally as likely to produce He-nuclei as are silver and bromine nuclei. This assumption appears improbable, and we therefore believe that the production rate for light nuclei given above may well be an overestimate of the true value.

† Due to the scanning bias against interactions with hydrogen, we have assumed that all stars in light elements will be in CNO.

In calculating the number of He-nuclei produced above the emulsions, we have used the production rate given previously. In addition, Sorensen has shown that the emission of He-nuclei is not isotropic, the median angle of the angular distribution about the primary being about 50°, whereas the primary particles are nearly isotropic over the upper hemisphere. For this reason we have taken the solid angle that He-nuclei are emitted into as being only 3π steradians.

Making the above assumptions, we find that in none of the groups of particles defined in the present experiment are more than 1 or 2% of the observed alpha-particles attributable to production of He-nuclei by singly or doubly charged particles. It appears, therefore, that this mode of production may be neglected.

That this conclusion is correct may be justified experimentally. Waddington (1956 b) working on a stack of emulsions exposed at a cut-off energy of about 650 Mev per nucleon. and an altitude of 106 000 feet, searched an area containing an estimated 230 fast alpha-particles, and found only one with a residual range less than 32 mm. Dainton *et al.* (1952) observed in emulsions exposed at a similar cut-off energy but at 60 000 feet, 9 slow alpha-particles in an area containing 70 heavy primary particles. These 70 particles are estimated to correspond to 1400 fast alpha-particles. The few slow alpha-particles observed in these experiments can all be attributed to the fragmentation of heavy particles rather than to production by the interaction of singly or doubly charged particles.

Acknowledgments

We wish to thank R. B. Thorness and Ray Maas for their help in the design and construction of the Saskatoon equipment ; W. Huch for his help with the balloon flights ; Dawn Copeland, Pamela Curry, Biruta Sommers, Janet Witchell and Leona Wurm for doing the very difficult and tedious scanning involved in this experiment.

We are grateful to Professor C. F. Powell for the hospitality of his laboratory. One of us, C. J. W., wishes to thank the Royal Society for the award of a Mackinnon Research Studentship.

References

Apper Rao, M. V. K., Daniel, R. R., and Neelakontan, K. A., 1956, *Proc. Ind. Acad.*, **43**, 181.

Bradt, H. L., and Peters, B., 1950, *Phys. Rev.*, **80**, 943.

Camerini, U., Davies, J. H., Fowler, P. H., Franzinetti, C., Muirhead, H., Lock, W. O., Perkins, D. H., and Yekutieli, G., 1951, *Phil. Mag.*, **42**, 1241.

Dahanayake, C., Francois, P. E., Fujimoto, Y., Iredale, P., Waddington, C. J., and Yasin, M., 1955, *Nuovo Cim.*, Ser. X, **1**, 888.

Dainton, A. D., Fowler, P. H., and Kent, D. W., 1952, *Phil. Mag.*, **43**, 729.

Ellis, R. A., Gottlieb, M. B., and Van Allen, J. A., 1954, *Phys. Rev.*, **95**, 304(a)

Jory, F. S., 1956, *Phys. Rev.*, **102**, 1167.

Linsley, J., 1955, *Phys. Rev.*, **97**, 1292.

Lock, W. O., March, P. V., Muirhead, H., and Rosser, W. G. V., 1955, *Proc. Roy. Soc.* A, **230,** 215.
Neher, H. V., and Stern, E. A., 1955, *Phys. Rev.*, **98,** 845.
Ney, E. P., 1955, reported at Mexico Conference.
Simpson, J. A., Fenton, K. B., Katzman, J., and Rose, D. C., 1956, *Phys. Rev.*, **102,** 1648.
Sorensen, S. O., 1951, *Thesis, University of Oslo* (see also *Phil. Mag.*, **42,** 188).
Waddington, C. J., 1954, *Phil. Mag.*, **45,** 1312 ; 1956 a, *Ibid.*, **1,** 105 ; 1956 b, *Nuovo Cim.*, **3,** 930.
Webber, W. R., and McDonald, F. B., 1955, *Phys. Rev.*, **100,** 1460.
Yasin, M., 1955, *Ph.D. Thesis,* University of Bristol.

A Simple Treatment of Meson–Nucleon Scattering †

By S. F. Edwards and P. T. Matthews
Department of Mathematical Physics, University of Birmingham

[Received April 26, 1956, Revised August 10, 1956]

Abstract

It is shown that the p-wave meson–nucleon scattering cross sections can be very simply explained by calculating the first order effective potential between meson and nucleon and the scattering in this potential. Some comments are made on the S-wave problem and virtual heavy meson effects.

§ 1. Introduction

The oldest and simplest application of field theory to the low energy nucleon–nucleon problem is the adiabatic approximation. An effective potential (the Yukawa potential) is calculated by Born approximation. This is then inserted in the non-relativistic Schrödinger equation for the relative motion of the two nucleons, which is then solved exactly for the binding energy and scattering. We show here that the qualitative features of the successful description of the p-wave meson–nucleon scattering, given by other authors on the basis of the no-recoil pseudovector theory (Sartori and Wataghin (1954), Chew and Low (1956)), may be derived in this, conceptually extremely simple, way. The effective potential for the meson is determined by Born approximation. This is then inserted in the relativistic Schrödinger (i.e. Klein–Gordon) equation for the meson, and the scattering in this potential calculated exactly. We shall refer to this as the potential approximation.

This procedure does not preserve the crossing symmetry. However, if the equation is symmetrized with respect to crossing and solved as an expansion in the energy one reproduces the results of the above authors.

If the interaction is supplemented by the ϕ^2 term in the non-relativistic approximation to γ_5 theory, there is an S-wave scattering, which is given exactly by the potential approximation. Taking the same coupling constant and cut-off as in the p-wave case, one obtains an S-wave of the required order of magnitude, but lacking the observed dependence on isotopic spin.

In the final section the possibility is investigated that this isotopic spin dependence is a consequence of virtual K-meson effects. It appears

† Communicated by Professor R. E. Peierls, C.B.E., F.R.S.

that these may well give a non-negligible contribution, but do not appear likely to give a simple explanation of the effect.

The equation from which we start is derived in closed form in the Appendix, which thus provides a more formal basis for the outlook adopted in § 2.

It is perhaps worth remarking that the Tamm–Dancoff approximation is not equivalent to the scattering in an effective potential, although it has been described in these terms (see for example, Gell-Mann and Watson 1954). The Tamm–Dancoff method excludes the effect of virtual meson pair creation, which may take place in any potential. (This is discussed in more detail by Feldman and Matthews 1956.) This approximation replaces an algebraic equation by an integral equation, which has been solved approximately by Chew (1953).

§ 2. The p-Wave Scattering

The scattering at energy ω, $(\omega^2=p^2+\mu^2)$, is determined by the equation

$$(p^2+\mu^2-\omega^2)(\mathbf{p}\,|\,\phi_r)-V_{rs}(\mathbf{p},\mathbf{q})(\mathbf{q}\,|\,\phi_s)=0. \quad . \quad . \quad . \quad (2.1)$$

Integration or summation over repeated variables is implied. The potential V is determined by Born approximation. If the interaction energy density is

$$H(x)=-j_r(x)\phi_r(x)=-g\delta(\mathbf{x})\tau_r\boldsymbol{\sigma}\cdot\nabla\phi_r(x), \quad . \quad . \quad . \quad (2.2)$$

then

$$V_{rs}(\mathbf{p},\mathbf{q})=(2\pi)^3[j_r(\mathbf{p}),j_s(-\mathbf{q})]/\omega, \quad . \quad . \quad . \quad . \quad . \quad (2.3)$$

where

$$j_r(\mathbf{p})=ig(\boldsymbol{\sigma}\cdot\mathbf{p})\tau_r/(2\pi)^3. \quad . \quad . \quad . \quad . \quad . \quad . \quad . \quad (2.4)$$

This is obtained by perturbation theory from the familiar 'crossed' and 'uncrossed' graphs. The cross section is proportional to the square of the modulus of the t-matrix, where the t-matrix satisfies†

$$t_{rs}(\mathbf{p},\mathbf{q})=V_{rs}(\mathbf{p},\mathbf{q})+V_{rt}(\mathbf{p},\mathbf{k})(k^2+\mu^2-\omega^2-i\epsilon)^{-1}t_{ts}(\mathbf{k},\mathbf{q}). \quad (2.5)$$

Introduce $t_{rs}{}^{\alpha\beta}(\omega)$ and $V_{rs}{}^{\alpha\beta}(\omega)$, defined by

$$t_{rs}(\mathbf{p},\mathbf{q})=p_\alpha t_{rs}{}^{\alpha\beta}(\omega)q_\beta,$$

$$V_{rs}(\mathbf{p},\mathbf{q})=p_\alpha V_{rs}{}^{\alpha\beta}(\omega)q_\beta. \quad . \quad . \quad . \quad . \quad . \quad . \quad (2.6)$$

---

† This equation is proved thus: if ϕ^{in} is the incoming wave function, satisfying $(p^2+\mu^2-\omega^2)\,\phi^{\mathrm{in}}=0$, then by (2.1), ϕ satisfies

$$\phi=\phi^{\mathrm{in}}+(p^2+\mu^2-\omega^2-i\epsilon)^{-1}\,V\phi. \quad . \quad . \quad . \quad . \quad (a)$$

The differential cross section, σ, is given by $\sigma\sim|\,t\,|^2$, where

$$\phi=\phi^{\mathrm{in}}+(p^2+\mu^2-\omega^2-i\epsilon)^{-1}\,t\,\phi^{\mathrm{in}}.$$

Thus $t\phi^{\mathrm{in}}=V\phi$. Hence, multiplying (a) by V,

$$t=V+V\,(p^2+\mu^2-\omega^2-i\epsilon)^{-1}\,t.$$

These matrices then satisfy the matrix equation (not an integral equation)

$$t_{rs}{}^{\alpha\beta}=V_{rs}{}^{\alpha\beta}+V_{rt}{}^{\alpha\delta}d''t_{ts}{}^{\delta\beta}, \quad . \quad . \quad . \quad . \quad . \quad . \quad (2.7)$$

where $d''(\omega)$ is the diagonal matrix

$$d''(\omega)=\frac{1}{3}\int\frac{k^2d^3k}{(k^2+\mu^2-\omega^2-i\epsilon)}. \quad . \quad . \quad . \quad . \quad . \quad . \quad (2.8)$$

The matrices t and V may be diagonalized by projection operators. For isotopic spin the projection operators for the $\frac{1}{2}$ and $\frac{3}{2}$ states are respectively

$$\begin{aligned} p^1{}_{rs}&=(1/3)\tau_r\tau_s,\\ p^3{}_{rs}&=\delta_{rs}-(1/3)\tau_r\tau_s, \end{aligned} \quad . \quad . \quad . \quad . \quad . \quad . \quad (2.9)$$

and similarly for total angular momentum. If P_α, ($\alpha=JT$), are the projection operators for states of angular momentum and isotopic spin $\frac{1}{2}J$ and $\frac{1}{2}T$ (i.e. $\alpha=11$, 13, 31, 33),

$$t(\omega)=\sum_\alpha P_\alpha t_\alpha(\omega), \quad . \quad . \quad . \quad . \quad . \quad . \quad . \quad . \quad (2.10)$$

and, expressing (2.3) in terms of (2.9),

$$V=(g^2/(2\pi)^3\omega)\sum_\alpha n_\alpha P_\alpha, \quad . \quad . \quad . \quad . \quad . \quad . \quad (2.11)$$

where $n_{11}=-8$, $n_{13}=n_{31}=-2$, $n_{33}=4$. Substituting into (2.7), and taking matrix elements for states of definite T and J, gives the algebraic equation

$$t_\alpha(\omega)=\frac{g^2n_\alpha}{\omega-g^2n_\alpha d''(\omega)/(2\pi)^3}. \quad . \quad . \quad . \quad . \quad . \quad . \quad (2.13)$$

The factor $d''(\omega)$ is cubically divergent. Mass renormalization consists of replacing it by

$$\bar{d}(\omega)=d''(\omega)-d''(0), \quad . \quad . \quad . \quad . \quad . \quad . \quad . \quad . \quad (2.14)$$

which gives $t(\omega)$ a pole at $\omega=0$, corresponding to the neutron. This approach agrees with the familiar renormalization of perturbation theory. If $\bar{d}$ is cut off at Λ, it can be simply evaluated :

$$\bar{d}(\omega)=(2\pi/3)\{2\Lambda\omega^2-\pi(\mu^3-ip^3)\}. \quad . \quad . \quad . \quad . \quad (2.15)$$

Finally in terms of the phase shifts

$$1/t_\alpha(\omega)\sim p^3\exp[-i\delta_\alpha]/\sin\delta_\alpha. \quad . \quad . \quad . \quad . \quad . \quad (2.16)$$

The constant of proportionality can be determined by equating the imaginary parts of (2.13) and (2.16). Then equating real parts one has

$$\frac{p^3\cot\delta_\alpha}{\omega}=+\frac{3}{n_\alpha}\left(\frac{4\pi}{g^2}\right)-\left[\frac{2\Lambda\omega}{\pi}-\frac{\mu^3}{\omega}\right]. \quad . \quad . \quad . \quad (2.17)$$

Making the approximation of dropping the final term, one can write this in the effective range form

$$\lambda_\alpha p^3\cot\delta_\alpha/\omega=1-\omega/\omega_\alpha, \quad . \quad . \quad . \quad . \quad . \quad . \quad (2.18)$$

where

$$\lambda_\alpha=+\frac{n_\alpha}{3}\left(\frac{g^2}{4\pi}\right), \quad . \quad . \quad . \quad . \quad . \quad . \quad . \quad . \quad (2.19)$$

and

$$\omega_\alpha=6\pi^2/n_\alpha g^2\Lambda. \quad . \quad . \quad . \quad . \quad . \quad . \quad . \quad . \quad (2.20)$$

A resonance occurs at $\omega=\omega_\alpha$ if n_α is positive, that is for $\alpha=33$.

§ 3. Unitarity and Crossing

The approximation of § 2 does not preserve the crossing symmetry of $t_{rs}(\omega)$. If we interpret V_{rs} of (2.7) as the exact potential (derived in the Appendix), the equation is exact and is unchanged if we write

$$t_{rs}(\omega)=V_{rs}(\omega)+\tfrac{1}{2}[V_{rt}(\omega)d''t_{ts}(\omega)+V_{st}(-\omega)d''t_{tr}(-\omega)]. \quad . \quad . \quad (3.1)$$

The imaginary part of t^{-1} is fully determined by unitary

$$\mathrm{Im}t^{-1}=-p^3/3\cdot 4\pi. \quad . \quad . \quad . \quad . \quad . \quad . \quad . \quad (3.2)$$

To obtain the effective range formula, which automatically satisfies crossing symmetry, we expand (3.1) for the real part of $t^{-1}(\omega)/\omega$ as a power series in ω, approximating for V_{rs} as in § 2. (Note that we are still handling an algebraic, not an integral equation.) This yields

$$\frac{\eta_\alpha g^2 \mathrm{R}(t_\alpha^{-1})}{\omega}=1-\frac{1}{2}\frac{\mathrm{R}(\bar{d})}{(2\pi)^3}\left\{\eta_\alpha+\frac{A\ \eta_\gamma^2}{\eta_\alpha}\right\}, \quad . \quad . \quad . \quad (3.3)$$

where $A^{\alpha\gamma}$ is the numerical matrix determined by

$$t_\alpha(\omega)=A^{\alpha\gamma}t_\gamma(-\omega). \quad . \quad . \quad . \quad . \quad . \quad . \quad . \quad (3.4)$$

This reproduces (2.18) with the definition of ω_α modified to

$$\omega_\alpha=6\pi^2/c_\alpha g^2 A \quad . \quad . \quad . \quad . \quad . \quad . \quad . \quad (3.5)$$

where $c_\alpha=(-6,\ 0,\ 6)$ in agreement with the above authors. The experimental data for the 33 wave are fitted by

$$g^2/4\pi=0{\cdot}08/\mu^2,$$
$$A=5\,\mu. \quad . \quad . \quad . \quad . \quad . \quad . \quad . \quad . \quad (3.6)$$

The other phases are then small and negative.

§ 4. The S-Wave

If the non-relativistic interaction is regarded as an approximation to the relativistic ps–ps theory, there is an additional term in the Lagrangian (g defined as before) of

$$L_s=-2g^2m\phi^2. \quad . \quad . \quad . \quad . \quad . \quad . \quad . \quad . \quad (4.1)$$

This gives rise to an S-wave scattering, which can be calculated exactly by the ' potential ' method :

$$t_s(\omega)=\frac{-2g^2m}{1+2g^2md(\omega)/(2\pi)^3} \quad . \quad . \quad . \quad . \quad . \quad (4.2)$$

where

$$d(\omega)=\int(k^2+\mu^2-\omega^2-i\epsilon)^{-1}d^3k. \quad . \quad . \quad . \quad . \quad (4.3)$$

$d(\omega)$ is linearly divergent, and it is consistent with our approximation to simulate the renormalization of the relativistic theory with a cut-off A. This leads to the expression for the S-phase shift

$$p\cot\delta=-\frac{2\pi}{mg^2}-\frac{2A}{\pi}. \quad . \quad . \quad . \quad . \quad . \quad . \quad . \quad (4.4)$$

Taking g^2 and Λ from the p-wave data, this gives an S-wave scattering of the observed magnitude, but the strong dependence on isotopic spin observed experimentally is completely lacking in this model.

This discrepancy might be corrected in a relativistic scheme, but another possibility arises in the contribution from virtual K-mesons. Since τ, θ and π mesons are all strongly coupled to nucleons, they must be strongly coupled to each other. For simplicity we assume there is a direct local coupling :

$$L_1 = m g_1 \tau^{\alpha\beta}{}_r (\bar{\chi}^\alpha \vartheta^\beta + \bar{\vartheta}^\alpha \chi^\beta)\phi_r, \quad . \quad . \quad . \quad . \quad . \quad (4.5)$$

where χ and ϑ are the τ and θ meson fields, respectively. We also assume

$$L_2 = g_2(\bar{\psi}^\alpha \Lambda \vartheta^\alpha + \bar{\Lambda}\psi^\alpha \bar{\vartheta}^\alpha \quad . \quad . \quad . \quad . \quad . \quad (4.6)$$

and

$$L_3 = g_3 \tau^{\alpha\beta}{}_r (\bar{\psi}^\alpha \Sigma_r \vartheta^\beta + \bar{\Sigma}_r \psi^\beta \bar{\vartheta}^\alpha) \quad . \quad . \quad . \quad . \quad . \quad (4.7)$$

consistent with the Gell-Mann–Nishijima scheme. The coupling constants g_i appearing in these interactions are pure numbers and we take $g_i^2/4\pi = 1$, which appears to be consistent with the observed production rates. A rough calculation of the resulting effective meson–nucleon potentials of order $g_1^2 g_2^2$ and $g_1^2 g_3^2$ indicates that these effects might give corrections to meson–nucleon scattering of the order of 10%. However, the factor m included in L, for dimensional reasons, might well be replaced by the K-meson or π-meson mass, so 10% should be regarded as an upper limit. Of this correction, crossing symmetry requires that the τ-dependent part is further reduced by a factor of (ω/K-meson mass). Thus although heavy mesons may play a part in a detailed theory of π-meson scattering, they do not offer a simple answer to the τ-dependence of the S-wave.

APPENDIX

We derive here in closed form the equation for the meson propagator, Δ', in the presence of the source $j_r(x)$.

Consider the Lagrangian

$$L = -\tfrac{1}{2}\phi_r(-\Box + \mu^2)\phi_r + (j_r + J_r)\phi_r \quad . \quad . \quad . \quad . \quad (A\ 1)$$

where $J(x)$ is a classical field. The propagator in Schwinger's (1951) notation is

$$\Delta'_{rs}(x, y) = \langle (\phi_r(x), \phi_s(y))_+ \rangle - \langle \phi_r(x) \rangle \langle \phi_s(y) \rangle . \quad . \quad (A\ 2)$$

Using the equation of motion for ϕ

$$\begin{aligned}(-\Box + \mu^2)\Delta'_{rs} &= \langle (j_r, \phi_s) \rangle - \langle j_r \rangle \langle \phi_s \rangle - i\delta_{rs} \\ &= -i\delta \langle j_r \rangle / \delta J_s - i\delta_{rs} . \quad . \quad . \quad . \quad . \quad . \quad . \quad . \quad (A\ 3)\end{aligned}$$

But

$$\begin{aligned}-i\frac{\delta\langle j_r\rangle}{\delta J_s} &= -i\frac{\delta\langle j_r\rangle}{\delta\langle\phi_t\rangle}\frac{\delta\langle\phi_t\rangle}{\delta J_s} \\ &= \frac{\delta\langle j_r\rangle}{\delta\langle\phi_t\rangle}\Delta'_{ts} . \quad . \quad . \quad . \quad . \quad . \quad . \quad . \quad (A\ 4)\end{aligned}$$

Thus

$$[(-\Box+\mu^2)\delta_{rt}-\delta\langle j_r\rangle/\delta\langle\phi_t\rangle]\Delta'_{ts}=-i\delta_{rs}. \quad . \quad . \quad . \quad \text{(A 5)}$$

Now

$$\delta\langle j_r\rangle/\delta\langle\phi_t\rangle=i\langle(j_r,j_t)_+\rangle-i\langle j_r\rangle\langle j_t\rangle, \quad . \quad . \quad . \quad \text{(A 6)}$$

where, for example,

$$\langle(j_r(x),j_t(y))_+\rangle=\frac{P\int j_r(x)j_t(y)\exp[i\int Ldx^4]\delta\phi}{P\int\exp[i\int Ldx^4]\delta\phi}, \quad . \quad \text{(A 7)}$$

the P denoting that the operators $j_r(x)$ must operate in their chronological order. Expanding (A 6) in powers of j gives, to order j^2.

$$\delta\langle j_r(x)\rangle/\delta\langle\phi_t(y)\rangle=-i[j_r(x),j_t(y)]\Theta(t_y-t_x), \quad . \quad \text{(A 8)}$$

where

$$\Theta(t)=1, \qquad t>0,$$
$$=0, \qquad t<0.$$

Substituting this into (A 5), and making a Fourier transform, leads directly to eqns. (2.1)–(2.3) for the meson wave function.

Acknowledgments

The authors wish to thank Dr. R. H. Dalitz and Professor R. E. Peierls for helpful conversations and suggestions.

References

Chew, G. F., 1953, *Phys. Rev.*, **89**, 591.
Chew, G. F., and Low, F., 1956, *Phys. Rev.*, **101**, 1570.
Feldman, G., and Matthews, P. T., 1956, *Phys. Rev.*, **103**, 1870.
Gell-Mann, M., and Watson, K. M., 1954, *Ann. Rev. Nuclear Sci.*, **4**, 219.
Sartori, L., and Wataghin, V., 1954, *Nuovo Cim.*, **12**, 145.
Schwinger, J., 1951, *Proc. Nat. Acad. Sci.*, **37**, 452.

The Reflection and Transmission of Shock Waves I: The Reflection of a Detonation Wave at a Boundary †

By D. C. Pack
Department of Mathematics, The Royal College of Science and Technology, Glasgow

[Received August 20, 1956]

Summary

It is shown that, for a shock wave advancing through any physically real barotropic medium, the nature of the reflected wave is uniquely determined by the relative shock impedances of the medium through which the incident wave passes and the medium upon which it falls. A simple criterion is found for determining the nature of the reflection of a detonation wave at the end of a block of explosive. Particular attention is paid to the examples of an explosive in contact with a gas, water or solid surface. Certain approximations, which may be useful when there is a reflected shock wave, are discussed.

§ 1. Introduction

As far as the author is aware the only published information on the reflection and transmission of shock waves at boundaries is contained in papers by Paterson (1948), Taub (1947) and in studies made at the Institute of Aerophysics in the University of Toronto (Bitondo *et al.* 1950, Bitondo 1950, and Ford and Glass 1954). These are all concerned with shock waves advancing through ideal gas and meeting another ideal gas. It is shown below that for a shock wave advancing through any physically real barotropic medium, the nature of the reflected wave is uniquely determined by the relative shock impedances of the medium through which the incident wave passes and the medium upon which it falls. A simple criterion is found for determining the nature of the reflection of a detonation wave at the end of a block of explosive. Particular attention is paid to the cases where the explosive is in contact with a gas, water or a solid surface. The paper ends with a discussion of approximations which may be useful when there is a reflected shock wave.

§ 2. Equations of Motion for the Incident Wave

If the incident shock wave and the boundary upon which it falls were plane and parallel and were contained in an infinite rigid unbreakable tube, and if viscosity, heat-conduction and all boundary effects were absent, the motion in each phase would be one-dimensional. The assumption of one-dimensional flow will be made in the following paragraphs,

† Communicated by the Author.

for, although one-dimensional flow cannot be exactly realized in practice (and in fact, there is a steep decay of pressure behind a detonation wave) the conclusions drawn for the interfaces will be valid at least for the initial instant in which the reflection occurs, over an area of the surface of contact which will depend upon the area over which the boundary may be assumed to be plane. Thus the equations will indicate the nature of the phenomena which occur and also the initial magnitudes of the physical quantities. Suppose that the velocity of the incident waves is V_1. Suppose that this wave is moving through a medium in which the equilibrium pressure and density are respectively p_0 and ρ_0. Suppose that these values rise instantaneously to p_1 and ρ_1 on the passage of the incident wave. Let u_1 and c_1 be the particle velocity and local speed of sound behind the incident wave. The conservation of mass requires that

$$\rho_0 V_1 = \rho_1 (V_1 - u_1) \quad . \quad . \quad . \quad . \quad . \quad . \quad . \quad . \quad (1)$$

and the conservation of momentum is expressed by the equation

$$p_1 - p_0 = \rho_0 V_1 u_1 = \rho_0 \rho_1 u_1^2 / (\rho_1 - \rho_0). \quad . \quad . \quad . \quad . \quad (2)$$

If the incident wave is a detonation wave, the Chapman–Jouget condition requires that

$$V_1 = u_1 + c_1, \quad . \quad . \quad . \quad . \quad . \quad . \quad . \quad . \quad . \quad (3)$$

and if it may be supposed that there is an effective ratio of specific heats γ for the products of detonation in the neighbourhood of the detonation wave, then

$$c_1^2 = \gamma p_1 / \rho_1. \quad . \quad . \quad . \quad . \quad . \quad . \quad . \quad . \quad . \quad (4)$$

In the detonation phenomena p_0 may be neglected in comparison with p_1. It then follows easily from eqns. (1)–(4) that

$$\left.\begin{aligned} \rho_1 &= \frac{\gamma + 1}{\gamma} \rho_0, \\ u_1^2 &= \frac{p_1}{(\gamma + 1)\rho_0} = \frac{p_1}{\gamma \rho_1}. \end{aligned}\right\} \quad . \quad . \quad . \quad . \quad . \quad . \quad (5)$$

§ 3. Equations of Motion after Reflection of the Wave

That a shock wave is transmitted to the medium ahead of the incident wave is physically obvious and will not be discussed theoretically. The nature of the reflected wave has to be determined.

Suppose that the shock wave transmitted to the medium upon which the incident wave falls has velocity V_2. Let ρ_2 be the density behind it and ρ_0 the (equilibrium) density ahead of it. Let u_2 be the velocity imparted to the medium by this shock wave and p_2 the pressure of the wave. Conservation of mass requires that

$$\rho_0 V_2 = \rho_2 (V_2 - u_2) \quad . \quad . \quad . \quad . \quad . \quad . \quad . \quad (6)$$

and conservation of momentum that

$$p_2 - p_0 = \rho_0 V_2 u_2. \quad . \quad . \quad . \quad . \quad . \quad . \quad . \quad . \quad (7)$$

If p_0 may be neglected in comparison with p_2, (6) and (7) give

$$p_2 = r_0 r_2 u_2^2/(r_2 - r_0). \quad \ldots\ldots\ldots \quad (8)$$

In the infinitesimal layer of the first medium immediately in contact with the second the pressure and velocity must be p_2 and u_2 respectively, equal to the pressure and velocity set up in the second medium by the transmitted wave. Let ρ_2 be the density in this layer. The boundary is an example of a contact discontinuity.

First suppose that the reflected wave is a shock wave moving with velocity W_2 in the direction opposite to that of the transmitted shock wave. The motion (supposed steady) in the first medium immediately behind this shock wave is then governed by the equations

$$\rho_2(u_2 + W_2) = \rho_1(u_1 + W_2) \quad \ldots\ldots\ldots \quad (9)$$

and

$$p_2 - p_1 = \frac{\rho_1 \rho_2}{\rho_2 - \rho_1}(u_1 - u_2)^2 = \rho_2(u_2 + W_2)(u_1 - u_2) \quad \ldots \quad (10)$$

representing the laws of conservation of mass and momentum, and the equation of conservation of energy, which in the *particular case* of a gas with effective ratio of specific heats γ takes the form

$$\rho_2/\rho_1 = \frac{(\gamma-1)+(\gamma+1)z_2}{(\gamma+1)+(\gamma-1)z_2}, \quad \ldots\ldots\ldots \quad (11)$$

where $z_2 = p_2/p_1$. Write $u_2 + W_2 = X_2$; then X_2 is the speed of the reflected shock wave relative to the medium downstream of it and is necessarily positive. It is easy to show from (2), (7), (9) and (10) that

$$(p_2 - p_1)/(p_1 - p_0) = \rho_2 X_2(r_0 V_2 - \rho_0 V_1)/\rho_0 V_1(r_0 V_2 + \rho_2 X_2).$$

Hence a reflected shock wave, requiring $p_2 > p_1$, requires also that $r_0 V_2 > \rho_0 V_1$. This result is not dependent upon the form of the energy equation nor has p_0 been neglected in deriving it: it is therefore true for any media and for any type of incident shock wave.

Next consider the case when a rarefaction wave is reflected at the contact discontinuity. The only difference in the equations occurs from the change of conditions to be satisfied behind this wave. There is no longer a discontinuity in the pressure in the first medium after the instant of impact of the incident shock wave upon the second medium, but only a discontinuity in the derivative of the pressure at the head of the wave as it moves upstream. The eqns. (9) and (10) therefore cease to apply. The condition for a receding rarefaction wave in any barotropic medium, i.e. one in which the pressure depends only upon density, is (see, for example, Courant and Friedrichs 1948),

$$u_2 = u_1 + \int_{\rho_2}^{\rho_1} c \frac{d\rho}{\rho}, \quad \ldots\ldots\ldots \quad (12)$$

where $c^2=dp/d\rho$. On substitution for u_2 from preceding equations it follows that

$$(r_0V_2-\rho_0V_1)u_1=p_2-p_1-r_0V_2\int_{\rho_2}^{\rho_1}c\frac{d\rho}{\rho},$$

showing that if p is a monotonic increasing function of ρ (as it is for any physically real barotropic medium) a reflected rarefaction wave ($p_2<p_1$) is only possible if $r_0V_2<\rho_0V_1$.

The only condition on the media required by the above proof is that the incident shock wave should be passing through a barotropic medium. The nature of the reflection is thus determined completely by the relative values of the *shock impedance* of the two media, the shock impedance of a medium being defined as the product of the equilibrium density of the medium and the speed of the shock wave moving downstream through it.†

Expressed in this way, the criterion for a reflected shock or rarefaction wave is very simple, but it requires knowledge of the speed of the transmitted shock wave, which will not be known until the whole reflection and transmission phenomenon has already been determined. In the following paragraphs a closer examination of the equations is made for an incident detonation wave and there is a discussion of the wave reflected after impact upon an ideal gas, water or a solid surface.

§ 4. Application to the Reflection of a Detonation Wave

When the wave reflected into the detonation products, treated as ideal gas with an effective ratio of specific heats γ, is a shock wave,

$$2p_1(z_2-1)^2=\rho_1(u_1-u_2)^2\{(\gamma-1)+(\gamma+1)z_2\}$$

from (10) and (11). By means of (8) and (5) this may be written in the form

$$f(Z)\equiv 2\gamma(Z^2-1)^2-\{(\gamma-1)+(\gamma+1)Z^2\}\{1-ZQ(Z)\}^2=0 \quad . \quad (13)$$

where $Z^2=z_2$, $ZQ(Z)=u_2/u_1$ and $Q(Z)=+\{(\gamma+1)(\rho_0/r_0)(1-r_0/r_2)\}^{1/2}$. [$Q$ depends only upon Z for given media and given values of p_1, p_0.] Equation (13) is therefore the equation determining the pressure behind the reflected shock wave when the incident wave is a detonation wave.

When u_2, u_1 and c in (12) are expressed in terms of p_2, p_1 and densities, the equation for the pressure behind a reflected rarefaction wave is obtained. By means of (5) and the assumption as before of the adiabatic relationship in the product gases of the detonation, Z is in this case the solution of the equation

$$g(Z)\equiv ZQ(Z)-1+\{2\gamma/(\gamma-1)\}(Z^{(\gamma-1)/\gamma}-1)=0 \quad . \quad . \quad . \quad (14)$$

where $Q(Z)$ is defined as above.

The type of reflection may be determined in general by seeking a root of $f(Z)=0$ with $Z>1$ for a reflected shock wave or a root of $g(Z)=0$ with $Z<1$ for a reflected rarefaction wave.

† If the boundary is in motion before the shock wave strikes it, the shock impedance is defined as the product of the density of the medium into which the shock wave is moving and the speed of the shock wave relative to this medium.

Now $g'(Z)=d(ZQ)/dZ+2Z^{-1/\gamma}$ which is positive for all positive values of Z since, as is easily seen, $dQ/dZ>0$ for given media with fixed p_1, ρ_0; but $g(0)<0$ and $g(1)=Q(1)-1$. Hence there is a solution with a rarefaction wave if, and only if, $Q(1)>1$. In this case, whenever $Z>1$, $ZQ(Z)>1$ and hence $u_2>u_1$. It follows from (4) that no shock wave solution ($p_2>p_1$) is possible and the solution with a reflected rarefaction wave therefore exists and is the unique solution of the problem.

If $Q(1)<1$, then $ZQ(Z)$ increases with Z until it reaches the value unity at $Z=Z_1$, say. There is no shock wave solution when $Z>Z_1$. However, $f(1)<0$ and $f(Z_1)>0$ and when $Q(1)<1$ it is clear that $f(Z)$ is a strictly monotonic increasing function of Z in the range $1\leqslant Z\leqslant Z_1$; thus there is a root, $Z=Z_0$ of $f(Z)=0$ in this range and it is the only physically valid root of (13).

The nature of the reflection is therefore determined uniquely by the value of $Q(1)$. The result may be expressed as follows:

There is a reflected shock wave or rarefaction wave according as

$$(\gamma+1)\frac{\rho_0}{r_0}\left(1-\frac{r_0}{r_1}\right)<\text{or}>1, \qquad \ldots\ldots \quad (15)$$

where r_1 is the density in the second medium corresponding to the passage through it of a shock wave with the pressure of the incident wave.

Examples

(*a*) *Explosive in contact with an ideal gas.*

If the medium ahead of the explosive is an ideal gas with ratio of specific heats Γ, the increase of density across the transmitted shock wave is given by

$$r/r_0=\{(\Gamma-1)+(\Gamma+1)p/p_0\}/\{(\Gamma+1)+(\Gamma-1)p/p_0\}.$$

For a shock wave with pressure $p_1\gg p_0$, $r_1/r_0\doteq(\Gamma+1)/(\Gamma-1)$. Then $Q^2(1)\doteq 2(\rho_0/r_0)(\gamma+1)/(\Gamma+1)$. For combinations of common explosives and gases $Q(1)$ has a value very much greater than unity, showing that a reflected rarefaction wave is the rule.

(*b*) *Explosive in contact with water.*

An equation of state for water given in Cole's book on underwater explosions (Cole 1948) and which has been found by Schall (1950) to be in good agreement with experimental work, is the following:

$$p=B(S)\left[\left\{\frac{r(T,\,p)}{r(T,\,0)}\right\}^n-1\right],$$

where p, S, T and r are respectively pressure, specific entropy, temperature and density, n is an index which may be given the value 7·15 with good accuracy, $B(S)$ is a slowly changing function of the entropy, and the density r is expressed as a function $r(T, p)$ of temperature and pressure ($p=0$ corresponds to atmospheric conditions). For the purpose of computations of pressures and velocities it is often useful to replace the above formula by

$$p=B(r^n-1) \qquad \ldots\ldots\ldots \quad (16)$$

where B is taken as a constant and put equal to 3·047 kilobars. This

form of the equation of state has been used in well known researches by Polachek and Seeger (1949) on shock waves in water-like substances and in a paper by Finkelstein (1947) on the reflection of a shock wave in water.

For a shock wave with a pressure $p_1 > 150\,000$ atmospheres, $r_1 > 1{\cdot}729$ g/cm^3. Then $Q^2(1) \doteq 0{\cdot}41\rho_0(\gamma+1) > 1$ (in general) and it follows that the reflected wave is a wave of rarefaction.

As a matter of interest eqn. (14) may be solved for the case examined experimentally by Schall, in which an explosive (PETN) was detonated in contact with water. The pressure p_1 was found experimentally to be 25×10^{10} dynes/cm^2 and ρ_0 was 1·6 g/cm^3. If $\gamma = 3$ is taken for the explosive gases, for want of a better value, then a numerical solution of (14) gives a value of Z corresponding to $p_2 = 16{\cdot}9 \times 10^{10}$ dynes/cm^2. The value obtained by Schall from his experiments was $p_2 = 19{\cdot}2 \times 10^{10}$ dynes/cm^2. The error is approximately 12%, which is not surprisingly high in view of the assumptions about the value of γ and the equation of state of water at these high pressures. In fact, the values of r derived from Cole's equation of state are really too high, hence Q^2 is also too high and consequently Z and p_2 are underestimated.

(c) *Explosive in contact with a solid.*

For the pressures set up by the detonation of an explosive it is not possible to treat a solid target as elastic. An equation of state for steel and lead suggested some years ago by Pack *et al.* (1948) has proved successful for comparison of theory with experiment in several instances, and is expressed in such a form that it may be used for any solid for which compressibility data are available for moderately high pressures. For metals in general $r_0 c_0 > \rho_1 V_1$, so that if the shock wave transmitted to a metal were to move into it with a supersonic velocity $V_2 (> c_0)$, it would follow at once from the general result on shock impedance that a shock wave would be reflected. However, it was shown in the paper by Pack *et al.*, quoted above, that the shock wave velocity in a metal may well be less than the velocity of sound. (This was found to be true theoretically and in experiments for a steel target.) Thus a general statement cannot be made without further investigation, and until more is known about the equations of state of solids (including metals). It seems likely, however, that a reflected shock wave will be the rule for most if not all combinations of explosive and metal, since $(\gamma+1)\rho_0 < r_0$ if the metal is not a light one, and even for a light metal such as aluminium the factor $(1 - r_0/r_1)$ is strongly damping on the left-hand side of the inequality in (15).

§ 5. Ablard's Approximation

The practical importance of calculations on the pressure set up by reflection of a shock wave lies in attempts which have been made to relate the velocity of the rear surface of a target block, which can be measured without too great difficulty, to the pressure applied to its front. A theoretical analysis illustrating the connection for a simple wave system

is given in Part II. In the interpretation of experiments in which a detonation wave is reflected from a metal block, Ablard's approximation is sometimes used, namely $\rho_2 X_2 = \rho_0 V_1$. Since, for a detonation wave, $\rho_0 V_1 = \rho_1 c_1$ from (1) and (3), this implies that $\rho_2 X_2 = \rho_1 c_1$. An examination of the equations of motion given above for a reflected shock wave (*not* necessarily a detonation wave) shows that

$$\rho_2 X_2 = \rho_1 c_1 \left[\left\{ (\gamma-1)+(\gamma+1)z_2 \right\} / 2\gamma \right]^{1/2}.$$

For $z_2 = 1+\epsilon$ $(\epsilon \ll 1)$, $\rho_2 X_2 \doteqdot \rho_1 c_1 \left\{ 1 + \frac{\gamma+1}{4\gamma}\epsilon - \frac{(\gamma+1)^2}{32\gamma^2}\epsilon^2 \right\}$.

When $\epsilon = 0{\cdot}315$ and $\gamma = 3$, $\rho_2 X_2$ differs from $\rho_1 c_1$ by 10%. To judge the error in another instance it may be noted that for the experiments on steel and lead reported by Pack *et al.* the calculated values of z_2 were 1·67 and 1·59 respectively; in these instances Ablard's approximation is 20% in error.

Ablard's approximation may be compared with the physically more understandable approximation that the reflected shock wave moves back with the local speed of sound relative to the gas in contact with the solid. It may be shown that

$$X_2 = c_2 \left[\left\{ (\gamma+1)+(\gamma-1)z_2 \right\} / 2\gamma z_2 \right]^{1/2},$$

which, when $z_2 = 1+\epsilon$ $(\epsilon \ll 1)$, gives

$$X_2 \doteqdot c_2 \left\{ 1 - \frac{\gamma+1}{4\gamma}\epsilon + \frac{(\gamma+1)(7\gamma-1)}{32\gamma^2}\epsilon^2 \right\}.$$

Thus $X_2 = c_2$ has the same percentage error as Ablard's approximation to the first order in ϵ, and is slightly better to the second order in ϵ. Some use of this approximation will be made in Part II of this work where, in discussion of the wave motion arising from the impact of a shock wave on an elastic target, the value of ϵ is small.

References

Bitondo, D., 1950, *Inst. of Aerophys., Univ. of Toronto*, UTIA Report No. 7.

Bitondo, D., Glass, I. I., and Patterson, G. N., 1950, *Inst. of Aerophys., Univ. of Toronto*, UTIA Report No. 5.

Cole, R. H., 1948, *Underwater Explosions* (Princeton: University Press).

Courant, R., and Friedrichs, K. O., 1948, *Supersonic Flow and Shock Waves* (New York: Interscience Publishers).

Finkelstein, R., 1947, *Phys. Rev.*, **71**, 42.

Ford, C. A., and Glass, I. I., 1954, *Inst. of Aerophys., Univ. of Toronto*, UTIA Report No. 29.

Pack, D. C., Evans, W. M., and James, H. J., 1948, *Proc. Phys. Soc.*, **60**, 1.

Paterson, S., 1948, *Proc. Phys. Soc.*, **61**, 119.

Polachek, H., and Seeger, R., 1949, *Proceedings First Symposium in Applied Mathematics* (New York: American Mathematical Society).

Schall, R., 1950, *Z. angew. Phys.* (6), **2**, 252.

Taub, A. H., 1947, *Phys. Rev.*, **72**, 51.

The Reflection and Transmission of Shock Waves II: The Effect of Shock Waves on an Elastic Target of Finite Thickness †

By D. C. Pack
Department of Mathematics, The Royal College of Science and Technology, Glasgow

[Received August 20, 1956]

Summary

An examination is made of the variation with time of the pressure and velocity in an elastic target of finite thickness subject to the impact of a shock wave. The cycle of reflections and transmissions at the boundaries of the target is described in detail.

§ 1. Introduction

A problem of some practical importance concerns the motion of an elastic target of finite thickness subject to the impact of a shock wave. The system of reflected and transmitted waves which is created by such an impact is examined in detail below for a one-dimensional system, and formulae are found for the variation with time of the pressure and velocity in the target. It is assumed that the shock impedance of the target is greater than that of the 'outer medium' through which the shock wave approaches the target, so that a shock wave is reflected as well as transmitted (see Part I, Pack 1956). The outer medium is supposed to be barotropic, i.e. in continuous flow it has an equation of state of the form $p=p(\rho)$, where p and ρ are respectively the pressure and density. The wave system in a target which is finite in all its dimensions is too complicated for analysis at present; calculations based upon a one-dimensional model are, however, very useful, since they represent the actual conditions for a limited interval of time depending upon the ratio of width to depth of the target, the area over which the incident shock wave may be considered to be plane and the distance behind this shock wave over which the conditions are uniform.

The shock wave will be supposed to be of such a magnitude that the pressure transmitted to the target block remains below the elastic limit of the block. When the medium ahead of the block is water, this restricts the magnitude of the impinging shock wave to about one-half of the elastic limit of the block, since the pressure is approximately doubled by impact (see, for example, Cole 1948). The magnitude is therefore restricted to about 1500 atmospheres for a shock wave passing through water and

† Communicated by the Author.

falling upon a target made of steel ; the restriction is greater when air is the medium through which the shock wave advances, since the multiplication on impact is more important. A theoretical treatment of the motion when plastic flow is present could be made, but the difficulties would be greatly enhanced, and a first attempt on the problem may well be concerned only with the propagation of elastic stresses in the target.

§ 2. Wave Motion in a Plate

Suppose that at time t the plane section S originally at distance x from the front surface has been displaced through a distance ξ. Its displacement from the original position of the front surface is then $x+\xi$. The displacement of the plane section originally at distance $x+\delta x$ is $x+\xi+\delta x+(\partial\xi/\partial x)\delta x$ to the first order in small quantities δx. Thus, the new width of the section originally of thickness δx is $\delta x(1+\partial\xi/\partial x)$. The engineering strain is therefore $\partial\xi/\partial x$. If the pressure in the target is $p(x, t)$, then the resultant pressure on the section of the target, opposing the motion of the target, is $(\partial p/\partial x)\delta x$. The velocity of S is $u=\partial\xi/\partial t$. Let r_0 be the equilibrium density of the target. Then the equation of motion for the section of thickness δx is

$$r_0 \cdot \frac{\partial^2\xi}{\partial t^2} = -\frac{\partial p}{\partial x}. \qquad \ldots\ldots\ldots \quad (1)$$

The pressure p is related to the strain $e_x=\partial\xi/\partial x$ by Hooke's Law. When the lateral dimensions do not enter the problem (plane strain), there is no strain except in the longitudinal direction, i.e. $e_y=e_z=0$. If ν is Poisson's ratio and $p_y=p_z$ are the principal lateral pressures,

$$Ee_x=-p+2\nu p_y ;$$

$$0=-p_y+\nu(p_y+p),$$

giving $Ee_x=-(1+\nu)\,(1-2\nu)p/(1-\nu)$. Hence

$$\frac{\partial\xi}{\partial x}=\frac{-(1+\nu)\,(1-2\nu)}{1-\nu}\,\frac{p}{E}=\frac{-(1+\nu)p}{3(1-\nu)K}$$

where K is the modulus of compression (bulk modulus), and eqn. (1) becomes

$$r_0\frac{\partial^2\xi}{\partial t^2}=\frac{3K(1-\nu)}{1+\nu}\frac{\partial^2\xi}{\partial x^2}. \qquad \ldots\ldots\ldots \quad (2)$$

Write $3K\,(1-\nu)/r_0\,(1+\nu)=c^2$, where c is the general speed of sound for dilatational waves ; then (2) becomes

$$\frac{\partial^2\xi}{\partial t^2}=c^2\frac{\partial^2\xi}{\partial x^2}. \qquad \ldots\ldots\ldots \quad (3)$$

This is the familiar form of the wave equation in one dimension. Since the independent variables here are x and t, displacements (and hence pressures, etc.) are propagated with the speed of sound *relative to the equilibrium positions of the particles of the target.* It follows that a pressure

pulse crosses a target of *equilibrium* thickness l in time l/c, whatever the motion of the target. The eqn. (3) has characteristics

$$\frac{dx}{dt}=\pm c, \quad \text{i.e. } x\mp ct=\text{constant},$$

and on these characteristics certain conditions of compatibility are required to be satisfied (see Courant and Friedrichs 1948). Thus

$$\left.\begin{aligned}&\text{on } x-ct=\text{constant}, \ r_0cu+p=\text{constant},\\ &\text{and on } x+ct=\text{constant}, \ r_0cu-p=\text{constant}.\end{aligned}\right\} \quad . \ . \ (4)$$

The density r in the section S is given by the equation of continuity

$$r_0\delta x=r\delta x\left(1+\frac{\partial\xi}{\partial x}\right).$$

Hence

$$-\frac{\Delta r}{r}=\frac{\partial\xi}{\partial x}, \quad . \ . \ . \ . \ . \ . \ . \ . \ . \ (5)$$

where

$$\Delta r=r-r_0.$$

§ 3. The Passage of the Shock Wave through the Target

The front surface of the block in what follows is the surface which, in the equilibrium position, is facing the shock wave. The time t is measured from the instant when the shock wave reaches the front face. Let there be an excess pressure p_1 in the shock wave. When the shock wave strikes the block it is reflected with pressure p_2 (say), and a shock wave of pressure p_2 is transmitted to the block. The value of the pressure p_2 in terms of p_1 is determined by the requirement that the particle velocity u_2 set up in the block must be equal to the particle velocity in the ' outer medium ' adjacent to the front face. The formulae governing the reflection phenomena have been given in Part I (Pack 1957). The velocity u_2 set up in the target by the pressure p_2 is equal to p_2/r_0c, as is immediately seen from a characteristics diagram in the (x, t) plane by following a characteristic of the family $x+ct=$constant which comes from any part of the target which remains in equilibrium ; on such characteristics the value of the constant in the condition of compatibility is zero, since $u=0$ and the pressure p in the target is neglected in the equilibrium state of the target.

In order to show the motion as it appears to a stationary observer, the coordinates used in the figure are $x+\xi$, for the displacement of the target relative to axes fixed in space, y for distance in the outer medium measured (positive in the same direction as x positive) from the original position of the boundary of the target.

The x-coordinates of the target are traversed with velocity c by the shock wave front. The $x+\xi$-coordinates are therefore crossed with velocity $c+u_2$; the transmitted shock wave is represented by the line OA in the figure. The reflected shock wave is represented by OL.

The characteristics in the outer medium have the equations $dy/dt=u\pm a$, a being the local speed of sound (see Courant and Friedrichs 1948).

On each side of OL the values of u and a are constant, although the values are different on the two sides. Thus the characteristics are straight lines in the outer medium with gradients equal to the local values of $u \pm a$.

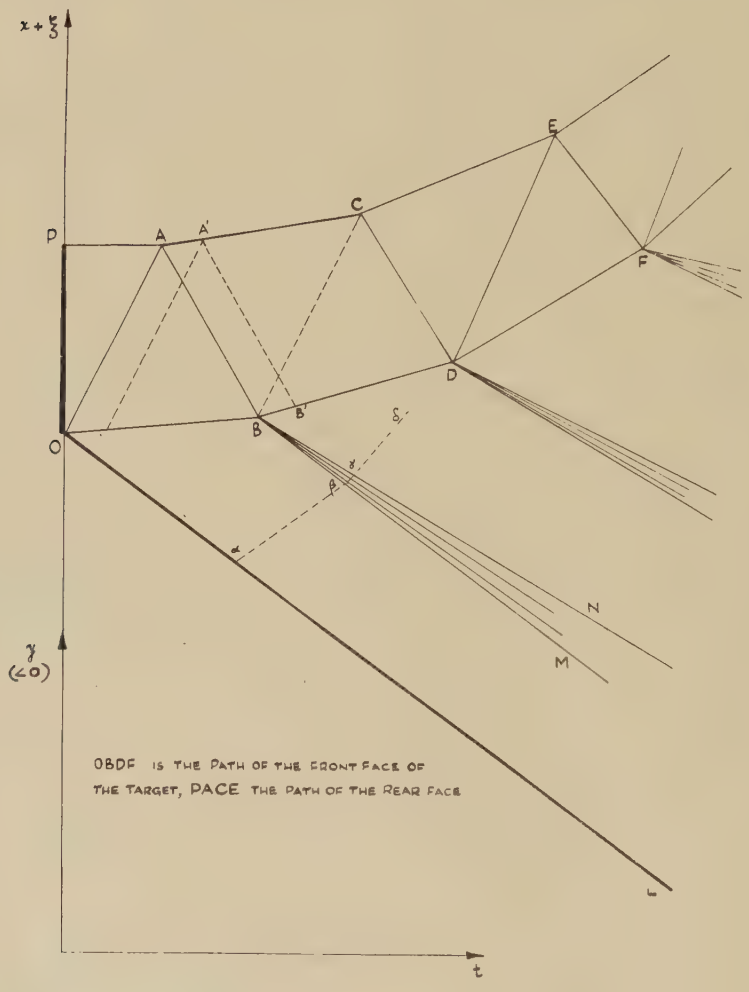

For pressures such as are considered in this paper, $u \ll a$. Also, when the multiplication of pressure on reflection is not too great, the value of a_2 is not very different from the speed W_2 of the receding shock wave; this follows from the approximation $Z_2 = u_2 + W_2 = a_2$ discussed in Part I. Thus one family of characteristics between OL and OB (the front face of the target) is nearly parallel to OL. However, a_2 is actually greater than $W_2 + u_2$, representing the physical fact that any disturbance

behind a shock wave is propagated faster than the shock wave and therefore eventually overtakes it.

The wave in the target, represented by OA, reaches the rear surface and is reflected. The pressure in the medium $x>l$ will be neglected in comparison with the pressure in the target. Thus the boundary condition on $x=l$ is $p=0$.

On a characteristic $x-ct=$constant in the region OAB,

$$r_0cu+p=r_0cu_2+p_2.$$

In the region ABC $p=0$; hence, in this region

$$u=u_3=u_2+\frac{p_2}{r_0c}=2u_2.$$

The arrival of the reflected wave AB at the front face of the block is the signal to the outer medium indicating the finiteness of the target. The rarefaction ($p=0$) which has passed through the target at the time t_B leads to a reflected shock wave in the target and a transmitted rarefaction wave in the outer medium. In view of the steady flow behind the receding shock wave OL this rarefaction wave is a simple wave (see Courant and Friedrichs 1948), represented in the characteristics diagram by a fan MBN. A characteristic such as $\alpha\ \beta\gamma\ \delta$ penetrating this fan becomes straight again after crossing BN (the last wavelet of the expansion at B). The pressure in the reflected wave BC and the transmitted wave BN is p_4 ($<p_2$), and the value of p_4, together with the velocity of the particles following these waves, may be obtained from the characteristic relationships (see Courant and Friedrichs 1948), thus :

$$\text{on } \alpha\beta\gamma\delta, \quad u+\int_{\rho^2}^{\rho} a\frac{d\rho}{\rho}=u_2, \qquad \ldots\ldots \quad (6\,a)$$

ρ_2 being the density in the outer medium corresponding to the velocity u_2 and pressure p_2 ;

$$\text{on } A'B',\ r_0cu-p=\text{constant}=2r_0cu_2 \quad \ldots\ldots \quad (6\,b)$$

The pressure p_4 and the velocity u_4 are obtained by solving (6 *a*) and (6 *b*) simultaneously.

From (6 *b*), $u_4=2u_2+p_4/r_0c$. Only a small change in the velocity is possible in the solid target ; but small changes in velocity in a slowly moving gas are associated only with relatively small changes of pressure. We can therefore calculate p_4 approximately by writing $p_4=p_2\ (1-\epsilon)$ and neglecting higher powers of ϵ than the first.

If the outer medium is a gas with $p=(k\rho)^\gamma$, k being a constant (since the entropy is constant behind a uniform shock wave), then

$$\frac{p_4}{r_0c}+2u_2+\frac{2a_4}{\gamma-1}=u_2+\frac{2a_2}{\gamma-1},$$

which leads to the result

$$\epsilon=\frac{2\gamma p_2/r_0ca_2}{1+\gamma p_2/r_0ca_2}.$$

For a steel target, $c=6\times10^5$ cm/sec and $r_0=7{\cdot}8$ g/cm^3. If $p_2=1$ kilobar, $a_2=3\times10^4$ cm/sec and $\gamma=1{\cdot}4$, then

$$\frac{2\gamma p_2}{r_0 c a_2}\doteqdot 0{\cdot}02.$$

Hence we may well expand ϵ in powers of p_2/r_0ca_2 and we have

$$p_4=p_2\left(1-\frac{2\gamma p_2}{r_0ca_2}\right). \quad . \quad . \quad . \quad . \quad . \quad . \quad . \quad . \quad (7)$$

The change in p is therefore of the order of 2% at this reflection. If the outer medium is water with the approximate equation of state $p=B(\rho^\gamma-1)$, in which $B=3{\cdot}047$ kilobars and $\gamma=7{\cdot}15$, then the formula equivalent to (7) is

$$p_4=p_2\left\{1-\frac{2\gamma(p_2+B)}{r_0ca_2}\right\}.$$

For a steel target, if $p_2=1$ kilobar as before, $a_2=1{\cdot}7\times10^5$ cm/sec, and

$$\frac{2\gamma(p_2+B)}{r_0ca_2}\doteqdot 0{\cdot}074.$$

The change in pressure is therefore of the order of 7%.

§ 4. The Cycle of Events

The phenomena described in § 3 repeat themselves over and over again; the proportionate fall of pressure at the front surface varies slightly at each step until such time as the first rarefaction (at B) has reached the shock wave OL and its reflection returned to the front surface to end the succession of steady states which have prevailed at this surface between each simple wave. It was shown in Part I that $u_2+W_2\doteqdot a_2$ if $z_2=p_2/p_1$ is not too much greater than unity; thus the rarefaction wave from B (which is the first to return) is almost parallel to OL and since the gradient of the characteristics in the target is in general so much steeper than the gradients in the outer medium, there will be many reflections of the type discussed above before the analysis is no longer valid. A calculation indicates that for shock waves in water, of strength up to 1500 atmospheres, there are at least 13 rarefaction waves (i.e. the target is crossed by waves in both directions at least 13 times) before the *shock wave* is affected by the rarefaction. The cycle of motion of the *target* will continue unchanged until this wave returns to the target. The velocity of the rear face of the target increases at intervals of $2l/c$ by an amount equal to p/r_0c, where p is the latest pressure to arrive at the rear surface and to be removed by this free boundary. The velocity *after n* reflections is therefore

$$u=(p_2+p_3+p_4+\ \ldots\ +p_{n+1})/r_0c.$$

When the outer medium is water the ratio of p_{n+1}/p_n tends to a constant limit, since $\epsilon\to 2\gamma B/r_0ca_0$ ($\sim0{\cdot}6$ for a steel target) where a_0 is the speed of sound corresponding to atmospheric pressure ($p=0$). The target has a

limiting speed and the ' acceleration ' of the target (as measured by the non-uniform jump in speed per double-traverse of the target by the wave system) is diminishing and tending to zero in the limit. When the outer medium is air the same phenomena will occur, but in this case $\epsilon \to 0$ as $p_2 \to 0$.

References

Cole, R. H., 1948, *Underwater Explosions* (Princeton : University Press).
Courant, R., and Friedrichs, K. O., 1948, *Supersonic Flow and Shock Waves* (New York : Interscience Publishers).
Pack, D. C., 1957, *Phil. Mag.*, **2**, 182.

A Comparison of Electron and Positron Single Scattering in Argon†

By C. Bowness and N. Cusack
Birkbeck College, London

[Received August 20, 1956]

Summary

A combination of lens spectrometer and diffusion cloud chamber was used to study the difference in the scattering of 0·3 Mev positrons and electrons by argon. 611 electron and 506 positron scatters were observed with projected angles $\phi > 30°$. The ratio of the number of electron scatters per unit track length to that of positrons was 1·21 with a standard error of 6% ; the theoretical value is 1·18. The measured absolute value of the cross section agreed with the theoretical value within the experimental error of about 10%.

§ 1. Introduction

Several physical causes make the cross section for the scattering of fast electrons and positrons by atoms differ from the simple Rutherford formula. The various causes show themselves most clearly at different values of the relevant variables. Current interest attaches mainly to the finite nucleus effect which is best investigated at very high energies (Hahn *et al.* 1956), and to the radiative effect which should be detectable at energies of a few Mev (Elton and Robertson 1952). The effect of spin can be detected at energies of the order 1 Mev and should be fully accounted for by the well known theory of Mott (1931), provided the scattering angles are sufficiently large to avoid the screening effect of the orbital electrons. Recent experiments leave little doubt of the correctness of the Mott cross section for electron scattering, both in its variation with angle and energy, and in its absolute value (see, for example, Pettus *et al.* 1956, Chapman *et al.* 1955).

The spin–orbit interaction is responsible for the difference in scattering between electrons and positrons (Massey 1942). Consequently, measurement of the ratio of electron to positron scattering is an alternative way of checking the Mott theory. A few such measurements have been attempted, of which the most successful is that of Ellis and Henderson (1955). Their work was done at energies of 0·7 and 1·4 Mev, using gold and aluminium foils. For the three angles 22·8°, 34·5° and 47·5°, it was shown that, within an error of 5%, the ratio of electron to positron scattering was correctly given by theory. References to earlier work are given by Ellis and Henderson. Since their paper, Bosley and Hughes

† Communicated by the Authors.

(1955) have published results consistent with theory for the scattering of 10 MeV particles in nuclear emulsion.

The present work gives additional evidence for the electron positron scattering difference by another technique and at different values of the relevant variables.

§ 2. The Experiment

2.1. *Preliminary Considerations*

For values of Z such that $Z/137 \ll 1$, the series expressions given by Mott's theory can be reduced to a much simpler equation for the cross section. In the form given by McKinley and Feshbach (1948), this formula is

$$I(\theta)=\left(\frac{Ze^2}{2m_0c^2}\right)^2 \frac{1-\beta^2}{\beta^4} \operatorname{cosec}^4\tfrac{1}{2}\theta[1-\beta^2 \sin^2\tfrac{1}{2}\theta \pm \pi\alpha\beta \sin \tfrac{1}{2}\theta(1-\sin \tfrac{1}{2}\theta)]. \quad (1)$$

The third term in the bracket is taken positive for electrons and negative for positrons and is responsible for the difference in scattering. This equation should be correct to at least 1% for argon, $Z=18$.

It is simpler and more accurate in cloud chamber work to measure, not θ, but the orthogonal projection of θ on to a plane containing the incident particle direction. Let ϕ be the projection of θ, and $P(\phi)d\phi$ be the number of scatters through ϕ per unit path length; then $\int_{\phi_1}^{\phi_2} P(\phi)d\phi$ can be computed very easily from eqn. (1) and the tables of O'Ceallaigh (1950), if the values of NZ^2 and β are known from the observations.

Consider equal lengths of positron and electron track, and scattering angles greater than some lower limit ϕ_1. Let the total number of electron scatters exceed that of positrons by δN; and let N be the total number of positron and electron scatters added together. If it is required to detect δN, it is desirable that the ratio of δN to the statistical uncertainty in N should be as large as possible, i.e. $\delta N/\sqrt{N}$ should be large. For a given Z and track length, this ratio increases as β decreases. It is therefore better to work with low velocity particles but not, of course, so low that other factors such as screening, energy loss, and multiple scattering become intolerable. Fortunately, a suitable compromise velocity can be chosen within the spectrum of ^{64}Cu which was desirable as a source for other reasons as described below.

Recent papers on screening (Gunmersen 1952, Mohr and Tassie 1954) suggest that screening can safely be ignored for the values of $\phi > 30°$ used in the present experiment. The smallness of the screening effect is also indicated by the fact that the accurate measurement of electron scattering by Pettus *et al.* (1956) agreed with unscreened theory down to 60° at 0·2 MeV in gold. In this connection it should be remembered that the ϕ's in the range 30° to 40° will be due to θ's anywhere in the range 30° up to 90°. Incidentally, since the positron–electron difference

increases with θ up to about 80° at the energy of this experiment, it will be somewhat accentuated by the use of ϕ instead of θ.

2.2. *Apparatus and Procedure*

The scattering occurred in the argon filling of a diffusion cloud chamber. Stereoscopic photography was carried out by conventional methods and projected angles were measured on full size reprojected images. The errors to which such experiments are subject have often been described and need not be detailed here ; a recent account has been given by Allen *et al.* (1956). To reduce some of the errors the following methods were adopted. No attempt was made to determine the incident energy by track curvature measurement ; instead, the particles were injected into the cloud chamber from a solenoidal lens spectrometer through a connecting tube containing. collimating slits. The spectrometer was calibrated by reference to the *F*-line of the thorium internal conversion spectrum and provided a beam of accurately known energy with a resolution of 4% in $H\rho$. Instead of a Wilson cloud chamber, a diffusion chamber capable of giving one photograph every 10 seconds was used. This enabled much more economical use to be made of the short lived radioactive source.

For the source, ^{64}Cu, of half-life 12·8 hours, was chosen because considerable importance was attached to scattering the electrons and positrons under identical conditions and this was materially assisted by a source which emitted both particles with comparable energies and intensities. The method of obtaining an output of either positrons or electrons from the lens has been described previously (Cusack and Stott 1955). In the present work, batches of 90 pictures of positron tracks were taken alternately with 90 of electron tracks ; in between batches, 10 control pictures were taken with the lens current switched off. The source was covered with a ray-tight shutter except for the 150 milliseconds before each photograph. By this procedure it was ensured that the electron and positron scattering occurred under identical circumstances. It is not impossible that conditions in a diffusion chamber should change slightly during 24 hours continuous work, but such changes would occur over much longer periods than the 15 minutes required for one batch of pictures and would therefore affect both types of particle equally. $H\rho$ was chosen at the value for which the beam intensity was the same for positrons and electrons so that equal numbers of pictures would give equal track lengths. In ^{64}Cu the peaks of the positron and electron spectra are at $H\rho = 2000$ and 1400 gauss cm respectively, but there are two electrons to one positron approximately and equal intensities were obtained from the spectrometer at $H\rho = 2250$ gauss cm.

At the cloud chamber end of the collimating tube the lens vacuum was separated from the atmosphere by a 0·75 mg/cm^2 terylene foil window supported on a brass grid of 80% transmission. The window in the cloud chamber wall was made of a similar foil and the two windows were separated by about 2 mm of air. The multiple scattering and energy loss

of the particles in the windows were small but would in any case be independent of the sign of charge to a high degree of approximation.

The considerations of the preceding two paragraphs make it practically certain that no systematic difference between electron and positron results could be introduced before scattering occurred. As a further precaution, the scanning and measurement of the photographs was done by observers who did not know which were positron and which electron pictures. The ratio of positron to electron scatters was therefore subject to statistical errors only. Among the errors which tend to cancel out when the ratio of positron to electron scattering is considered are : errors in NZ^2 due to uncertainty in the exact value of the supersaturation in the sensitive layer ; errors due to scanning inefficiency even if the latter is a function of ϕ as, indeed, it probably is ; errors arising from the fact that all the incident particles do not move exactly right-angles to the camera axis as they should if O'Ceallaigh's orthogonal projection tables are used.

A more detailed discussion of the apparatus and of the suitability of a glass walled atmospheric pressure diffusion chamber to this type of work can be found elsewhere (Bowness 1956).

2.3. *The Observations*

1533 positron and 1563 electron pictures were taken in a single run. The current through the lens coil and the pressure and temperature in the diffusion chamber were kept constant and measured. From these observations the following quantities were obtained.

(i) The total track length. To find this, certain selection criteria were applied to the tracks. The diffusion chamber is continuously sensitive to background from cosmic radiation and annihilation rays emanating from the source. Most of the latter had been removed by a suitable distribution of lead in and around the spectrometer. Of the remaining background, a considerable fraction consisted of dense highly contorted electron tracks which could easily be distinguished and ignored. All other tracks were counted if they were more than 1 cm long and if their initial direction made an angle of less than 45° with the incident beam direction. These two criteria were applied with the help of a rigid Perspex arm which could both slide and rotate in the plane of reprojection about a point corresponding to the focus of the spectrometer. To indicate the critical length and direction, the end of the arm carried fiducial marks which could be superimposed on any track in any part of the image. The criteria were arrived at after trials based on the examination of the 10% of the pictures which were taken with the lens focusing current switched off. These pictures usually contained one or two pieces of track and after applying the above criteria to them it was found that background accounted for 4% of the accepted track length. Finally, tracks showing electron–electron collisions were accepted only as far as the fork.

It was not necessary to measure the length of every single track. All tracks were measured on a sample of the pictures which was chosen

sufficiently large to make the statistical error in the total track length small compared with that in the observed number of scatters. This condition required that all accepted tracks on 30% of the pictures should be measured. The results are given in table 1.

(ii) The particle velocity. The lens current was measured with a potentiometer and it was found from the calibration that $H\rho = 2246$ gauss cm for the focused particles. Small corrections for the average energy loss in the windows and the cloud chamber gas were calculated from Landau's formula. The value of β for insertion into eqn. (1) was 0·783 which corresponds to $H\rho = 2154$ gauss cm or energy 0·311 MeV.

(iii) NZ^2. The chamber was at atmospheric pressure throughout and the condensant was methyl alcohol. The temperature of the sensitive layer was known from auxiliary measurements with thermocouples. It is not easy to find directly the vapour pressure but it can be estimated from the degree of supersaturation known to be required for track formation. However, any slight uncertainty here is not important because the

Table 1. Analysis of Accepted Track Lengths

Particle	Number of frames	Number in sample	Mean length per frame (cm)	Total track length (metres)
Electrons	1563	482	27·66	432·3
Positrons	1533	454	28·15	431·5

condensant only contributes 2·4% of the value of NZ^2, and, as pointed out above, does not enter the comparative measurements. The final value of NZ^2 was $8{\cdot}44 \times 10^{21} \pm 1\%$ per cm^3.

(iv) The scattering angles. Scattering angles $\phi > 30°$ were measured directly on the reprojected images with a protractor. The mean of four readings was taken in each case and the error in measuring any one of them should not exceed 2° and will often be less. The quantity $\delta N/\sqrt{N}$, referred to above increases as ϕ decreases, nevertheless it was decided not to measure angles down to 20° or less because smaller angles are less easy to detect with certainty and might also involve consideration of screening. The result of the angle measurement is given in table 2 together with the expected angular distribution of the same total number of particles. A little calculation shows that, of the observed ϕ's$>30°$, approximately 70% were derived from θ's$>40°$, 46% from θ's$>50°$, and 30% from θ's$>60°$. Examination of the control pictures shows that 4·5% of the scatters might have been due to background.

§ 3. Discussion and Comparison with Theory

Evidence for the excess of electron over positron scattering can be obtained from the ratio of the total numbers of scatters with $\phi > 30°$

for equal track lengths. Denote the ratio of electron to positron scatters by r. Then

$$r(\text{obs.}) = \frac{611}{506} \times \frac{431{\cdot}5}{432{\cdot}3} = 1{\cdot}205.$$

The standard statistical error in each of the track lengths is 1·6% and in the numbers of scatters 4·3%. The standard error in r(obs.) is therefore 6%.

From eqn. (1) and O'Ceallaigh's tables, r(theor.)=1·181, giving $r(\text{obs.})/r(\text{theor.}) = 1{\cdot}02 \pm 6\%$. The observed difference between positron and electron scattering is therefore accounted for satisfactorily by the Mott theory.

Table 2. Angular Distribution of Scatters

Angular range	Electrons		Positrons		Both	
	Obs.	Theor.	Obs.	Theor.	Obs.	Theor.
30–40	286	279·1	222	234·4	508	513·5
40–50	150	127·2	135	104·5	285	231·7
50–60	81	67·9	55	55·0	136	122·9
60–70	23	40·3	30	32·4	53	72·7
70–80	20	25·8	17	20·7	37	46·5
80–90	23	17·5	7	14·0	30	31·5
90–100	7	12·4	7	10·1	14	22·5
100–110	5	9·2	7	7·6	12	16·8
110–120	7	7·1	5	5·9	12	13·0
120–150	5	14·4	15	12·4	20	26·8
150–180	4	10·1	6	9·0	10	19·1
30–180	611	611·0	506	506·0	1117	1117·0

Using the values of NZ^2 and β, and the track lengths, the total expected number of scatters can be calculated and compared with the number found. This provides a check on the absolute value of the cross section $I(\theta)$. For ϕ's$>30°$, the ratio of observed to expected numbers was $0{\cdot}92 \pm 4\%$ for electrons, $0{\cdot}90 \pm 5\%$ for positrons and $0{\cdot}91 \pm 3\%$ for both together. The errors quoted are statistical standard errors, but of course these ratios are also subject to some systematic errors which are absent from r(obs.). The most important error is probably the number of scatters missed in the scanning. Although the pictures were examined twice, independently, with the use of both cameras, and every effort made to count all ϕ's, the possibility cannot be excluded that some scatters were missed, particularly in the range 30° to 40°. It should be recalled that O'Ceallaigh's tables are given as functions of $\rho \cdot \lambda_c/2a$ where λ_c=the minimum track length accepted after scatters and $2a$ is the depth of the illuminated region. Since the attempt was made to count all scatters,

the tables were entered at $\rho=0$. However, scatters with very short λ_c are the more likely to be missed and if, for example, λ_c is put equal to 2 mm, the difference between observed and expected numbers practically vanishes. The reasonable conclusion is, therefore, that the observations show agreement with the theoretical absolute value of the cross section to within an experimental error of about 10%. The figure shows the observed and theoretical angular distributions, although this type of

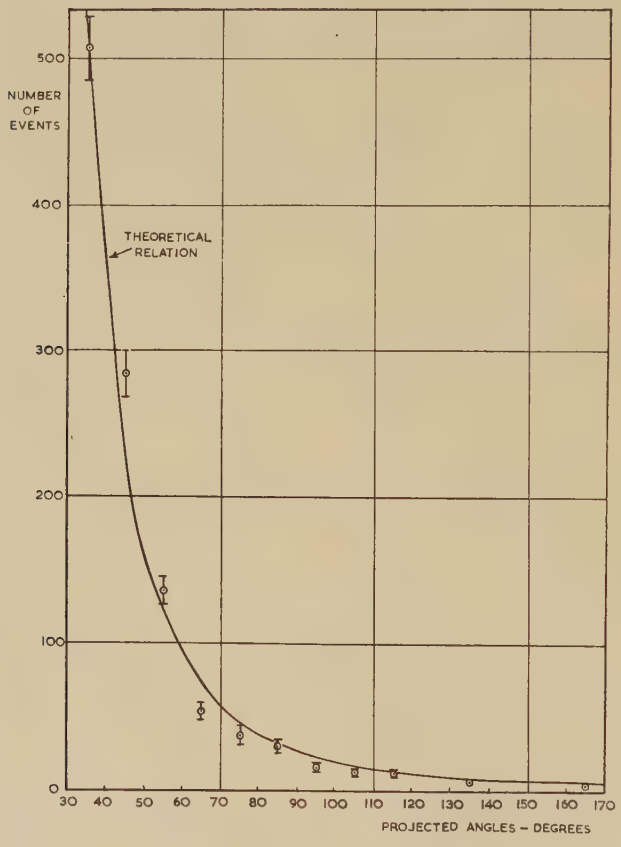

Angular Distribution of Scatters.

experiment cannot be expected to provide a close check on the distribution shape. The points show the measured number of scatters, electrons and positrons together, in 10° ranges of projected angles centred on the points and the standard errors are indicated. The full line shows the theoretical distribution of the same number of scatters. There is rough agreement between the points and the curve although the observed ratio of the number of 30° to 40° scatters to that of 40° to 50° ones is smaller than theory predicts. This is probably due to a combination of statistical error with scanning inefficiency in the lower range.

Acknowledgments

The authors wish to thank Professor J. D. Bernal for facilities in his department ; the Central Research Fund of the University of London for financial support ; the technical staff of Birkbeck College for making apparatus ; and Miss J. Locke and Mr. R. Miles for their help with some of the routine measurements.

References

Allen, K. R., Lipsicas, N. M., Major, D., and Phillips, K., 1956, *Proc. Phys. Soc.* A, **69,** 141.
Bosley, W., and Hughes, I., *Phil. Mag.*, **46,** 1281.
Bowness, C., 1956, *Ph.D. Thesis, University of London.*
Chapman, K. R., Matsukawa, E., Rose, P. H., and Stewardson, E. A., 1955, *Proc. Phys. Soc.* A, **68,** 928.
Cusack, N., and Stott, P., 1955, *Phil. Mag.*, **46,** 632.
Ellis, J., and Henderson, C., 1955, *Proc. Roy. Soc.* A, **229,** 260.
Elton, L., and Robertson, H., 1952, *Proc. Phys. Soc.* A, **65,** 145.
Gunnersen, E. M., 1952, *Austral. J. Sci. Res.* A, **5,** 258.
Hahn, B., Ravenhall, D. G., and Hofstadter, R., 1956, *Phys. Rev.*, **101,** 1131.
Masset, H. S. W., 1942, *Proc. Roy. Soc.* A, **181,** 14.
McKinley, W. A., and Feshbach, H., 1948, *Phys. Rev.*, **74,** 1759.
Mohr, C. B. O., and Tassie, L. J., 1954, *Proc. Phys. Soc.* A, **67,** 711.
Mott, N. F., 1931, *Proc. Roy. Soc.* A, **235,** 429.
O'Ceallaigh, C., *Proc. Roy. Irish Acad.*, 53A, **53,** 133.
Pettus, W., Blosser, H. G., and Hereford, F. L., 1956, *Phys. Rev.*, **101.** 17.

The Elastic Scattering of Protons by Protons at 925 MeV †

By P. J. Duke, W. O. Lock and P. V. March ‡
University of Birmingham

W. M. Gibson and J. G. McEwen
Queen's University, Belfast

and

I. S. Hughes and H. Muirhead
University of Glasgow

[Received July 31, 1956]

Summary

Ilford G5 emulsions have been exposed to a 925 MeV beam from the Birmingham proton synchroton. Sixty-five examples of the elastic scattering of protons by free protons in the emulsion have been found in 1539 metres of track. After removal of events having azimuthal angles $\psi > 45°$ where ψ is the angle between the plane of the two secondary particles and the plane of the emulsion, the remaining 44 events yielded a total elastic cross section of 17 ± 3 mb. The angular distribution of all the events shows a strong forward peak in the centre of mass system. The shape of this distribution has been compared with the predictions of a simple optical model and a value of $(0{\cdot}9 \pm 0{\cdot}1) \times 10^{-13}$ cm has been found for the interaction radius of the proton. The results are compared with other experimental work.

§ 1. Introduction

In this paper we present a detailed account of a study of the elastic scattering of protons by free protons in Ilford G5 nuclear research emulsions. A preliminary report of this experiment has already been published (Duke *et al.* 1955 b). Subsequently the mean energy of the proton beam has been more precisely determined, and the track length followed in emulsions of known shrinkage factor has been doubled.

It is intended that the present discussion should also serve as an introduction to the two following communications. These concern investigations of the ' quasi-elastic ' scattering of protons with protons bound inside a nucleus (McEwen, Gibson and Duke 1957) and of the inelastic scattering of protons with free protons in the emulsion (Hughes, March, Muirhead and Lock 1957).

† Communicated by P. B. Moon, F.R.S.
‡ Now at Department of Natural Philosophy, University of Glasgow.

The results of experiments using protons with energies up to 450 MeV have been tabulated by Berretta *et al.* (1954). The distinctive features of these results are the constant value of the total elastic cross section above 100 MeV and the isotropy of the differential cross section above 20° in the centre of mass system (C-system). Indications of a rise in the cross section at angles of less than 30° in the C-system resulting from a purely nuclear interaction (as opposed to that resulting from Coulomb repulsion) were first observed by Hartzler and Siegel (1954) at 428 MeV. This deviation from isotropy was confirmed at 437 MeV (Sutton *et al.* 1955). Following the construction of the large proton accelerators in the U.S.A., the U.S.S.R., and Great Britain, the maximum proton energy at which elastic scattering experiments have been carried out has been increased to about 6 BeV. The published results indicate that the anisotropy of the scattering becomes more pronounced as the energy of the protons is increased. There is also an indication that the value of the total elastic cross section begins to decrease slowly with energy above 400 MeV. These results will be reviewed in more detail later and compared with those of the present experiment.

§ 2. Experimental Procedure

The experiment was performed using protons scattered out from the circulating beam of the Birmingham synchrotron (Moon *et al.* 1955). The target material was the free hydrogen normally present in Ilford G5

Fig. 1

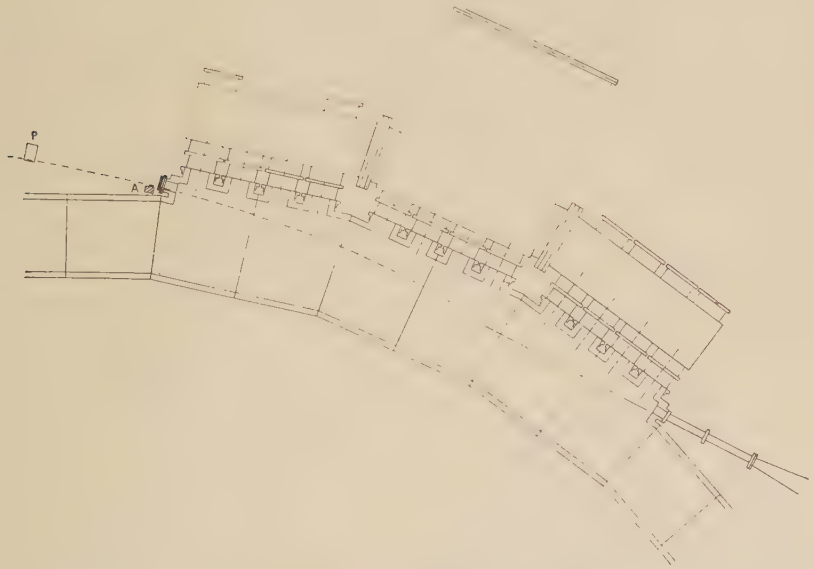

Plan of part of the synchrotron vacuum box and pumping manifolds showing the inflector tip and the trajectory of a scattered proton beam.

emulsions. The protons emerged through a circular glass window which was clamped to the wall of the vacuum box by a steel annulus, as shown in fig. 1. The trajectories of these scattered protons in the stray magnetic field were computed graphically and are shown in the same figure. The exposure position at P along the trajectory was chosen to give a maximum value for the ratio of the main beam intensity to that of the background of lower energy particles.

In order to verify experimentally that the beam which had passed directly through the window was reaching the plates, standard x-ray films were exposed perpendicular to the beam at several points along the trajectory. An exposure of about 100 pulses of protons of full energy (about 10^5 protons/cm^2/pulse) was sufficient to give a sharp image of the proton beam. Two of these x-ray films are shown in figs. 2 (*a*) and (*b*). That in 2 (*a*) was exposed at about 15 cm from the window and that in 2 (*b*) at the exposure position. The different areas covered by the beam in (*a*) and (*b*) were due to the horizontal defocusing and the vertical focusing action of the magnetic field. The latter effect, which was also the cause of the elliptical shadow of the steel annulus in (*a*), was not considered when the trajectory was computed. Because of this focusing effect and the finite extent of the emulsions at P, it was clear from the x-ray films that the plates were accepting not only protons of almost the full energy which had emerged through the window but also protons of slightly lower energy which had passed through the porcelain wall of the step and through the steel annulus. The actual extent of these three regions was determined from the position of the shadows cast on (*a*) and (*b*) by a block of absorbing material placed near the window, at A in fig. 1. The fairly sharp line of the shadow on film (*b*) corresponded to the inner limit of the exposure position and hence the shadow cast by the same block on (*a*) indicated the region of the step from which the emerging protons were being accepted by the emulsions. From the area and thickness of the steel annulus, the porcelain wall and the glass window, the mean energy of the beam was found to be 925 ± 30 Mev. This value should be compared with the previous estimate of 950^{+30}_{-50} Mev (Duke *et al.* 1955 b). The value of 925 ± 30 Mev found from the geometry of the experiment is also consistent with the value of 870 ± 35 Mev found from measurements on 8 elastic scatters in which one of the secondary protons came to rest in the emulsion.

A few of the recent exposures were made with a beam which was scattered out by a carbon target through a similar window further round the synchrotron. The relative positions of the target, the window, and the emulsions were the same as those described above and so the beam energy was assumed to be unchanged.

The plates were scanned by following the tracks of protons using Cooke M4000 microscopes fitted with $\times45$ oil immersion objectives. The intensity of the exposures (about 2×10^4 particles/cm^2) corresponded to about 8 tracks per field of view (100 μ square) so that the probability of an observer changing from one track to another while following it was

negligible. Only those tracks which were within $2\frac{1}{2}°$ of the mean beam direction and of minimum ionization were selected and followed. All interactions of protons in the emulsion were recorded; 2p and 4p stars and deviations of the primary proton were subjected to a more detailed examination. In this notation a star of type Np has been produced by a proton and has N secondary prongs of length greater than $5\,\mu$. All secondary tracks with length less than $5\,\mu$ were classified as recoil tracks. A deviation of the primary proton unaccompanied by any observable change in grain density was attributed to elastic scattering in the field of a large nucleus (Lock *et al.* 1955). The 4p stars were examined to detect any which could have been due to the reaction $\mathrm{p}+\mathrm{p}\rightarrow\mathrm{p}+\mathrm{p}+\pi^{+}+\pi^{-}$.

§ 3. Analysis of 2p Stars

The application of the principles of conservation of momentum and energy to the elastic collision of a proton with a free proton initially at rest yields the following results :—

(i) The track of the incident proton and the two secondary tracks are coplanar, that is, the angle, ϕ, between the incident proton and the plane of the two secondary tracks is zero.

(ii) The true angles of scatter, α_1, and α_2, are related by the expression

$$\tan\alpha_1\tan\alpha_2=2/E \quad . \quad . \quad . \quad . \quad . \quad . \quad . \quad (1)$$

where E is the total energy in the laboratory system expressed in units of the rest mass of a proton. For protons with an energy of 925 ± 30 MeV, $2/E$ is equal to $0{\cdot}670\pm0{\cdot}008$. Thus the true opening angle of the interaction, $\alpha_1+\alpha_2$, must lie between $78\frac{1}{2}°$ and $90°$.

These properties were used to separate the true elastic events from inelastic events and interactions with complex nuclei. The angles and approximate grain densities of the secondary tracks of all 2p stars were carefully measured, apart from those stars having a secondary caused by an α-particle or a heavier nucleus, or a definite recoil stub. The angle of scatter, projected on the horizontal plane, was measured to $\pm\frac{1}{4}°$ using the hair line in the eyepiece graticule. The dip angle of each track was measured using a $\times95$ oil immersion objective to $\pm\frac{3}{4}°$. Each time an event was measured, the shrinkage factor of the emulsion was determined to $\pm1\%$ using a method described elsewhere (Duke *et al.* 1955 a). The error of $\pm\frac{3}{4}°$ specified for the dip angle includes that introduced in the shrinkage factor determination. The angles α_1 and α_2 were obtained from the measured angles by :

$$\cos\alpha=\cos\theta\cos\delta\cos\delta_0+\sin\delta\sin\delta_0 \quad . \quad . \quad . \quad . \quad . \quad (2)$$

and ϕ was given by :

$$\sin\phi=\frac{\cos\delta_0\cos\delta_1\cos\delta_2}{\sin(\alpha_1+\alpha_2)}\left[\tan\delta_2\sin\theta_1-\tan\delta_1\sin\theta_2+\tan\delta_0\sin(\theta_2-\theta_1)\right]$$
$$. \quad . \quad . \quad (3)$$

where δ_0, δ_1 and δ_2 are the dip angles of the primary and the two secondary tracks and θ_1 and θ_2 are the projected angles of scatter. A measure of the departure from the perfect angular correlation required for an elastic collision was obtained by inserting the measured value of the larger α into eqn. (1) and hence calculating the value of the smaller α. The difference between this value and that obtained by direct measurement was denoted by $\Delta\alpha$. For a true elastic event $\Delta\alpha$ should be zero. The estimated average statistical errors for both the measured and the derived quantities are given in table 1. The values stated include an allowance for a small emulsion distortion. In particular cases systematic errors of about 1°

Table 1

Projected angle	θ	$\pm 15'$
Dip angle	δ	$\pm 45'$
True angle of scatter	α	$\pm 50'$
Departure from angular correlation	$\Delta\alpha$	$\pm 1° 15'$
Coplanarity angle	ϕ	$\pm 1°$

Fig. 3

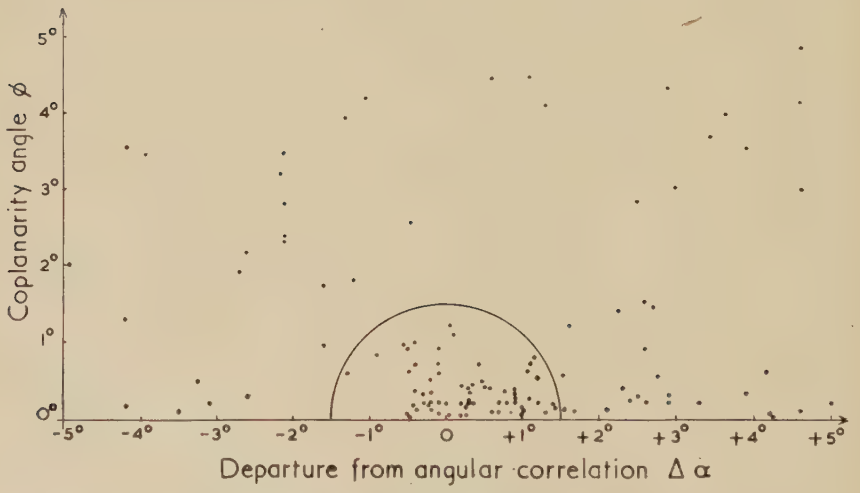

Graph of the coplanarity angle ϕ, plotted against the departure from angular correlation, $\Delta\alpha$.

may be introduced by large distortion effects, a small angle scatter of a secondary near the event or random irregularities in the fine focus movement of the microscope. The statistical error itself would be increased if the track being measured left the emulsion after less than about 200 μ had been traversed.

All those events which had $\alpha_1+\alpha_2$ between 70° and 95° and gave values of $\phi \leqslant 5°$ and $|\Delta\alpha| \leqslant 5°$ were plotted on the graph of ϕ against $\Delta\alpha$ shown in fig. 3. The large limits were taken to ensure that no true elastic interaction could be missed. There is a definite clustering of points near $\phi = 0$

and $\Delta\alpha=0$. Semicircular arcs of radii 0·5°, 1·0°, 1·5° etc. centred on $\Delta\alpha=0$ and $\phi=0$ were drawn on fig. 3. The number of events per unit area included between each pair of arcs plotted against the radius of the arc is shown in fig. 4. The distribution has a roughly Gaussian form which approaches zero at a radius of 1·5° and continues thereafter as a 'long tail', indicating a random background distribution. The radius of 1·5° was taken as the cut-off value, and all the events outside the corresponding semicircle were assumed to be inelastic events or interactions with complex nuclei. This value of 1·5° for the cut-off is consistent with the estimated errors in ϕ and $\Delta\alpha$ shown in table 1.

Fig. 4

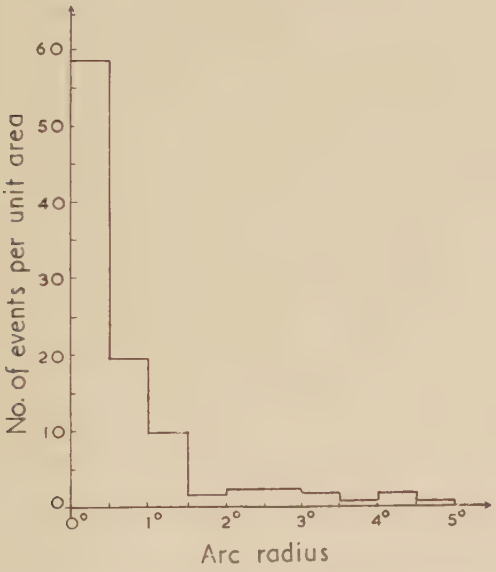

Graph of the number of events per unit area included between successive arcs, drawn on fig. 3, plotted against the arc radius.

Of the 122 events shown in fig. 3, 57 fall outside and 65 inside the semicircle. These 65 events were taken to be examples of the elastic scattering of the incident protons by free protons in the emulsion.

§ 4. Scanning Efficiency

A histogram of the total number of elastic events in four equal ranges of azimuthal angle, ψ, defined as the angle between the plane of the two secondaries and the emulsion plane, is shown in fig. 5(*a*). There is a definite decrease in the number of events with large values of ψ. Figures 5(*b*) and (*c*) are similar histograms for those events having the smaller angle of scatter $\alpha_s > 12°$ and $\leqslant 12$ respectively. The loss is more marked

in fig. 5(*c*) although it is still appreciable in (*b*). It appears that a considerable number of events having values of $\psi > 45°$ have been lost in the scanning or in the analysis. The lost events are predominantly those having $\alpha_s \leqslant 12°$.

There are several reasons for the loss of those events having large values of ψ and small values of α_s. It is inherently more difficult to detect events which take place in a plane almost perpendicular to that of the emulsion. In these cases the main component of the small deviation of the proton primary is in the dip angle. Such deviations are difficult to observe when scanning along the track. Furthermore it is these events which are most likely to be affected by errors in shrinkage factor measurement, by the shortness of the recoil track, by distortion, or by small angle scattering of one of the tracks near the event.

Fig. 5

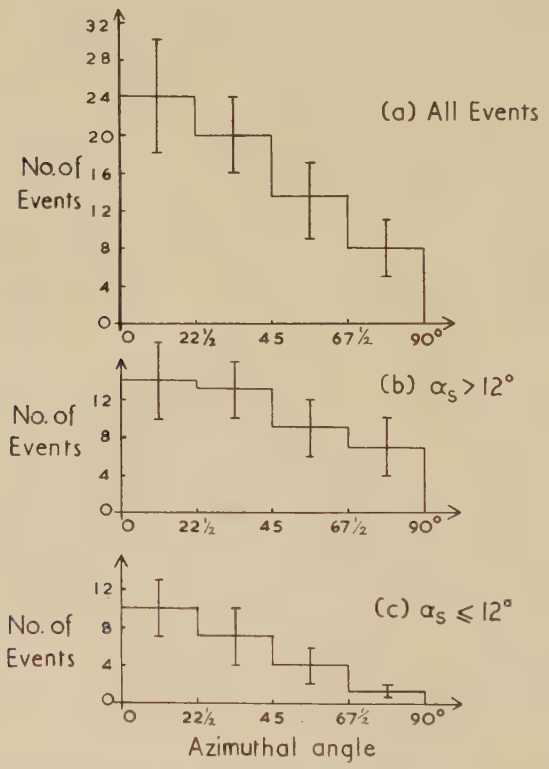

Histograms of the number of events in equal intervals of ψ, the azimuthal angle ; (*a*) all events, (*b*) events having the smaller angle of scatter $\alpha_s > 12°$, (*c*) events having $\alpha_s \leqslant 12°$.

In order to calculate the total cross section we have assumed that there is no loss of events with $\psi \leqslant 45°$(44 cases) and that the number of events with any ψ is twice the number with $\psi \leqslant 45°$.

§ 5. Results

The 44 elastic events having $\psi \leqslant 45°$ were found in 1539 metres of track length. Two events were subtracted from this number to allow for those background events which were included within the semicircle leaving 42 ± 7 elastic collisions with $\psi \leqslant 45°$ and therefore 84 ± 14 events with any ψ value. The mean free path for the elastic scattering of protons in Ilford G5 emulsions is therefore $18{\cdot}3\ ^{+3{\cdot}7}_{-2{\cdot}6}$ metres. The free hydrogen content of the emulsions used in the experiment was obtained from data supplied by Ilford Limited (Waller, private communication), together with a knowledge of the humidity at which the plates were stored immediately prior to their exposure. The mean value of the hydrogen content was $(3{\cdot}17 \pm 0{\cdot}06) \times 10^{22}$ atoms/cm^3. From this figure a value of 17 ± 3 mb was obtained for the total elastic cross section. If the loss of events with large values of ψ was neglected, the 65 events gave a total elastic cross section of 13 ± 3 mb.

Fig. 6

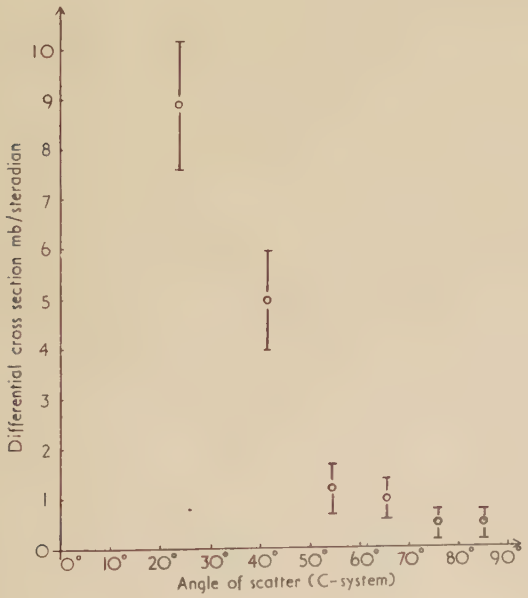

Differential cross section plotted as a function of the angle of scatter in the centre of mass system.

The angles α^* of the secondary tracks in the C-system with respect to the direction of the primary may be calculated using the relationship:

$$\tan \frac{\alpha^*}{2} = \sqrt{\frac{E}{2}} \tan \alpha. \quad . \quad . \quad . \quad . \quad . \quad . \quad . \quad (4)$$

For a 925 MeV proton eqn. (4) reduces to $\tan \frac{1}{2}\alpha^* = 1{\cdot}22 \tan \alpha$. Values of α^* have been obtained for all 65 elastic events. The differential cross section has been calculated for six equal intervals of solid angle after making a correction for the loss of those events having large values of ψ. This correction was made by including in the first angular interval only those events which had $\psi \leqslant 45°$, giving 23 events or 46 for all values of ψ. The total number of events for all 6 intervals was increased to 84 (the number used in obtaining the total elastic cross section) by distributing the 3 extra events required amongst the other 5 angular intervals in the ratio of the number of events actually observed. The result of this calculation is shown in table 2 and the values obtained for the differential cross section are plotted graphically in fig. 6.

Table 2

Angular Range C-system degrees	Observed number of events	Corrected number of events	$\frac{d\sigma}{d\Omega}$ in mb/ster.
0–33½	30	46	8·9±1·3
33½–48¼	22	23·9	4·6±0·9
48¼–60	5	5·4	1·0±0·4
60–70½	4	4·3	0·8±0·4
70½–80½	2	2·2	0·4±0·3
80½–90	2	2·2	0·4±0·3

§ 6. Discussion

The experimental values of the total cross section for elastic scattering obtained at energies between 437 and 5700 MeV are given in table 3. There appears to be a tendency for the total elastic cross section to decrease slowly with increasing energy. It should be noted that in all the experiments carried out using counter techniques, the value obtained for the elastic cross section depends on an extrapolation of the observed angular distribution. Measurements were made only at angles greater than about 30° in the C-system in all experiments except that of Meshcheryakov *et al.* (1956) who made measurements down to 5°.

The values obtained in the present work for the differential cross section are in general agreement with those obtained by Smith *et al.* (1955) at 1000 MeV. The increase in the value of the scattering cross section at forward angles is part of a general tendency which begins at about 430 MeV (Sutton *et al.* 1955) and continues up to the present experimental limit of about 6 BeV (Cork and Wenzel 1955). Reference should be made to the report of Hess (1956) for a complete summary of the differential cross section measurements at different energies.

It has been pointed out by Serber and Rarita (1955) that the results of Smith *et al.* (1955) for the differential cross section can be fitted by the expression

$$\frac{d\sigma}{d\Omega} \propto \left[\frac{J_1(kR \sin \alpha^*)}{\sin \alpha^*}\right]^2 \quad \ldots\ldots \quad (5)$$

where k is the wave number of the incident proton in the C-system, R is an interaction radius of the proton, and J_1 is a first-order Bessel function. We have fitted eqn. (5) to our results and have obtained a value of $(0{\cdot}9\pm0{\cdot}1)\times10^{-13}$ cm for R. This is in good agreement with that obtained by Batson and Riddiford (1956), Fowler *et al.* (1956 a, b) and Chen *et al.*

Table 3

Energy (MeV)	Total elastic cross section in mb	Technique	Reference
437	$23{\cdot}8\pm1{\cdot}2$	C	Sutton *et al.* (1955)
440	$23{\cdot}5\pm1{\cdot}2$†	C	Smith *et al.* (1955)
460	$24{\cdot}0\pm0{\cdot}6$	C	Meshcheryakov *et al.* (1956)
560	$26{\cdot}0\pm0{\cdot}8$	C	Meshcheryakov *et al.* (1956)
590	$25{\cdot}2\pm2{\cdot}0$†	C	Smith *et al.* (1955)
650 ± 50	$26{\cdot}3\pm1{\cdot}8$	Cl. Ch.	Batson and Riddiford (1956)
660	23 ± 2	C	Bogachev and Vzorov (1954)
660	$24{\cdot}7\pm1{\cdot}0$	C	Meshcheryakov *et al.* (1956)
800	$21{\cdot}5\pm2{\cdot}0$†	C	Smith *et al.* (1955)
810 ± 100	24 ± 3	Cl. Ch.	Morris *et al.* (1956)
925	17 ± 3	Em	Present work.
1000	$19{\cdot}2^{+3}_{-2}$†	C	Smith *et al.* (1956)
1500	$20\pm4{\cdot}5$	Cl. Ch.	Fowler *et al.* (1956 a, b)
2700	$15\pm4{\cdot}5$	Cl. Ch.	Block *et al.* (1956)
5300	$5{\cdot}7\pm2{\cdot}3$	Cl. Ch.	Wright *et al.* (1956)
5700	13 ± 6	Em	Giles (1955)

† Normalized to the value of $d\sigma/d\Omega$ at 90° obtained by Sutton *et al.* (1955) at 437 MeV; the values given are those quoted by Hess (1956).

Key: C, counters; Cl. Ch., Cloud chambers; Em, Emulsions.

(1956) from a study of proton scattering at energies between 600 and 2700 MeV. Interaction radii of the same order of magnitude have been obtained from pion–proton scattering experiments at 1·4 BeV (Eisberg *et al.* 1955, Walker and Crussard 1955). From electron scattering experiments McAllister and Hofstadter (1956) have obtained a value of $(0{\cdot}74\pm0{\cdot}24)\times10^{-13}$ cm for the r.m.s. radius of both the charge and the magnetic moment distributions of the proton.

Acknowledgments

We wish to express our thanks to Miss O. Archibald, Mrs. S. E. Baker, Miss P. Gavigan, Miss M. J. Lewis, Mrs. E. R. Lock, Mrs. N. Palmer, Miss M. T. Parkes, Miss E. Rose, Mrs. B. R. Stephens and Mrs. M. Whitaker for carrying out the tedious scanning involved. We are indebted to Mr. C. Waller of Ilford Limited for supplying data on the properties of G5 emulsion, to Mr. C. J. Batty and Dr. S. J. Goldsack for their invaluable assistance with the calculations of the trajectories and to Dr. G. Feldman, Mr. R. McKeague, Mr. B. A. Munir and Dr. J. Vilain for many useful

discussions. We also thank Dr. J. L. Symonds and other members of the synchrotron team for ensuring the successful operation of the machine.

The authors at Belfast (W. M. G. and J. G. McE.) and Glasgow (I. S. H. and H. M.) would like to express their thanks to Professor Moon for enabling them to take part in this work, which was carried out as part of a programme of research supported by the Department of Scientific and Industrial Research. Two of us (P. J. D. and P. V. M.) are indebted to this body for maintenance grants.

References

Batson, A., and Riddiford, L., 1956, *Proc. Roy. Soc.* A, **237,** 175.

Berretta, L., Villi, C., and Ferrari, F., 1954, *Nuovo Cim.* (*Suppl.*), **12,** 499.

Block, M. M., Harth, E. M., Cocconi, V. T., Hart, E., Fowler, W. B., Shutt, R. P., Thorndike, A. M., and Whittemore, W. L., 1956, *Phys. Rev.*, **103,** 1484.

Bogachev, N. P., and Vzorov, V. K., 1954, *Dokl. Akad. Nauk. S.S.S.R.*, **99,** 931.

Chen, F. F., Leavitt, C. P., and Shapiro, A. M., 1956, *Phys. Rev.*, **103,** 211.

Cork, B., and Wenzel, W. A., 1955, *University of California Physics Report,* UCRL 3223, p. 16.

Duke, P. J., Lock, W. O., March, P. V., and Munir, B. A., 1955 a, *J. Sci. Instrum.*, **32,** 365.

Duke, P. J., Lock, W. O., March, P. V., Gibson, W. M., McKeague, R., Hughes, I. S., and Muirhead, H., 1955 b, *Phil. Mag.*, **46,** 877.

Eisberg, L. M., Fowler, W. B., Lea, R. M., Shephard, W. D., Shutt, R. P., Thorndike, A. M., and Whittemore, W. L., 1955, *Phys. Rev.*, **97,** 797.

Fowler, W. B., Shutt, R. P., Thorndike, A. M., and Whittemore, W. L., 1956 a, *Phys. Rev.*, **103,** 1479.

Fowler, W. B., Shutt, R. P., Thorndike, A. M., Whittemore, W. L., Cocconi, V. T., Hart, E., Block, M. M., Harth, E. M., Fowler, E. C., Garrison, J. D., and Morris, T. W., 1956 b, *Phys. Rev.*, **103, 1489.**

Giles, P. C., 1955, *University of California Physics Report,* UCRL. 3223, p. 12.

Hartzler, A. J., and Siegel, R. T., 1954, *Phys. Rev.*, **95,** 185.

Hess, W. N., 1956, *University of California Physics Report,* UCRL. 4639.

Hughes, I. S., March, P. V., Muirhead, H., and Lock, W. O., 1957, *Phil. Mag.*, **2,** 215.

Lock, W. O., March, P. V., Muirhead, H., and Rosser, W. G. V., 1955, *Proc. Roy. Soc.* A, **230,** 215.

McAllister, R. W., and Hofstadter, R., 1956, *Phys. Rev.*, **102,** 851.

McEwen, J. G., Gibson, W. M., and Duke, P. J., 1957, *Phil. Mag.*, **2, 231.**

Meshcheryakov, M. G., Bogachev, N. P., Leksin, E. A., Neganov, B. S., and Piskarev, E. V., 1956, *CERN Symposium,* Vol. II, p. 125, Geneva 1956.

Moon, P. B., Riddiford, L., and Symonds, J. L., 1955, *Proc. Roy. Soc.* A, **230,** 204.

Morris, T. W., Fowler, E. C., and Garrison, J. D., 1956, *Phys. Rev.*, **103,** 1472.

Serber, R., and Rarita, W., 1955, *Phys. Rev.*, **99,** 629 (A).

Smith, L. W., McReynolds, A. W., and Snow, G., 1955, *Phys. Rev.*, **97,** 1186.

Sutton, R. B., Fields, T. H., Fox, J. G., Kane, J. A., Mott, W. E., and Stallwood, R. A., 1955, *Phys. Rev.*, **97,** 783.

Walker, W. D., and Crussard, J., 1955, *Phys. Rev.*, **98,** 1416.

Wright, R. W., Saphir, G., Powell, W. M., Maenchen, G., and Fowler, W. B., 1956, *Phys. Rev.*, **100,** 1802 (A).

The Production of π-Mesons in Proton–Proton Collisions at 925 MeV †

By I. S. Hughes, P. V. March, H. Muirhead
University of Glasgow

and W. O. Lock
University of Birmingham

[Received July 31, 1956]

Summary

A study has been made of the production of π-mesons in the collisions of protons having an energy of 925 MeV, with the hydrogen present in nuclear emulsions. The results yield the following cross sections :

$p+p \rightarrow \pi^+ + n + p$	27 ± 3 mb,
$\pi^+ + D$	$0{\cdot}6 \pm 0{\cdot}4$ mb,
$\pi^0 + p + p$	6 ± 2 mb,
$\pi^+ + \pi^- + p + p$	$\leqslant 0{\cdot}2$ mb.

Angular and momentum distributions have been obtained for particles emitted in the first process. The results may be interpreted in terms of the production of mesons by the decay of an excited nucleon.

§ 1. Introduction

Recent measurements of the magnitude of the total cross sections for proton–proton collisions have shown a rise from the nearly constant value of about 23 mb over the region from 150 to 400 MeV (Berretta *et al.* 1954) to about 48 mb at 900 MeV (Shapiro *et al.* 1954). Above 900 MeV the cross section decreases slowly to at least 2·7 BeV and reaches a value of 41 mb at that energy (Shapiro 1956).

In contrast to these measurements, those on the cross section for the elastic scattering of protons have shown a slow decrease from a value of 25 mb at 400 MeV to about 15 mb at 2·75 BeV (Block *et al.* 1956 ; Smith *et al.* 1955).

The difference between the cross sections for the total and the elastic scattering represents the cross section for meson production. The present paper describes measurements on the characteristics of meson production when the incident proton possesses an energy of 925 ± 30 MeV. The measurements were made in nuclear emulsions, which were exposed to the external beam from the Birmingham proton synchrotron.

† Communicated by the Authors.

In table 1 the possible processes are given for the production of π-mesons which may occur at this energy. In the present experiment the energy in the centre of momentum C-system is 429 MEV ; that required for the production of one, two or three π-mesons is about 140, 280 and 420 MEV respectively. No attempt was made to find examples of triple production.

The method of identification of events representing π-meson production utilizes the principles of the conservation of energy and momentum. Hence processes involving the emission of two uncharged particles could not be distinguished.

Table 1

$p+p \rightarrow \pi^+ + n + p$	(*a*)
$\pi^+ + D$	(*b*)
$\pi^0 + p + p$	(*c*)
$\pi^+ + \pi^- + p + p$	(*d*)
$\pi^+ + \pi^0 + n + p$	(*e*)
$\pi^+ + \pi^+ + n + n$	(*f*)
$\pi^0 + \pi^0 + p + p$	(*g*)
3-meson production	(*h*)

§ 2. Experimental Procedure

2.1. *Preliminary Examination*

The methods used for the exposure and examination of the nuclear emulsions are described in the previous paper (Duke *et al.*). All events having two or four secondary charged particles were examined. Those accompanied by the emission of an electron or in which one of the tracks was produced by an α-particle or by a nuclear recoil were rejected. All events identified as elastic scatterings between free protons were also excluded.

In proton–proton collisions at 925 MEV the maximum angles of emission of the nucleons with respect to the primary direction are 57° and 35° respectively, in the laboratory system of coordinates, for the emission of one and two π-mesons.

If an event satisfied these conditions the angles of emission and the grain density of each secondary track were measured. Further events could then be rejected since the energy (and hence the grain density) of the protons emitted in processes (*a*), (*c*) and (*d*) had to fall within prescribed limits for any permitted angle of emission. The simultaneous production of a π^+-meson and a deuteron could be recognized at this stage since unique relations exist between the angles of emission and the grain densities of the meson and the deuteron ; the tracks of the primary proton and the two secondary particles must also be coplanar. Considerations of the balance of energy and momentum permit the identification of process (*d*) since all four secondary particles are observed.

2.2. *The Method of Identification for Events Involving One Uncharged Particle*

The details of the procedure used to balance energy and momentum are given in an Appendix. The probability that an event can conserve energy and momentum is expressed in terms of a ratio R, defined by

$$R = \frac{|G_M - G|}{\Delta G_M}$$

where G_M is the measured grain density for one secondary track, ΔG_M is the maximum error of this quantity, and G is the grain density which this track must have if energy and momentum are conserved. A gaussian distribution is expected for the values of this ratio. The calculated distribution of R shows that the majority of genuine examples of π-meson production should have values of $R < 1{\cdot}5$. Whenever possible, measurements of the multiple scattering of the secondary tracks were made in

Fig. 1

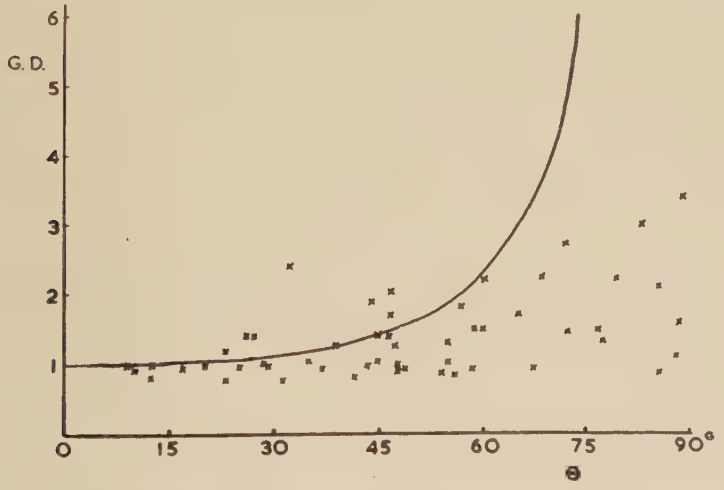

Distribution in grain density and angle with the primary, of secondary tracks assumed to be mesons for which a positive indentification, by means of multiple scattering measurements, was not possible. Each cross represents one track. Proton tracks arising from elastic scattering of the primary particle by a free nucleon must lie on, or to the left of, the curve drawn.

order to decrease the limits of error of the energy determinations and to check the assignments of identity made on the basis of energy and momentum balance. As a result of these measurements new values of R were obtained in a few cases. It was found that of 136 of the events with $R < 1{\cdot}5$, the track assigned to a π-particle was positively identified as

a π-meson in 36 events and a proton in 44 while for the remaining 56 events the measurements were inconclusive.

If the unidentified events are accepted or rejected in the ratio of the numbers of identified mesons to protons the cross section for the process $p+p \rightarrow \pi^+ + n+p$ is 18 mb. If all the uncertain events are accepted this cross section becomes 27 mb.

We believe that the latter value is probably the better one for the following reasons :

(i) An examination of the unidentified events shows that in the majority of cases the track assigned to a π-meson has a large angle of dip and a low grain density. If these tracks were due to protons they would have an

Fig. 2

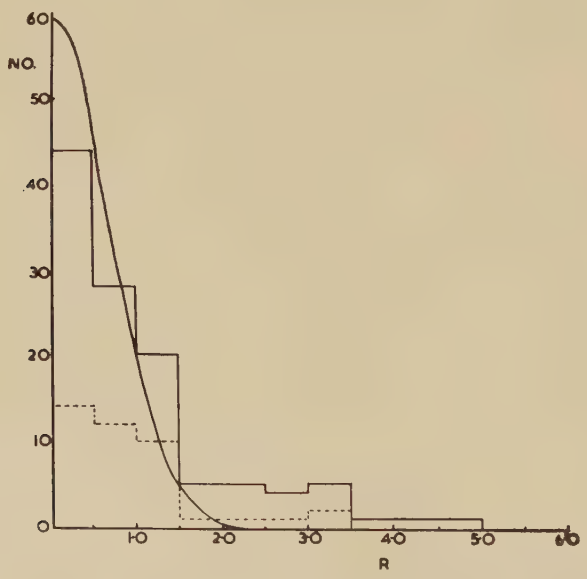

Distribution of the ratio R for events not rejected by multiple scattering measurements. In this and the following figures the full line histograms represent the distribution for all the events, the dotted line histograms those for events in which the π-meson was positively identified. The full line curve is the calculated distribution for all events.

energy in excess of that allowed for an elastically scattered proton at the same angle of emission (see fig. 1). Since the background events can only arise from complex nuclei in the emulsion an improbable sequence of collisions inside a nucleus would be required to produce such protons.

(ii) Most of the measurements of multiple scattering were made on tracks of low grain density. If a proton produces a track of low grain density the conservation of momentum requires that it should be emitted at a small angle to the direction of the primary proton. Therefore,

such protons tend to produce the long tracks in the emulsion which are necessary for multiple scattering measurements. Since mesons which produce tracks of low grain density may be emitted at any angle, multiple scattering measurements are biased in favour of protons.

It was found that the majority of the 44 events in which the track assigned to the meson was in fact a proton, were events in which the range of error in the determination of the energy of one of the secondary particles was large.

In view of these considerations we have accepted the 56 events in which the multiple scattering measurements were inconclusive, as genuine examples of the process $p+p \rightarrow \pi^+ + n + p$.

The distribution of R for all events in which R is less than 5, except those rejected by multiple scattering measurements, is shown in fig. 2. The calculated distribution has been normalized to the total number of events with R less than 1·5.

The method of identification we have used for events in which one meson is produced is more selective for the production of π^0- than for π^+-mesons. This is so because energy conservation restricts the possible energy values of the neutral particle, and if this particle is a meson the range of possible momenta is smaller than that for a neutron. Thus the region over which a momentum balance is possible is restricted for the production of π^0-mesons. For the production of π^0-mesons, however, there exist no criteria equivalent to the identification of π^+-mesons by measurements of multiple scattering and by the angle–grain density plot (fig. 1).

§ 3. Results

A total of 453 and 298 events having two and four secondary particles respectively were found. In table 2 we display the numbers of accepted events remaining at each stage of elimination. These events

Table 2

Number of events	2 Prongs	4 Prongs
Found	453	298
After preliminary examination	238	0
With $R<1{\cdot}5$	160	—
After multiple scattering	116†	—

† This includes all events involving single meson production.

were found in a total length of 1076 metres of track of the 925 MeV protons; the hydrogen content at the time of exposure was $(3{\cdot}17 \pm 0{\cdot}06) \times 10^{22}$ atoms/cm^3; the cross sections for processes observed could thus be found and are listed in table 3.

The angular and momentum distributions in the C-system for the π-mesons, neutrons and protons are given in figs. 3, 4 and 5. The experimental angular distributions were found to be symmetrical about 90° as is to be expected for a collision between two identical particles. To improve the statistical accuracy of the results the distributions have been folded about this angle. For all the distributions, we have plotted

Table 3

Process	No. of events	Cross-section
$p+p \rightarrow \pi^+ + n + p$	92	27 ± 3 mb.
$\pi + D$	2	$0{\cdot}6 \pm 0{\cdot}4$ mb.
$\pi^0 + p + p$	22	6 ± 2 mb.
$\pi^+ + \pi^- + p + p$	0	$\leqslant 0{\cdot}2$ mb.

Fig. 3

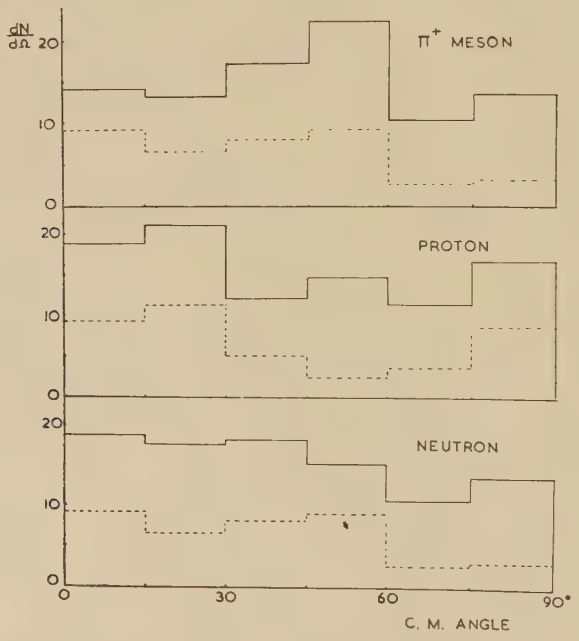

Angular distributions in the C-system of the secondary particles from the reaction $p+p \rightarrow \pi^+ + p + n$.

values of the quantities such that energy and momentum are conserved exactly (' consistency ' values—see Appendix), rather than the measured values. The small differences between the measured and ' consistency ' values are due to the experimental errors but the distributions of both sets of values are very similar for all the quantities.

A satisfactory feature of the results is that the distribution of the azimuthal angles shows no evidence of loss of events when this angle is large.

Fig. 4

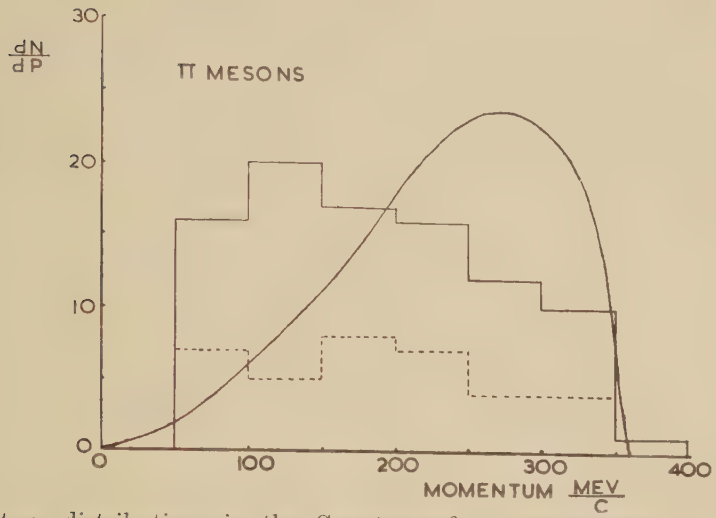

Momentum distributions in the C-system of π^+-mesons from the reaction $p+p \rightarrow \pi^+ + p + n$. The full line curve represents the form of the distribution calculated from purely statistical considerations.

Fig. 5

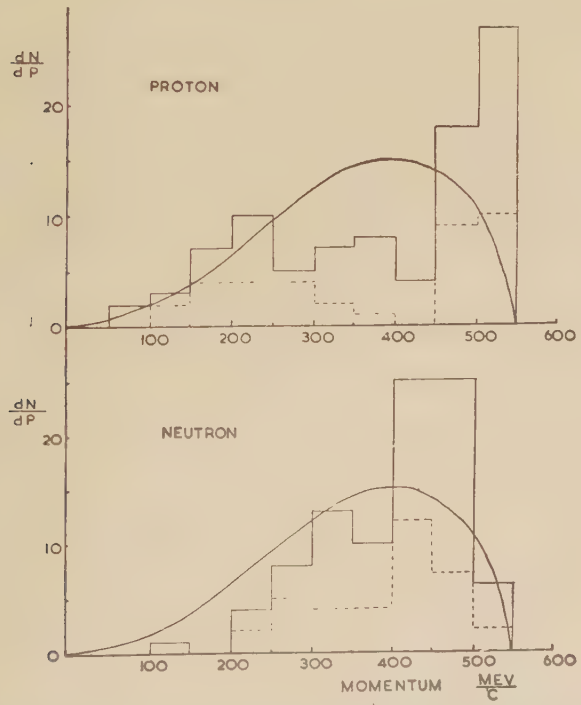

Momentum distributions in the C-system of the proton and the neutron from the reaction $p+p \rightarrow \pi^+ + p + n$. The full line curve represents the form of the distribution calculated from purely statistical considerations.

§ 4. Discussion

4.1. *Cross Sections*

The measured cross section for inelastic scattering is 34 ± 4 mb. That for elastic scattering, obtained from the same exposure and examination of the emulsions, is 17 ± 3 mb (Duke *et al.* 1956). These results compare favourably with those obtained using counter techniques (Shapiro 1956 Smith *et al.* 1955), but less satisfactorily with those found by using cloud chambers (Block *et al.* 1956). They are displayed in table 4; in the region of energies surveyed the total cross section for the scattering of free protons remains nearly constant at a value of 48 mb (Shapiro 1956).

Table 4

Energy in Mev	Technique	Cross section in mb	
		Elastic	Inelastic
800	Counter	21 ± 2	26 ± 3
800	Cloud chamber	24 ± 3	24 ± 3
925	Emulsions	17 ± 3	34 ± 4
1000	Counter	19 ± 3	$29 \pm 3{\cdot}5$
1500	Cloud chamber	20 ± 2	27 ± 3

The values quoted by Block *et al.* were obtained by a normalization of the observed ratio of inelastic to elastic scatterings to the measurements of total cross sections made by Shapiro *et al.* The cross sections for inelastic scattering from counter experiments represent the difference between the measured values for total and elastic scattering.

The results displayed in table 4 suggest that the events accepted by us as examples of the production of mesons from free hydrogen are not seriously contaminated by spurious examples arising from the more complex atomic constituents of the emulsion.

Unfortunately, firm theoretical predications cannot at present be made concerning either the absolute or relative magnitudes of these cross sections. The observed angular distributions for the elastic scattering between free protons suggest that the scattering is of a diffraction character for incident protons with energies between 650 Mev and 3 Bev (Smith *et al.* 1955; Cester *et al.* 1956). Over this range of energies the observed distributions may be successfully fitted by an expression of the form $[J_1(kR \sin\theta)/\sin\theta]^2$ where J_1 is a first-order Bessel function, k is the wave number of the incident proton in the C-system and R is an interaction radius for the proton (Serber and Rarita 1955).

Despite the successful representation of the experimental results by this simple expression, an examination of table 4 strongly suggests that the cross sections cannot be simply described in terms of optical 'black body' scattering, since, with the exception of the cloud chamber result at 800 Mev, the cross section for elastic scattering is invariably less than that for inelastic scattering.

It is of interest to attempt to relate the concept of optical scattering to the statistical theory of Fermi (1950, 1953). This theory assumes the formation of an excited compound system which may decay into its parent particles or into a mixture of mesons and nucleons. The former mode of decay will represent compound elastic scattering which would interfere coherently with the diffraction scattering. If a compound system is formed and decays in the manner proposed by Fermi then the observed shape of the differential cross section for elastic scattering suggests either that the interference takes place in such a manner that the characteristic pattern for diffraction scattering is preserved, or that the compound elastic scattering is negligible.

Since the probability for the occurrence of any process may be represented by an expression of the form $|H|^2W$ where H is the interaction term for the process and W is a statistical weighting factor covering the density of final states, either or both of the above proposals could be satisfied by the form and magnitude of $|H|^2$.

We will compare the relative cross sections for the decay of the compound system by assuming the formation of the following three states, (*a*) two nucleons, (*b*) two nucleons and a π-meson, (*c*) a nucleon and an excited nucleon.

State (*c*) represents the assumption that the production of the meson proceeds through the formation of a nucleon in an excited state with spatial and isotopic spin quantum numbers of 3/2 (Peaslee 1954). The energy available in the C-system for all the experiments listed in table 4 is well above the threshold for the production of this state.

We will consider the extreme assumptions that either the states (*a*) and (*b*) completely dominate (*c*), or that states (*a*) and (*c*) dominate (*b*). The first assumption represents the original statistical theory of Fermi. For this assumption

$$\frac{\sigma_b}{\sigma_a}=0{\cdot}43 \qquad \text{(Block 1956).}$$

For the second assumption we may write

$$\frac{\sigma_c}{\sigma_a}=\frac{|H_c|^2\,W_c}{|H_a|^2\,W_a} \qquad \text{and} \qquad \frac{W_c}{W_a}=\frac{\rho_c}{\rho_a}\cdot\frac{f_c}{f_a}\cdot\frac{S_c}{S_a}\cdot 2$$

where ρ=density of momentum states available, f=factor to allow for conservation of isotopic spin and, S=weighting factor for the spins of the systems and where the factor 2 occurs since indistinguishable particles appear in the elastic scattering. Inserting numerical values and assuming that the mass of the excited nucleon is 1·27 proton masses (see end of this section), the weights may be written as

$$\frac{W_c}{W_a}=0{\cdot}66\times 1\times 2\times 2=2{\cdot}6.$$

If we take $|H_c|^2=|H_a|^2$ then $\sigma_c/\sigma_a=2{\cdot}6$. Thus it may be seen that inelastic scattering is favoured if it is assumed that the production of the meson proceeds through the 3/2, 3/2 state This is in accord with

the suggestion made above that compound elastic scattering should be small, but it must be borne in mind that we have assumed $|H_c|^2=|H_a|^2$ which may not necessarily be true.

4.2. *Relative Yield of π^+- and π^0-Mesons*

Our measured ratio for the yield of π^+- to π^0-mesons is $4{\cdot}2\pm1{\cdot}0$. In table 5 we list published data for this ratio obtained in experiments over the energy range from 650 to 925 MeV. The data at higher energies suffer from uncertainties through the production of two π-mesons.

Table 5

Energy in MeV	Technique	Ratio	Reference
650	Cloud chamber	$3{\cdot}8+1{\cdot}9$ $-0{\cdot}9$	(*a*)
660	Counters	$3{\cdot}1\pm1{\cdot}0$	(*b*)
800	Cloud chamber	17 ± 8	(*c*)
925	Emulsions	$4{\cdot}2\pm1{\cdot}0$	Present experiment

(*a*) Batson and Riddiford (1956).
(*b*) Dzhieliopov *et al.* (1955), Tyapkin *et al.* (1955).
(*c*) Block *et al.* (1956).

It can be seen from table 5 that the results show anomalously large fluctuations. It should be borne in mind that the measurement from the present experiment is almost certainly contaminated by events from interactions in complex nuclei, which could conceivably affect this ratio. The ratio of 17 ± 8 quoted by Block *et al.* must be treated with caution since positive assignments of events as the production of π^+- or π^0-mesons could not be made in about 25% of the events found.

In view of these reservations no serious comparison can be made between the statistical model (scheme (*b*) above), which predicts ratios of 1, 3 or ∞, and the excited nucleon model which predicts a ratio of 5.

4.3. *Angular and Momentum Distributions for* $p+p\rightarrow\pi^++n+p$

The experimental angular distributions of the secondary particles in the centre of momentum system are approximately isotropic. The distribution of the angles between the π-meson and the proton, shown in fig. 6, shows a stronger correlation than would be expected from the statistical theory.† There is no marked correlation in the angle between the π-meson and the neutron. The correlations are readily explained in terms of an excited nucleon since nine-tenths of the π-mesons would be produced by the decay of the excited nucleon into a π^+-meson and a proton and only one-tenth by the decay into a π^+-meson and a neutron.

† Unless it is specifically stated in the following discussion we shall assume that the statistical theory and momentum space considerations predict the same results.

The curves superimposed on the experimental momentum distributions (figs. 4 and 5) are those expected from considerations of the momentum space available to each particle on the statistical theory (Block 1956). It can be seen that there is a tendency for the mesons to be emitted with low values of momentum.

The statistical theory predicts that the momentum distributions of the neutrons and of the protons should be identical. The experimental distributions appear to differ, that for the neutrons shows a broad peak about 400 MeV while that for the protons is wider and has a tendency to peak at the maximum possible momentum.

Fig. 6

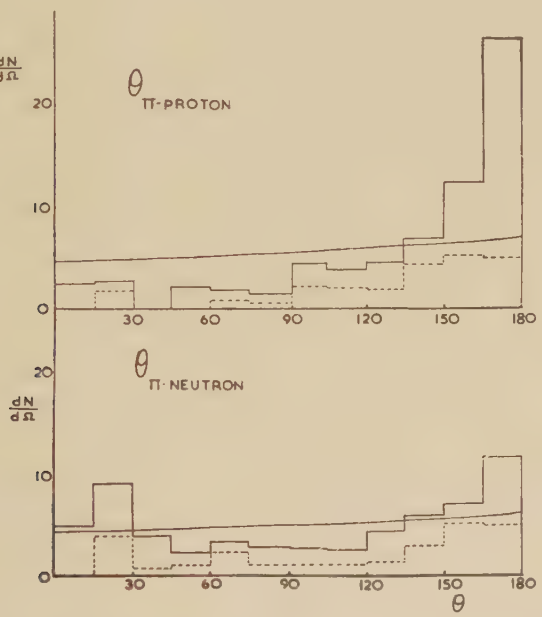

Distributions of the angles in the C-system between the π^+-meson and the proton and the π^+-meson and the neutron, from the reaction

$$p + p \rightarrow \pi^+ + p + n.$$

The full line curve represents the form of the distribution calculated from purely statistical considerations.

When the assumption is made that the π-meson and one of the nucleons result from the disintegration of an excited nucleon it is of interest to examine the energy released in the disintegration (Q-value), since experiments on the scattering of π^+-mesons by protons suggest that this quantity should be $\sim$160 MeV. The experimental distribution obtained for the Q-values together with that predicted by statistical theory (Block 1956) are shown in fig. 7. It can be seen that if an excited nucleon is formed, factors other than those occurring in the scattering of π^+-mesons on protons influence the disintegration of this state since the experimental

distribution peaks at about 110 MeV. The corresponding distribution for π^+-meson and neutron does not show a peak ; this is to be expected since no correlation was observed in the spatial angle between these particles (fig. 6). If the existence of an excited nucleon is assumed, then the angular distribution of the π-meson and proton in its coordinate system may be obtained ; this is displayed in fig. 8. The mesons have a tendency to be emitted in the backward direction in this coordinate system. In this context we mean the backward direction with respect

Fig. 7

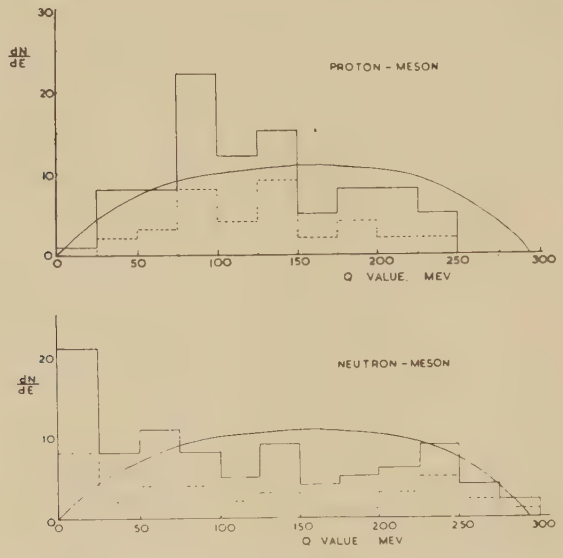

Distribution of Q-values for the decay into a π^+-meson and a proton and π^+-meson and a neutron, of an excited nucleon in the reaction

$$p+p \rightarrow n+N^* \rightarrow \pi^+ + p + n.$$

The curves represent the distribution anticipated from purely statistical considerations when no excited nucleon is formed.

to the direction of motion of the excited nucleon in the C-system. Thus they tend to be emitted with low energy in the system of the two colliding protons while the protons preferentially appear with the maximum energy consistent with the conservation of energy and momentum. The curves superimposed on the histogram are the distributions obtained by Ashkin *et al.* (1956) at 150 MeV and by Ferrari *et al.* (1956) at 124 MeV in experiments on the scattering of π^+-mesons by protons. Since the distribution of Q-values shows a peak at 100–120 MeV, the meson distribution should be compared with the results obtained at the lower energy. The comparison is surprising. The data given in fig. 8 indicates that meson production does not result from the decay of a pure isobar state since this would lead to a symmetrical angular distribution about 90° in the coordinate system of the excited nucleon. However, the distribution

would be modified by the presence of any meson production taking place through state (*b*).

For the production of π^0-mesons the numbers available were too few to provide useful information on angular or momentum distributions.

Fig. 8

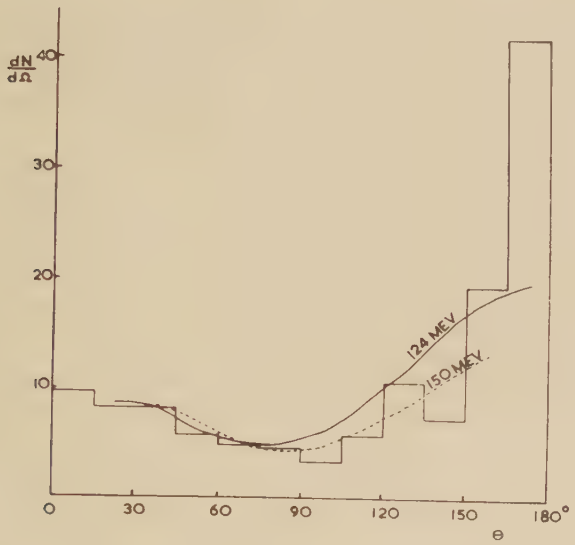

Angular distribution of the π^+-meson from the reaction

$$p+p \rightarrow n+N^* \rightarrow \pi^+ + p + n$$

in the coordinate system of the excited nucleon. The curves superimposed on the distribution represent the measured angular distributions in the C-system, of π^+-mesons from the scattering of mesons by protons at 124 and 150 MeV.

§ 5. Conclusions

The results show that the production of a single π^+-meson with a neutron and a proton predominates over all other processes and that the production of two π-mesons rarely occurs in proton–proton collisions at 925 MeV.

Whilst the topics discussed in § 4 indicate that factors other than the availability of momentum space influence the production of π^+-mesons, the predictions for the excited nucleon model are not sufficiently unique to conclude that firm experimental evidence exists for the formation of a 3/2, 3/2 state. A disturbing feature of the experimental data on π-meson production in the energy range from 600 MeV to 1·5 BeV is the lack of agreement between this experiment and that of Block *et al.* at 800 MeV. Where comparisons can be made our results at 925 MeV appear to be in general agreement with those at 650 MeV and 1·5 BeV but not that at 800 MeV. In all the experiments except the counter work at at 660 MeV the statistical accuracy of the results is low, and the marked difference between the results at 800 MeV and ours at 925 MeV could

conceivably represent extreme statistical fluctuations. The recent evolution of the hydrogen bubble chamber with its considerable advantages in the rate of collection of experimental data, should now make possible a more satisfactory study of meson production when the energy of the primary proton is in the region of 1 Bev.

Acknowledgments

We wish to express our thanks to Miss O. Archibald, Miss P. Gavigan, Miss M. J. Lewis, Mrs. E. R. Lock, Miss M. T. Parkes, Miss E. Rose and Mrs. M. Whitaker for carrying out the scanning involved, and to Mr. W. T Toner for his assistance in the analysis of the measurements.

We are indebted to Dr. R. H. Dalitz for clarifying for us many of the points raised in the discussion and to Mr. P. J. Duke, Dr. W. M. Gibson and Mr. J. G. McEwen for many conversations and to Dr. J. L. Symonds and the members of the synchrotron team for their collaboration in obtaining the exposures. We are also grateful to Dr. Quareni for permission to use the results obtained by himself and his collaborators before publication.

The authors at Glasgow wish to thank Professor P. I. Dee for his interest and encouragement, and Professor P. B. Moon for permission to take part in this research which was supported by the Department of Scientific and Industrial Research. One of us (I. S. H.) is indebted to this body for a Research Fellowship, and another (P. V. M.) to the Imperial Chemical Industries for a Research Fellowship.

APPENDIX

Procedure for Momentum and Energy Balance in Single Meson Production

If assumptions are made regarding the identity of a secondary particle, three values for its energy and momentum may be found corresponding to the observed grain density, and its maximum error (1·5 times the standard deviation in this instance).

Since the energy of the incident proton is known it is possible, using the principle of the conservation of energy, to obtain nine values for the energy of the neutral particle in the laboratory system by combining the possible values for the energy of one charged secondary with those of the other. Nine values of the momentum and angle of emission of the neutral particle were determined in a similar manner by an application of the principle of the conservation of momentum. Thus a further nine values can be obtained for the energy of the neutral particle.

In a three dimensional system with axes corresponding to the laboratory energies of the three secondary particles, the nine values for the energy of the neutral particle, obtained from energy conservation, lie on three parallel, coplanar and straight lines. The nine values obtained from momentum balance can be joined by three curves corresponding to the three straight lines obtained from energy conservation. If the curves

and the straight lines intersect then points on the line of intersection represent energies of the secondary particles for which momentum and energy are conserved for the measured angles of emission.

In fig. 9 the three straight lines, and the line of intersection LMN are shown ; for clarity the nine points obtained from momentum balance are omitted.

It was found in practice that the point of maximum probability on the line of intersection always lay on one of the straight lines, DOE or GOB in fig. 9 ; it is point M in this instance. Thus the ratio OM/OD is a measure of the probability that energy and momentum are conserved for the event.

Fig. 9

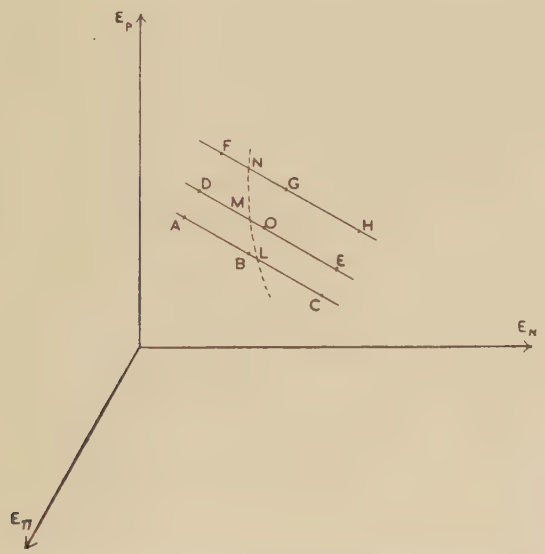

Illustration of the energy and momentum balancing technique.

In practice this procedure was modified by projecting on to a plane containing the axes representing the energy of the neutral particle and one of the charged particles. The ratio OM/OD is unaffected by the change to two dimensions. In order to obtain an acceptance criterion related to the measured quantities we define a quantity R :

$$R = \frac{|G_M - G|}{\Delta G}$$

G_M is the measured grain density for one secondary track, ΔG_M is the maximum error of this quantity and G is the grain density which the track must have if energy and momentum are conserved. Thus G_M is the grain density corresponding to an energy represented by the point O. Similarly G corresponds to the point M and ΔG_M corresponds to the length OD. The energies of the particles corresponding to the point M

are those used to obtain the ' consistency ' values of quantities in the C-system for which the distributions are plotted in the figures.

If the variation of the three values of energy of one of the charged secondary particles was small compared with that of the other, only the central value was taken and thus the nine values obtained for the energy of the neutral particle were reduced to three, so simplifying the procedure.

References

Ashkin, J., Blaser, J. P., Feiner, F., and Stern, M. O., 1956, *Phys. Rev.*, **101**, 1149.

Batson, A. P., and Riddiford, L., 1956, *Proc. Roy. Soc.* A, **237**, 175.

Berretta, L., Villi, C., and Ferrari, F., 1954, *Nuovo Cim.* (*Suppl.*), **12**, 499.

Block, M. M., Harth, E. M., Fowler, W. B., Shutt, R. P., Thorndike, A. M., Whittemore, W. L., Cocconi, V. T., Hart, E., Fowler, E. C., Garrison, J. D., and Morris, T. W., 1956, *CERN Symposium*, Vol. II, 374.

Block, M. M., 1956, *Phys. Rev.*, **101**, 796.

Cester, R., Hoang, T. F., and Kernan, A., 1956, *Sixth Rochester Conference* and private communication.

Duke, P. J., Lock, W. O., March, P. V., Gibson, W. M., McEwen, J. G., Hughes, I. S., and Muirhead, H., 1957, *Phil. Mag.*, **2**, 204.

Dzhieliopov, V. P., Moskaliev, V. I., and Miedvied, S. V., 1955, *Dokl. Akad. Nauk., S.S.S.R.*, **104**, 380.

Fermi, E., 1950, *Prog. Theor. Phys.*, **5**, 570 ; 1953, *Phys. Rev.*, **92**, 452 and **93**, 1434.

Ferrari, G., Ferretti, L., Gessaroli, R., Manaresi, E., Puppi, G., Quareni, G., Ranzi, A., Stanghellini, A., 1956, *CERN Symposium*, Vol. II, 230.

Peaslee, D. C., 1954, *Phys. Rev.*, **94**, 1084 and **95**, 1580.

Serber, R., and Rarita, W., 1955, *Phys. Rev.*, **99**, 629.

Shapiro, A. M., 1956, *Sixth Rochester Conference.*

Shapiro, A. M., Leavitt, C. P., and Chen, F. F., 1954, *Phys. Rev.*, **95**, 663.

Smith, L. W., McReynolds, A. W., and Snow, G., 1955, *Phys. Rev.*, **97**, 1186.

Tyapkin, A. A., Kozadaev, M. S., and Prokoshkin, Yu.D., 1955, *Dokl. Akad. Nauk., S.S.S.R.*, **100**, 689.

Quasi-Elastic Collisions of 925 MeV Protons†

By J. G. McEwen and W. M. Gibson
Department of Physics, Queen's University, Belfast

and P. J. Duke
Department of Physics, University of Birmingham

[Received 31 July 1956, and in revised form September 19, 1956]

Summary

Quasi-elastic collisions of protons with protons bound in nuclei have been examined in G5 emulsions exposed to 925 MeV protons from the Birmingham synchrotron.

The directions of the secondary particles have been used to obtain values for two components of the momentum of the bound protons. The observed momentum distribution may be described approximately by the function $\exp(-K/7)+0{\cdot}05\exp(-K/40)$, where K is the energy of the bound proton in MeV. The results show that $(2{\cdot}2\pm0{\cdot}3)\%$ of all nuclear reactions in the emulsion are quasi-elastic collisions with angle greater than 30° in the C-system of the two protons. This figure agrees with a calculation based on a semi-transparent nuclear model. The calculation indicates that such events contribute about 5% of the interactions with the light nuclei and about 0·7% of those with the heavy nuclei in the emulsion.

§ 1. Introduction

The search for elastic proton–proton collisions in G5 emulsion exposed to 925 MeV protons from the Birmingham synchrotron has been described by Duke *et al.* (1957). In the course of this search, measurements were made on events with only two emergent particles. Those in which the primary and secondary tracks were coplanar and at suitably related angles were considered to be elastic collisions with free protons. The events which lay close to, but definitely outside, the experimental limits for elastic scatterings were interpreted as due mainly to quasi-elastic collisions of protons with protons bound in nuclei.

In analysing these events we have assumed that since the binding energy is very small compared with the kinetic energy of the incident proton, the only difference from a free elastic collision is that the struck particle may have appreciable momentum. We have shown that the deflection of the protons while leaving the field of the nucleus is unimportant in most cases.

† Communicated by the Authors.

Quasi-elastic collisions of 340 MeV protons in light nuclei have previously been studied by Wilcox and Moyer (1955), and those of 1·4 BeV π-mesons in nuclear emulsions have been observed by Walker and Crussard (1955).

§ 2. Experimental Procedure

During the search for elastic proton–proton collisions, the angles and approximate grain densities of the tracks were measured for all disintegrations in which two charged particles were emitted (2p stars) provided :

1. Neither track was identified as due to an α-particle or heavier nucleus.

2. No sign of an additional track, however short, was seen.

For the purpose of the present analysis, only those 2p stars which satisfied three further criteria were considered :

3. The projections of the two tracks on the plane perpendicular to the direction of the incident particle made an angle greater than 90°.

4. The event was not identified as due to the reaction $p+p \rightarrow \pi^+ + d$.

5. Neither secondary track was identified from its scattering as due to a meson.

Fig. 1

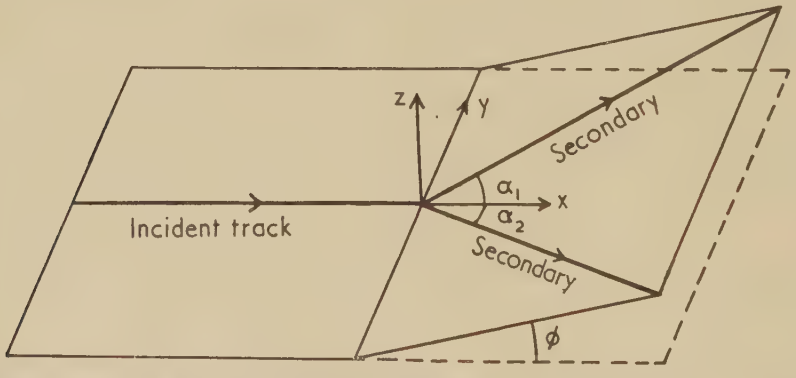

The geometry of a 2p star, showing the angles α_1, α_2 and ϕ, and the x-, y- and z-axes.

In those events which satisfied the above conditions, the measured values of the horizontal and vertical projections of the directions of the incident and emergent particles were used to give the angles shown in fig. 1, α_1, α_2 and ϕ. α_1 and α_2 are the angles between the secondary tracks and the direction of the primary. The formula for ϕ, the angle between the incident direction and the plane containing the emergent tracks, is quoted by Duke *et al.* (1957). Exact formulae were used except when a graphical method employing stereographic projection was accurate enough.

§ 3. Calculations

Separate calculations have been made of the effect of the three components of the momentum of the struck proton on the direction of the emergent protons.

If the three tracks are not coplanar, this may be attributed to a component of momentum of the struck proton, perpendicular to the incident proton direction and in the plane perpendicular to that of the two emergent particles, equal to $p_z = p_{\text{inc}} \tan \phi$; p_{inc} is the momentum of the incident particle.

Fig. 2

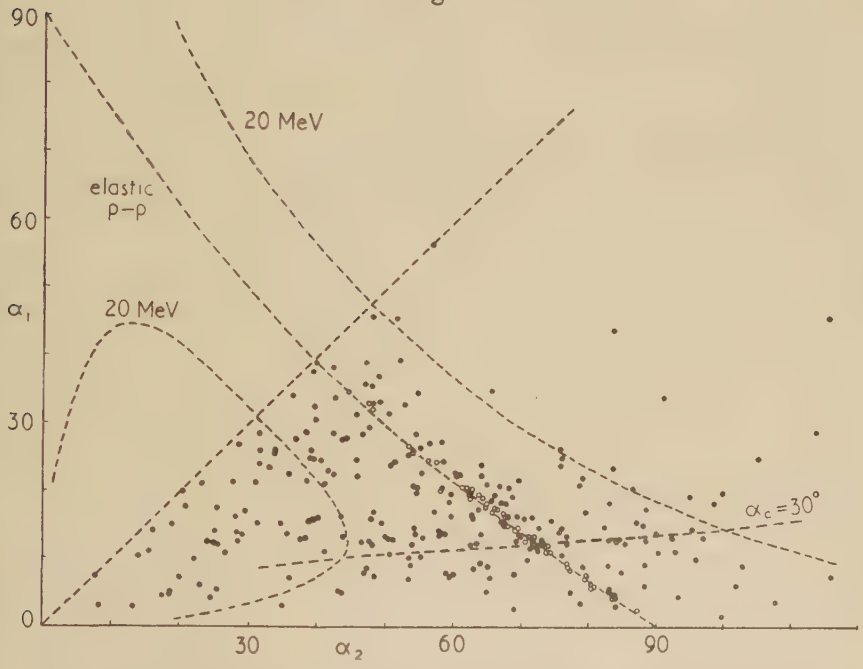

The values of α_1 and α_2 for all 2p events which satisfy the criteria in § 2 and have ϕ less than 7° ; the dotted curves show the angles calculated for elastic p–p events and for quasi-elastic events with $p_x = \pm 0{\cdot}12 p_{\text{inc}}$; the line corresponding to angles α_c of 30° and 150° for the two protons in their centre-of-mass system is drawn also. Open circles represent events considered to be elastic.

A component of momentum p_x, parallel to the incident direction, causes both values of α to decrease (or increase if p_x is negative) : fig. 2 shows curves giving the relation between α_1 and α_2 in the case of quasi-elastic collisions of protons with protons of $p_x = \pm 0{\cdot}12 p_{\text{inc}}$. This momentum corresponds to a kinetic energy of 20 Mev for the struck protons, in one direction or the other. The value of p_x for each accepted

event was obtained by interpolation between curves of this type, or where p_x is small by the approximate formula

$$p_x = p_{\text{inc}} \frac{T(1-ET/2)}{\tan^2\alpha_1 + \tan^2\alpha_2 + (E-2)T + ET^2} ,$$

$T = \tan\alpha_1 \tan\alpha_2$, and E is the total energy of the system measured in units of the rest-mass of the proton.

Fig. 3

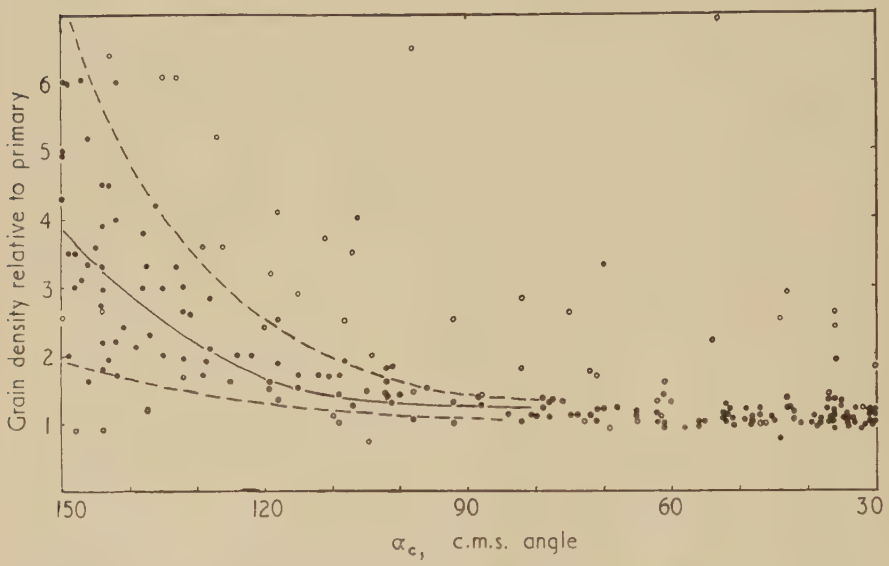

Grain density of individual tracks in 2p stars with $\phi < 7°$ and $|p_x| < 0{\cdot}12 p_{\text{inc}}$; α_c is the centre-of-mass angle obtained by assuming that the event is a quasi-elastic collision. The full curve gives the grain density for elastic collisions, while the broken curves give values for quasi-elastic collisions with $p_y = \pm 0{\cdot}12 p_{\text{inc}}$. Open circles refer to events rejected because the grain density of at least one track falls outside the limits $p_y = \pm 0{\cdot}24 p_{\text{inc}}$.

A component p_y, perpendicular to the incident proton direction, and in the plane of the two emergent protons, tends to increase one angle and decrease the other. Within the region of C-system angle considered, the effect can be distinguished from those of other components only by measurements of the energies of the secondary particles. To a good approximation the grain densities of the secondaries of a quasi-elastic collision depend only on p_y and on their angles in the C-system; fig. 3 shows the curves for quasi-elastic collisions with zero p_y, and for p_y corresponding to an energy of 20 MeV. In principle the distribution of p_y could be obtained from the energies, but experimental errors in the grain densities are too large for this measurement to be significant.

The C-system for a particular quasi-elastic collision is the system in which the centre of mass of the incident proton and the moving struck proton is stationary. The angle α_c of emission of two protons in this system may be obtained from their directions α_1 and α_2 in the laboratory system, though an unknown component p_y is liable to give serious uncertainty in the assigned value of α_c when $\alpha_c \ll 30°$. In practice, we have plotted lines of constant α_c on diagrams resembling fig. 2, and obtained values of α_c for individual events by interpolation.

§ 4. Treatment of Data

The problem is to separate quasi-elastic events from the background of other nuclear events which by chance have also produced two tracks : it is similar to the problem of separating the elastic p-p events from those now being considered.

In fig. 2 are plotted the values of α_1 and α_2 for all 2p events satisfying the criteria given in § 2, and with ϕ less than 7°, i.e. $|p_z| < 0{\cdot}12 p_{\text{inc}}$. Elastic p–p events lie within experimental error of the line

$$\tan \alpha_1 \tan \alpha_2 = 2/E,$$

and quasi-elastic events lie close to it. The rest, due to other processes, have angles which are not closely correlated, though small values are rather more probable. The majority of quasi-elastic events are expected to lie between the lines corresponding to $p_x = \pm 0{\cdot}12 p_{\text{inc}}$.

Figure 2 shows also a line of constant angle α_c in the C-system : α_c is 30° for one proton, 150° for the other. Provided α_c is over 30°, the values of α_1 and α_2 give a satisfactory measure of p_x which is almost independent of the existence of a component p_y. When α_c is less than 30° (or greater than 150°), the apparent value of p_x is liable to be much affected by experimental error in α_1 or α_2, by the existence of a component p_y, and by the greater probability that the slower proton, with energy of the order of 100 MeV, has suffered further deflection in crossing the potential barrier of the nucleus. Events which could correspond to quasi-elastic collisions with c.m.s. angle $< 30°$ (or $> 150°$) are therefore not considered.

The grain density of each track of a 2p star is plotted as a function of α_c : fig. 3 shows this plot for stars with $\phi < 7°$ and $|p_x| < 0{\cdot}12 p_{\text{inc}}$. If the points corresponding to both tracks of an event do not both lie within experimental error of the limits $p_y = \pm 0{\cdot}24 p_{\text{inc}}$ the event is rejected.

For the remaining events, with $\alpha_c > 30°$ and $\phi < 13{\cdot}5°$, the values of p_x are obtained from the angles α_1 and α_2 by interpolation on exact curves, or from the approximate formula given above. They are plotted in fig. 4 against the corresponding values of p_z obtained from the departure from coplanarity. The semicircle encloses all quasi-elastic events with energy of the struck proton less than 20 MeV. The ellipse corresponds approximately to the limits which are set as bounds for elastic collisions

with free protons by Duke *et al.* (1957). The axes of this ellipse give a rough measure of the limits of experimental error for each point on the diagram.

§ 5. Results

The distribution of momentum of the struck protons may be obtained from fig. 4. Circles are drawn on the p_x–p_z diagram, and the number of points per unit area is plotted in fig. 5 as a function of the proton energy obtained from the resultant momentum in the x–z plane.

Fig. 4

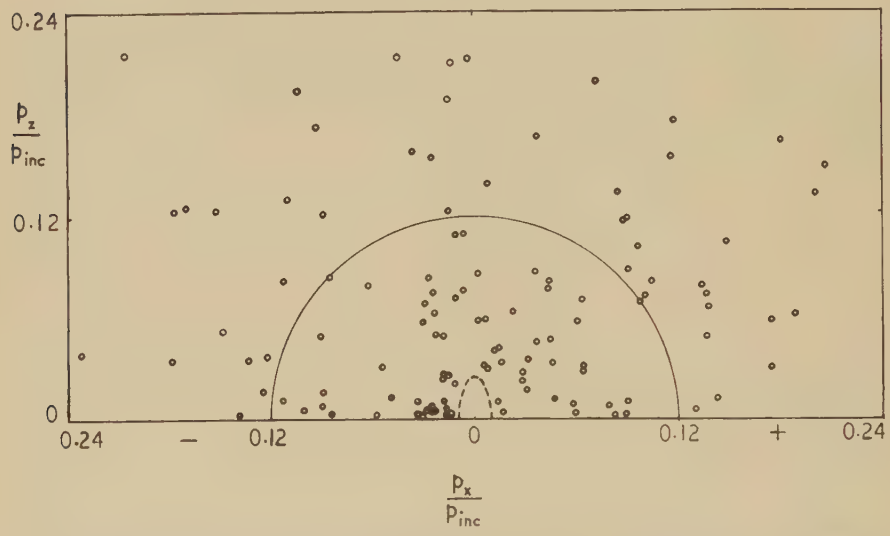

The values of p_x and p_z for events with $\alpha_c > 30°$. The semicircle encloses all events with energy of the struck proton less than 20 MeV. The ellipse encloses the elastic events, which are not plotted individually, and quasi-elastic events estimated to number four.

Apart from the quasi-elastic events, there is a background in the p_x–p_z plot which is thought to consist mainly of events in which a meson has been produced but not recognized, and a few cases where one of the protons, quasi-elastically scattered in a heavy nucleus, has suffered further deflection before emerging; almost all cases where a scattered nucleon has formed a deuteron by pick-up are excluded by the grain density criterion. In the background events there is little likelihood of coplanarity or angular correlation; to estimate their effect on fig. 5 we have assumed that they include half the events whose equivalent resultant momentum is between $0{\cdot}15p_{inc}$ and $0{\cdot}24p_{inc}$ (corresponding to energy between 30 MeV and 80 MeV) and that they are distributed uniformly over p_x and p_z. A similar result is obtained if we assume that all the events beyond $0{\cdot}24p_{inc}$ are background. The corrected numbers are shown as open circles in fig. 5.

If the momentum distribution is Gaussian, it may be described by a function $N(p_x)$ which is the probability per unit p_x of a given value of the component p_x, and

$$N(p_x)dp_x=\exp(-p_x^2/p_0^2)dp_x. \quad . \quad . \quad . \quad . \quad . \quad (1)$$

Fig. 5

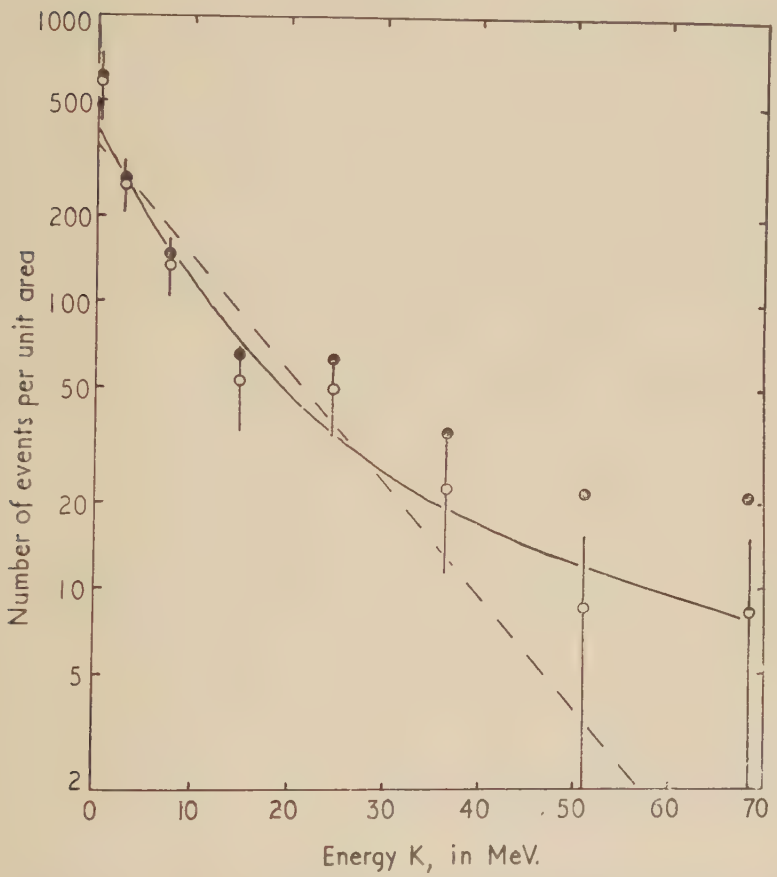

The number of points per unit area of fig. 4 plotted in arbitrary units against the energy of the struck proton. The open circles represent numbers corrected for background, and the full circles the uncorrected numbers; the probable errors of the latter are the same as those shown for the former. The full line is obtained from a probability per unit volume in momentum space proportional to $\exp(-K/7)+0{\cdot}05\exp(-K/40)$, while the broken line represents a Gaussian distribution falling to $1/e$ at $K_0=11$ MeV. The probable errors of K for individual events are about $\frac{1}{4}$ of the horizontal spacing between the points plotted.

Also the probability per unit area of a p_x–p_z plot is the same function of the resultant momentum $\sqrt{(p_x^2+p_z^2)}$:

$$N[\sqrt{(p_x^2+p_z^2)}]dp_xdp_z=\exp[-(p_x^2+p_z^2)/p_0^2]dp_xdp_z \quad . \quad . \quad (2)$$

and the probability per unit volume in momentum space is the same function of the resultant momentum $|p|$:

$$N(|p|)dp_x\,dp_y\,dp_z=\exp\left[-(p_x^2+p_y^2+p_z^2)/p_0^2\right]dp_x\,dp_y\,dp_z$$
$$=\exp\left(-K/K_0\right)dp_x\,dp_y\,dp_z, \quad . \quad . \quad . \quad . \quad . \quad (3)$$

where K is the kinetic energy of the struck proton.

Fitting an equation of form (2) to the corrected momentum distribution shown in fig. 5, we find that p_0 is a momentum corresponding to an energy $K_0=11$ MeV, with an uncertainty of ± 3 MeV resulting mainly from the correction for background events. The r.m.s. value of a single component corresponds to 5·5 MeV, which gives a mean nucleon energy of 16·5 MeV. But there is evidence that the distribution cannot be fitted by any single Gaussian curve (see § 6).

If we apply a less rigorous grain density criterion, there is no significant change in the momentum distribution obtained, but a somewhat greater uncertainty in the background.

If we take distributions of p_x and p_z separately from fig. 4, and fit equations of type (1) to them, we obtain values of p_0 which agree well with each other and with that given by the number per unit area. This gives extra confidence in the reliability of the results and the analysis.

§ 6. Discussion

Henley (1952) found that of several possibilities a Gaussian momentum distribution gave the best agreement with experimental work on π-meson production from carbon by 340 MeV protons (Richman and Wilcox 1950). The width of this distribution was chosen to give an average kinetic energy of 19·3 MeV, to fit the results of Hadley and York (1950) on deuterons formed by the pick-up of protons in carbon nuclei by 90 MeV neutrons (Chew and Goldberger 1950). Selove (1956) has examined in greater detail the pick-up of neutrons in carbon and beryllium by 95 MeV protons: the momentum distributions derived from these results in the same way appears to be the sum of two Gaussian distributions described by $\exp(-K/7)+0{\cdot}15\exp(-K/50)$.

Cladis *et al.* (1952) examined the energy spectrum of single protons, incident at 340 MeV, scattered quasi-elastically from carbon and oxygen at 40°; they found the best fit to be given by a Gaussian distribution of internal momentum, falling to $1/e$ at a momentum corresponding to about 16 MeV: the average kinetic energy of the nucleons was therefore about 24 MeV. Wilcox and Moyer (1955) detected in coincidence both protons from quasi-elastic collisions of 340 MeV protons with protons in various target nuclei, and found for beryllium a Gaussian momentum density distribution falling to $1/e$ at about 20 MeV; this gives a mean nucleon energy of 30 MeV.

Wattenberg *et al.* (1956) have fitted the nucleon momentum distributions in carbon and oxygen, which they obtained from experiments on the

photodisintegration of quasi-deuterons, to Gaussian distributions falling to $1/e$ at 19 MeV.

If our results are to be fitted to a single Gaussian distribution, this must fall to $1/e$ at 11 ± 3 MeV. The distribution found by Selove fits our results rather less well than does the single Gaussian distribution. A better fit, however, is given by a distribution of the form

$$\exp(-K/7)+0{\cdot}05\exp(-K/40).$$

It should be noted that this function gives the probability per unit volume in momentum space: since it is not a simple Gaussian function, the probability per unit area of a p_x–p_z plot is not given by the same expression: the curve shown in fig. 5 has been obtained by the appropriate transformation.

It is difficult to estimate the background correction exactly: if, as an extreme course, we make no correction whatever for background events, the best single Gaussian distribution falls to $1/e$ at about 18 MeV, and a good fit with two Gaussian distributions is given by

$$\exp(-K/7)+0{\cdot}07\exp(-K/50).$$

According to calculations based on a semi-transparent nucleus model (see Appendix), about 30% of the observed quasi-elastic events should come from the heavy nuclei in the emulsion. Thus, although the momentum distribution will refer mainly to protons in light nuclei, heavy nuclei will make a significant contribution and may be responsible for the large proportion of protons with low momentum.

The mean free path in emulsion for quasi-elastic collisions with $\alpha_c>30^\circ$ is 16 ± 2 m, compared with 0·35 m for all nuclear interactions. Thus $(2{\cdot}2\pm0{\cdot}3)\%$ of all events are observed as quasi-elastic events with angle greater than 30° in their centre-of-mass system.

Scanning efficiency has been discussed by Duke *et al.* (1957): their results show that the chief loss is among the events which we have excluded by the criterion $\alpha_c>30^\circ$. The loss of events with $\alpha_c>30^\circ$ is slight, and does not cause any significant uncertainty in the above figures; the form of the momentum distribution is quite unaffected, since there is little correlation between the probability of loss of an event and the values of p_x or p_z.

The calculations outlined in the Appendix give 1·7% as the probability that an event is a quasi-elastic collision with a single proton, with both protons escaping from the nucleus at angles between 30° and 150° in the C-system. In view of the approximations involved, the agreement between this value and that observed is satisfactory. The calculations indicate that quasi-elastic collisions contribute about 5% of the interactions with light nuclei and about 0·7% of the interactions with heavy nuclei in the emulsion.

Acknowledgments

We should like to thank Dr. W. O. Lock, Dr. H. Muirhead, Dr. R. McKeague, Dr. P. V. March and Dr. I. S. Hughes for supplying some of

the data and for much discussion, Mr. J. B. A. England for his cooperation in the absorption model calculations, and Miss O. Archibald, Mrs. S. E. Baker, Miss P. Gavigan, Miss M. J. Lewis, Mrs. E. R. Lock, Mrs. N. Palmer, Miss M. T. Parkes, Miss E. Rose, Mrs. B. R. Stephens and Mrs. M. Whitaker for most of the microscope work. We are also grateful to Dr. J. M. Wilcox of the University of California Radiation Laboratory for his very helpful comments on our results. Two of us (W.M.G. and J.G.McE.) would like to thank Professor K. G. Emeleus for his interest and assistance, and Professor P. B. Moon for allowing them to take part in this investigation, which formed part of a programme supported by the Department of Scientific and Industrial Research. One of us (P.J.D.) wishes to thank this body for a maintenance grant.

APPENDIX

Calculation of the Cross Section for Quasi-Elastic Events

By J. G. McEwen and J. B. A. England

The nucleus is assumed to behave like a uniform sphere in which the probability of a moving proton colliding with a nucleon is given by a constant coefficient as is the absorption of light in a semi-transparent medium. The probability of a particular quasi-elastic event being observed is the probability of the initial collision multiplied by the probability that each particle will escape without further collision. Calculations have been made for different types of collision at different points in the nucleus and mean values for the whole nucleus have been obtained by numerical integration. The procedure is shorter than the Monte Carlo method in this application, and could be modified to deal with other nuclear reactions at high energies in which few particles are involved.

Figure 6 represents a plane in a nucleus in which a quasi-elastic collision is assumed to take place. The incident proton travels a distance l_1 in the nucleus before making a collision, and the secondary protons travel distances l_2 and l_3 before emerging. The probability that such a collision will take place when the primary has travelled a distance between l_1 and l_1+dl_1, and that both secondaries will escape, is

$$k_1 dl_1 \exp(-k_1 l_1) \exp(-k_2 l_2) \exp(-k_3 l_3)$$

where k_1, k_2 and k_3 are the absorption coefficients in nuclear matter for the primary and secondaries respectively. It is required to integrate this expression over all parts of the nucleus where collisions could occur, the directions of the secondary particles having the appropriate angular distributions, and the plane of the primary and secondaries at any point being allowed to take all orientations.

For simplicity quasi-elastic events are treated as being coplanar and having the same angular distribution inside the nucleus as free proton–proton collisions. Since only events with C-system angle $\alpha_c > 30°$ were observed, the angular distribution was divided into four intervals of equal probability between $\alpha_c = 30$ and $\alpha_c = 90°$, and representative angles α_1 and α_2 for each interval were used in the calculation.

Fig. 6

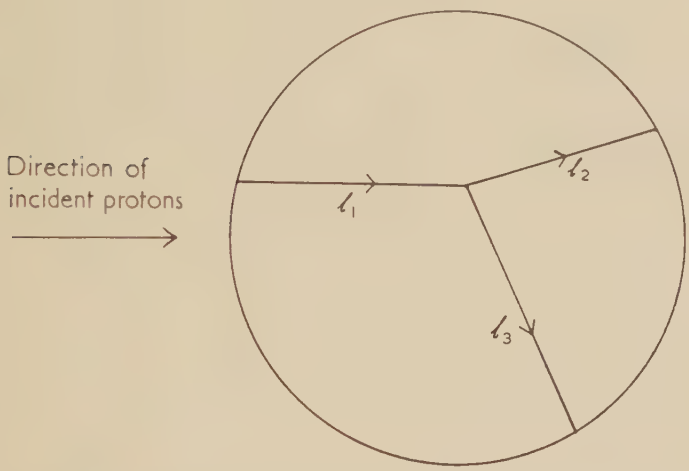

Diagram of a plane in a nucleus, containing the paths of an incident proton (length l_1) and two secondary protons (lengths l_2 and l_3).

The cross section of the nucleus projected on a plane normal to the direction of the incident protons is divided into five zones of equal area as shown in fig. 7 (*a*). The dotted circles divide each zone in half. Representative points are taken, one on each of these circles, and protons are considered incident at each point. The paths of these protons through the nucleus are shown as lines in fig. 7 (*b*).

Along each path points are taken representing intervals of equal collision probability (calculated from the absorption coefficient). The secondaries from collisions along a given path can lie with equal probability in any plane containing the path, but the probability that the secondary particles will emerge from the nucleus without further interaction varies with the position of the collision and with the angle ψ between the plane of the collision and the plane through the centre of the nucleus, i.e. the plane shown in fig. 7 (*b*).

In a given plane through a particular path, the path lengths in the nucleus l_2 and l_3 of the secondary particles from collisions along this path are measured. The collisions are considered to take place at the representative points mentioned above, unless one of them lies very near the nuclear surface.

In practice lines representing the directions of the primary and secondaries of each type of event are drawn on tracing paper and placed on the appropriate point on the proton path in the given plane as in fig. 6. Since paths in only half the plane in fig. 7 (*b*) are being considered, an equal number of events in which the angles are reversed must be used. Symmetry then limits ψ to values between 0 and $\frac{1}{2}\pi$.

Fig. 7

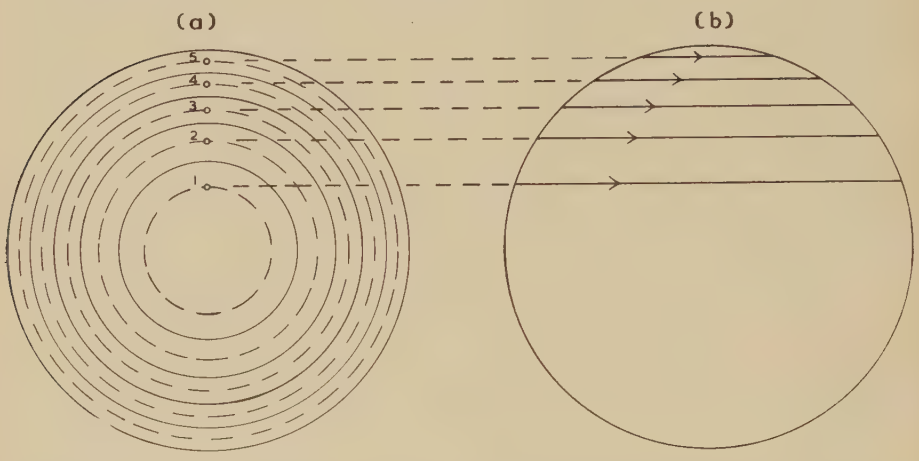

(*a*) Cross section of a nucleus, perpendicular to the incident protons, divided into five zones of equal area. (*b*) Paths through the nucleus of five incident protons, one representative of each zone.

The whole set of collisions is not used at each point. To keep the calculation reasonably short and at the same time to give it reasonable accuracy, two events were considered at each point, one with normal angles, and one with reversed. These were selected at random, within certain restrictions imposed to avoid extreme fluctuations.

The probability of escape is calculated for each collision with the absorption coefficient appropriate to each track. In the actual calculations the absorption coefficient always occurs multiplied by the nuclear radius. The value of the product used for the incident proton was that found at 860 Mev by Chen *et al.* (1955), viz. $k_1R=0{\cdot}70A^{1/3}$. The values for the secondary protons in each representative event were calculated from the known proton–free nucleon total cross sections at lower energies, with an allowance for the suppression by the Pauli principle of collisions with low momentum transfer (Goldberger 1948).

The average probability taken over all events along a given proton path in one plane varies with the angle ψ of the plane. The variation is small for paths near the centre of the nucleus but large and rapid for those near the edge. In order to obtain a reliable average probability

over all events, planes and angles, more planes were considered for the outer paths than for the inner.

For each path the average probability per collision in each plane is plotted against the angle ψ; twice the area under this curve measures the contribution from collisions along this path. The total probability of escape per collision of an incident proton in the nucleus is the average of contributions from all the paths. This total was obtained for light and heavy elements separately.

The accuracy obtained with this method is limited by the failure of the uniform model for paths too near the edge of the nucleus. The calculations for this region give a rather high probability of quasi-elastic collisions. This probability will be reduced by several effects: there is believed to be a shortage of protons near the nuclear surface (Hess and Moyer 1956): also secondary particles produced near the surface are especially likely to approach the surface at large angles of incidence, and to suffer internal reflection or refraction by the potential barrier.

To compare the results with experiment we allow for the fact that only events with $\alpha_c > 30^\circ$ were identified, by multiplying by a factor which we estimate to be 0·63. This figure includes an allowance for the suppression by the Pauli principle of collisions with low momentum transfer. Further, since only collisions in which the struck particle is a proton are observed as quasi-elastic, we multiply by Z/A. The measured values of total (elastic and inelastic) and of elastic cross sections for the collisions of protons with free protons at this energy (Chen *et al.* 1956, Smith *et al.* 1955, and Duke *et al.* 1957) show that mesons are produced in two-thirds of these interactions. With the assumption that this is also true when the struck proton is bound, the calculations give the probability that an event is a quasi-elastic collision with a single proton, with both protons escaping from the nucleus at angles between 30° and 150° in the C-system, as 5% in light nuclei and as 0·7% in heavy nuclei.

With the known composition of the emulsion and the absorption cross sections obtained by interpolating from the work of Chen *et al.* (1955) the results for light and heavy nuclei combine to give the total probability for quasi-elastic events in emulsion: this is 1·7% in the range of C-system angle considered.

References

Chen, F. F., Leavitt, C. P., and Shapiro, A. M., 1955, *Phys. Rev.*, **99**, 857; 1956, *Phys. Rev.*, **103**, 211.

Chew, G. F., and Goldberger, M. L., 1950, *Phys. Rev.*, **77**, 470.

Cladis, J. B., Hess, W. N., and Moyer, B. J., 1952, *Phys. Rev.*, **87**, 425.

Duke, P. J., Lock, W. O., March, P. V., Gibson, W. M., McEwen, J. G., Hughes, I. S., and Muirhead, H., 1957, *Phil. Mag.*, **2**, 204.

Goldberger, M. L., 1948, *Phys. Rev.*, **74**, 1269.

Hadley, J., and York, H. F., 1950, *Phys. Rev.*, **80**, 345.

Henley, E. M., 1952, *Phys. Rev.*, **85**, 204.

Hess, W. N., and Moyer, B. J., 1956, *Phys. Rev.*, **101**, 337.

Richman, C., and Wilcox, H. A., 1950, *Phys. Rev.*, **78**, 496.
Selove, W., 1956, *Phys. Rev.*, **101**, 231.
Smith, L. W., McReynolds, A. W., and Snow, G., 1955, *Phys. Rev.*, **97**, 1186.
Walker, W. D., and Crussard, J., 1955, *Phys. Rev.*, **98**, 1416.
Wattenberg, A., Odian, A., Stein, P. C., and Weinstein, R., 1956, *Bull. Amer. Phys. Soc.*, **1**, 170.
Wilcox, J. M., and Moyer, B. J., 1955, *Phys. Rev.*, **99**, 875.

Some Remarks about Electron-Correlation †

By O. Krismeent
British Council Fellow at the Cavendish Laboratory,
University of Cambridge‡

[Received June 13, 1956]

Abstract

A comparison is made between the theories of Wigner (1934), Wigner and Seitz (1934), and of Pines (1953, 1955), Bohm and Pines (1951, 1953), Pines and Bohm (1952), which both represent different approaches to an inclusion of correlation in the wave mechanical treatment of a free electron gas. Starting with a determinantal wave function for the electron gas, correlation is taken into account by means of a 'modulating' function by which the complete wave function must be multiplied. It can be shown that in both theories these modulating functions are nearly the same. A more detailed consideration of Wigner's treatment gives a 'cut-off' wavelength for the collective behaviour which is numerically nearly equal to the 'cut-off' wavelength in the theory of Bohm and Pines.

§ 1. Introduction

The Hamiltonian for a gas of N electrons is given by the expression

$$H=\sum_{i=1}^{N}(-\hbar^2/2m\cdot\Delta_i)+1/2\cdot\sum_{i,j=1}^{N}{}' e^2/r_{ij}, \quad . \quad . \quad . \quad . \quad . \quad (1)$$

where the first term denotes the kinetic operator and the second term denotes the Coulomb interaction of the electrons. The summation in the second term is over all pairs (i,j) of indices, and the prime indicates that all pairs with $i=j$ are excluded. If we build up an approximate eigenfunction corresponding to the Hamiltonian (1) by taking a product of plane waves ψ_i

$$\Psi_{\mathrm{H}}=\psi_1\ldots\psi_N \quad . \quad . \quad . \quad . \quad . \quad . \quad . \quad . \quad (2)$$

or a determinant of plane waves

$$\Psi_{\mathrm{HF}}=\det\{\psi_1,\ldots,\psi_N\} \quad . \quad . \quad . \quad . \quad . \quad . \quad . \quad (3)$$

Ψ_{H} and Ψ_{HF} are known as the solutions of the Hartree (H) or Hartree–Fock (HF) approximation. With the approximations (2) or (3), the one-electron functions ψ_i have to satisfy the Hartree or Hartree Fock equations respectively and for the Hamiltonian (1) a set of plane waves is

† Communicated by the Author.

‡ Permanent address: Max Planck Institut für Eisenforschung, Düsseldorf, West Germany.

known to give a self-consistent solution of these equations. Assuming doubly occupied levels, one for each spin, then no more than two electrons can have identical wave functions, i.e. the same wave vector for the plane waves, and those which have identical wave vectors belong to electrons of opposite spin.

Obviously the Hartree function Ψ_{H} does not include correlation, as the wave function of the ith electron is ψ_i and therefore independent of the positions of the other electrons. Some correlation is brought about by using the Hartree–Fock function Ψ_{HF}, but these correlations are purely accidental, originating from the use of the determinantal eigenfunction and not from a proper inclusion of the Coulomb interaction. As a determinant is the simplest antisymmetric combination of one-electron functions, it can also be said that these accidental correlations arise from the inclusion of the Pauli principle.

That electron correlation plays an important rôle is immediately seen by calculating the lowest eigenvalues for a free electron gas using the Hartree and Hartree–Fock approximations. In the Hartree approximation, this energy is given in atomic units by

$$E_{\mathrm{H}}=2{\cdot}21/r_s^{\,2}+1{\cdot}2/r_s \qquad . \quad . \quad . \quad . \quad . \quad . \quad . \quad (4)$$

and in the Hartree–Fock approximation

$$E_{\mathrm{HF}}=2{\cdot}21/r_s^{\,2}+1{\cdot}2/r_s-0{\cdot}916/r_s. \qquad . \quad . \quad . \quad . \quad . \quad (5)$$

Here r_s is the interelectronic spacing defined by $N \,.\, (4\pi/3) \,.\, a_0^{\,3} \,.\, r_s^{\,3}=L^3$, where a_0 is the Bohr radius and L the side of the cubical box in which the electrons are included. The first and second term in (4) and (5) are the kinetic energy and the potential energy in the field of the smeared-out charge of the electrons, while the additional term in (5) is the so-called 'exchange-energy'. Both approximations give far too high energies. According to the Hartree energy (4) no cohesion would exist in the alkali metals, and using the Hartree–Fock energy (5) the cohesion in these metals would be much weaker than actually observed. Therefore the inclusion of correlation should improve the wave function and consequently the energy. It has become a common usage to define the correlation energy as an energy gain compared to the Hartree–Fock energy, so that (5) has to be replaced by

$$E=2{\cdot}21/r_s^{\,2}+1{\cdot}2/r_s-0{\cdot}916/r_s-E_{\mathrm{corr.}} \qquad . \quad . \quad . \quad (5')$$

where $E_{\mathrm{corr.}}$ denotes the correlation energy.

§ 2. Improvement of the Wave Function

Starting with an approximation of the N-electron wave function made up by a combination of one-electron functions, for example the Hartree function Ψ_{H} or Hartree–Fock function Ψ_{HF}, it is easily seen how an improvement can be achieved. We discuss the question using the Hartree function Ψ_{H}. As in this approximation the probability density of finding two electrons (i,j) a distance $|\,\mathbf{x}_i-\mathbf{x}_j\,|$ apart is completely independent of

the distance $|\mathbf{x}_i-\mathbf{x}_j|$, an improvement of the Hartree function could obviously be achieved by modulating Ψ_{H} with a function $f(|\mathbf{x}_i-\mathbf{x}_j|)$ which has the following properties :

(*a*) $f(|\mathbf{x}_i-\mathbf{x}_j|)$ is positive for all values of $|\mathbf{x}_i-\mathbf{x}_j|$.

(*b*) $f(|\mathbf{x}_i-\mathbf{x}_j|)$ is smallest for $|\mathbf{x}_j-\mathbf{x}_j|=0$, does not decrease with increasing $|\mathbf{x}_i-\mathbf{x}_j|$ and approaches a constant value for large $|\mathbf{x}_i-\mathbf{x}_j|$.

Such a function reduces the probability density when two electrons are close together and does not affect the probability density (excluding a normalization factor) when the electrons are far apart. Furthermore it can be seen that the potential energy of the electron gas is decreased because $f(|\mathbf{x}_i-\mathbf{x}_j|)$ decreases when $1/|\mathbf{x}_i-\mathbf{x}_j|$ increases. The suggested improvement of the Hartree function then would be

$$\Psi=\Psi_{\mathrm{H}}\cdot\prod_{i,j=1}^{N}{}' f(|\mathbf{x}_i-\mathbf{x}_j|)$$

where the prime indicates that $i=j$ is excluded. The same is true if we use the Hartree–Fock function Ψ_{HF} instead of Ψ_{H}.

To determine the modulating function

$$F(\mathbf{x}_i,\mathbf{x}_j)=\prod_{i,j=1}^{N}{}' f(|\mathbf{x}_i-\mathbf{x}_j|) \quad . \quad . \quad . \quad . \quad . \quad . \quad (6)$$

the methods of Bohm and Pines and of Wigner have been used up till now. They will be dealt with more thoroughly in the next sections. Wigner does not give the modulating function explicitly but it can be derived from his results. Another attempt has been made by Mayer (1955) using the density matrix method but his results cannot be compared numerically with the other treatments.

§ 3. The Treatment of Bohm and Pines

The method of these authors (Bohm and Pines 1953, Pines 1953) can be shortly summarized as follows : By a series of canonical transformations, the Hamiltonian (1) is transformed into the sum of three Hamiltonians :

$$H=H_{\mathrm{part.}}+H_{\mathrm{coll.}}+H_{\mathrm{s.r.}} \quad . \quad . \quad . \quad . \quad . \quad . \quad . \quad (7)$$

where $H_{\mathrm{part.}}$ is defined by

$$H_{\mathrm{part.}}=-\hbar^2/2m\cdot\sum_{i=1}^{N}\Delta_i(1-N'/3N)-2\pi Ne^2\sum_{k<k_c}1/k^2$$

and describes the behaviour of independent particles, and where

$$H_{\mathrm{coll.}}=\sum_{k<k_c}\hbar\omega/2\cdot(A_k^*A_k+A_kA_k^*)$$

describes collective oscillations in the collective coordinates A_k, A_k^* and where $H_{\mathrm{s.r.}}$ corresponds to a collection of individual electrons interacting with a weak short-range force (s.r. =short range), so that $H_{\mathrm{s.r.}}$ can be neglected in a first approximation. For a complete definition for the

letters occurring above see Bohm and Pines (1953). k_c denotes the absolute value of a wave vector smaller than k_0, where k_0 is the absolute value of the wave vectors at the top of the Fermi-distribution. That means that there are just as many collective degrees of freedom as there are wave vectors smaller than k_c. The frequency of the oscillations to a first approximation is given by

$$\omega \approx \omega_P = (4\pi N e^2/m)^{1/2}.$$

Normally, these collective oscillations are not excited as their energy is far higher than the energy of an electron at the top of the Fermi-distribution, therefore the collective part of the Hamiltonian enters merely as a zero-point energy. Introducing the dimensionless parameter

$$\beta = k_c/k_0$$

which is related to the number of collective degrees of freedom N' and the number of electrons N by

$$\beta^3/6 = N'/3N,$$

Bohm and Pines determine this parameter by minimizing the total energy obtained by the splitting-off of the total Hamiltonian into an individual and a collective part.

Under these assumptions, neglecting the weak short-range part $H_{s.r.}$ of the Hamiltonian and taking subsidiary conditions imposed on the complete wave function into account, the complete wave function is found to be

$$\Psi = \Psi_{HF} \cdot \prod_{i,j=1}^{N}{}' \exp\{-g(\mathbf{x}_i - \mathbf{x}_j)/2\hbar\omega_P\}, \quad . \quad . \quad . \quad . \quad . \quad (8)$$

where $g(\mathbf{x}_i - \mathbf{x}_j)$ is given by

$$g(\mathbf{x}_i - \mathbf{x}_j) = 2\pi e^2 \cdot \sum_{|\mathbf{K}|<k_c} \exp(i\mathbf{k}(\mathbf{x}_i - \mathbf{x}_j))/k^2 \quad . \quad . \quad . \quad . \quad (9)$$

and therefore has just the same form as we have suggested in § 2.

We wish now to evaluate the modulating factor

$$f(\mathbf{x}_i - \mathbf{x}_j) = \exp(-g(\mathbf{x}_i - \mathbf{x}_j)/2\hbar\omega_P)$$

which enters the wave function (8). The argument of the exponential function can be transformed into a sine integral and we get

$$f(\mathbf{x}_i - \mathbf{x}_j) = \exp\{-(e^2/2\hbar\omega_P|\mathbf{x}_i - \mathbf{x}_j|) \cdot (2/\pi) \cdot Si(k_c|\mathbf{x}_i - \mathbf{x}_j|)\},$$

where $Si(x)$ is defined by

$$Si(x) = \int_0^x (\sin y/y)dy.$$

By setting

$$|\mathbf{x}_i - \mathbf{x}_j| = a_0 \cdot r_{ij}$$

where a_0 is the Bohr radius and introducing the values for the constants we finally obtain

$$f(r_{ij}) = \exp\{-(\tfrac{1}{2}) \cdot (\tfrac{1}{8})^{1/2} \cdot (r_s^{3/2}/r_{ij}) \cdot (2/\pi) \cdot Si((9\pi/4)^{1/3} \cdot \beta \cdot (r_{ij}/r_s))\}. \quad (10)$$

This modulating factor has the properties (*a*) and (*b*) stated in the preceding sections and plots of $f(r_{ij})$ for the interelectronic spacings $r_s=2$ and $r_s=4$ are given in figs. 1 and 2. These figures also contain the plots for the modulating functions derived from Wigner's investigations and we will deal with them in § 4. The values $r_s=2$ and $r_s=4$ are very close to the actual electronic densities found in Al and Na.

Fig. 1

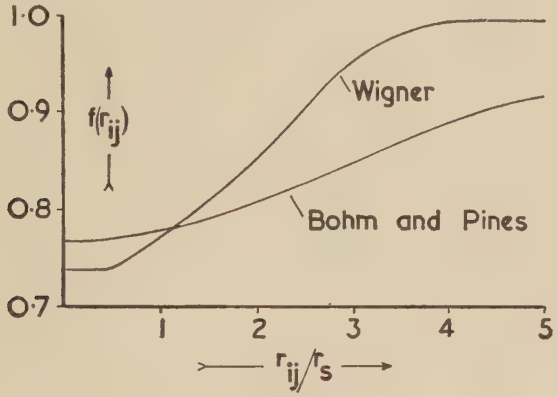

The modulating function $f(r_{ij})$ for $r_s=2$.

Fig. 2

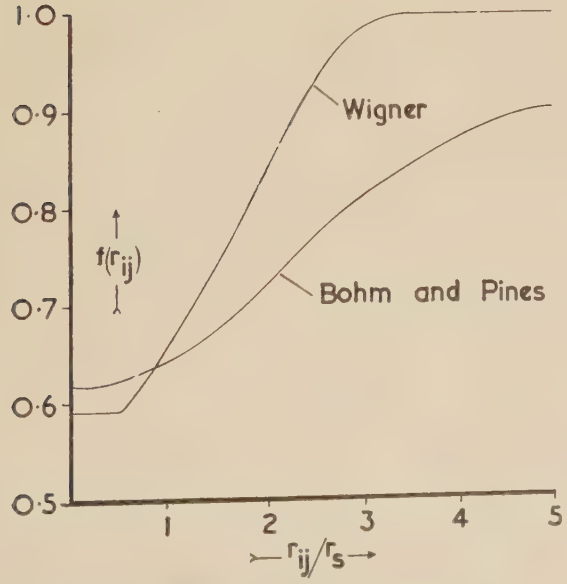

The modulating function $f(r_{ij})$ for $r_s=4$.

It is interesting to note what values the modulating function $f(r_{ij})$ takes for $r_{ij}=0$. Calculating these values from (10) we find

$$f(0)= \exp(-0{\cdot}352 \,.\, r_s^{1/2} \,.\, \beta). \quad . \quad . \quad . \quad . \quad . \quad (11)$$

The quantity β giving the 'cut-off' wavelength k_c for the collective coordinates depends on the interelectronic spacing r_s. Taking the numerical values of β given by Bohm and Pines, values of (11) have been calculated in the range $r_s=1$ to $r_s=5$. The results are given in table 1 and fig. 3.

Table 1. Values of $f(r_{ij})$ for $r_{ij}=0$ derived from Bohm and Pines' results

r_s	β	$f(0)$
1	0·428	0·86
2	0·532	0·77
3	0·612	0·69
4	0·690	0·62
5	0·736	0·56

Fig. 3

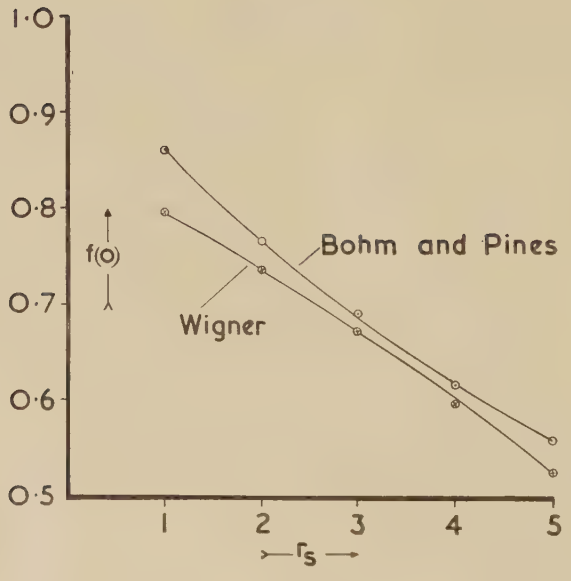

Values of $f(0)$.

From formula (11) and table 1 it can be seen that the value of the modulating factor for $r_{ij}=0$ drops to zero when the electron gas becomes very dilute and approaches unity when the density increases. In the range of actual metallic densities the factor takes an intermediate value between both extremes. For extremely high densities, the modulating

factor $f(r_{ij})$ approaches unit for all values of r_{ij} in that case electrons behave more and more like non-interacting particles.

§ 4. The Treatment of Wigner

The method of Wigner for including correlation is actually based on the application of second order Rayleigh-Schrödinger perturbation theory. For the wave function without Coulomb interaction Wigner and Seitz (1934) starts with a normalized product of two determinants made up from plane waves

$$\Psi_{\mathrm{HF}}=\frac{1}{n!}\cdot\begin{vmatrix}\psi_1(\mathbf{x}_1) & \dots & \psi_1(\mathbf{x}_n)\\ \vdots & & \\ \vdots & & \\ \psi_n(\mathbf{x}_1) & \dots & \psi_n(\mathbf{x}_n)\end{vmatrix}\cdot\begin{vmatrix}\psi_1(\mathbf{y}_1) & \dots & \psi_1(\mathbf{y}_n)\\ \vdots & & \\ \vdots & & \\ \psi_n(\mathbf{y}_1) & \dots & \psi_n(\mathbf{y}_n)\end{vmatrix}. \qquad (12)$$

The first determinant contains all electrons with upward spin and the second determinant all with downward spin, so that $N=2n$ is the total number of electrons. Such a wave function has been shown to give the same energy as a single determinant including spin functions for doubly occupied levels (Dellbrück 1930). To include correlation, Wigner (1934) assumes that correlation is brought about by the positions of all electrons with downward spin influencing every electron with upward spin. That means the wave function for the νth electron with upward spin

$$\psi_\nu(\mathbf{x})=L^{-3/2}\cdot\exp(2\pi i\boldsymbol{\nu}\mathbf{x}/L)$$

normalized in a box of sidelength L is replaced by a perturbed wave function

$$\psi_\nu(\mathbf{y}_1,\dots,\mathbf{y}_n;\ \mathbf{x})=\psi_\nu(\mathbf{y};\ \mathbf{x})=L^{-3/2}\cdot\{\exp(2\pi i\boldsymbol{\nu}\mathbf{x}/L)+\sum_\mu\alpha_{\nu\mu}\cdot\exp(2\pi i\boldsymbol{\mu}\mathbf{x}/L)\}\quad\dots\quad(13)$$

where the $\alpha_{\nu\mu}$ depend on the positions $\mathbf{y}_1,\dots,\mathbf{y}_n$ of all the electrons with downward spin and $\mathbf{y}$ is an abbreviation for the complete set $\mathbf{y}_1,\dots,\mathbf{y}_n$. The major difference in the methods of Bohm and Pines and of Wigner lies in the fact that Wigner contents himself with the accidental correlation brought about by the determinantal form of the wave function for electrons with parallel spin and introduces correlation only for electrons with opposite spin.

Carrying through the perturbation method for the determination of the $\alpha_{\nu\mu}$ in (13) Wigner (1934) finally gets for the perturbed wave function

$$\psi_\nu(\mathbf{y};\ \mathbf{x})=\psi_\nu(\mathbf{x})\cdot\{1-h_\nu(\mathbf{y}_1-\mathbf{x})-\dots-h_\nu(\mathbf{y}_n-\mathbf{x})\} \qquad (14)$$

where $h_\nu(\mathbf{y}-\mathbf{x})$ is given by

$$h_\nu(\mathbf{y}-\mathbf{x})=\sum_{\substack{2\nu-\mu\\ \text{occ.}}}\frac{\exp[2\pi i(\boldsymbol{\nu}-\boldsymbol{\mu})(\mathbf{y}-\mathbf{x})/L]}{(\boldsymbol{\mu}-\boldsymbol{\nu})^2\cdot(t_{\nu\mu}+t_{\nu\mu}')\cdot(\pi L/e^2)}+\sum_{\substack{2\mu-\mu\\ \text{unocc.}}}\frac{\exp[2\pi i(\boldsymbol{\nu}-\boldsymbol{\mu})(\mathbf{y}-\mathbf{x})/L]}{(\boldsymbol{\mu}-\boldsymbol{\nu})^2\cdot(t_{\nu\mu}+t_{\nu\mu}'+t_{\nu\mu}t_{\nu\mu}'/t_{\nu,2\nu-\mu})\cdot(\pi L/e^2)}. \qquad (15)$$

The summation in the first sum is over all wave vectors $\boldsymbol{\mu}$ of the Fermi-distribution for which $2\boldsymbol{\nu}-\boldsymbol{\mu}$ is an occupied state and in the second sum over all $\boldsymbol{\mu}$ for which $2\boldsymbol{\nu}-\boldsymbol{\mu}$ is unoccupied. The quantities $t_{\nu\mu}$ and $t_{\nu\mu}'$ are defined by

$$t_{\nu\mu}=(4\pi^2\hbar^2/mL^2)\,.\,(\boldsymbol{\mu}-\boldsymbol{\nu})\,.\,\boldsymbol{\mu}, \quad t_{\nu\mu}=(2/3\pi^2)^{1/3}\,.\,(e^2/r_s)\,.\,\epsilon'(|\boldsymbol{\mu}-\boldsymbol{\nu}|/k_0),$$

where

$$\epsilon'(\sigma)=\frac{1}{\sigma^2(1+\sigma^2/2{\cdot}56)}-\frac{0{\cdot}415}{(1+\sigma^2/2{\cdot}56)^2}-\frac{1{\cdot}465}{(1+\sigma^2/2{\cdot}56)^3}$$

and where k_0 is the absolute value of the wave vectors at the top of the Fermi-distribution. As usual, e denotes the electronic charge and r_s the interelectronic spacing.

If we replace now the unperturbed wave functions in the first determinant of the complete wave function (12) by the perturbed ones (14), we would not get a wave function which consists of the wave function (12) multiplied by a modulating factor, so that a comparison with the Bohm and Pines result and the form of our wave function in § 2 would not be possible. To make this comparison possible we have therefore adopted the following procedure: Firstly we have replaced the function $h_\nu(\mathbf{y}-\mathbf{x})$ in (15) by an averaged mean $h_{\text{av.}}(\mathbf{y}-\mathbf{x})$. Secondly after inserting these averages in (14) and (12), every term in the same column of the first determinant in (12) consists of the unperturbed plane wave multiplied with the same factor, so that these factors can be taken out of the determinant. Then the complete wave function gets the form of the unperturbed wave function (12) multiplied by a modulating factor. As already mentioned above, the Wigner treatment does not include correlation of electrons with parallel spin apart from the accidental correlations brought about by the use of the determinantal wave function. Therefore the modulating factors depend only on the differences $|\mathbf{x}_\nu-\mathbf{y}_\mu|$, where $\mathbf{x}_\nu$ is the position of the νth electron with upward spin and $\mathbf{y}_\mu$ the position of the μth electron with downward spin.

§ 5. The Average Coefficients and the 'Cut-off' Wavelength

To find the average value of the function $h_\nu(\mathbf{y}-\mathbf{x})$ in (15), averaged over all $\boldsymbol{\nu}$ of the Fermi-distribution, we look at the coefficients of

$$\frac{\exp\,(2\pi i(\boldsymbol{\nu}-\boldsymbol{\mu})\,(\mathbf{y}-\mathbf{x})/L)}{(\boldsymbol{\mu}-\boldsymbol{\nu})^2}$$

in the two sums on the right side of (15). These coefficients are either

$$c_{\nu\mu}=(t_{\nu\mu}+t_{\nu\mu}')^{-1}\,.\,(e^2/\pi L)$$

if $2\boldsymbol{\nu}-\boldsymbol{\mu}$ is an occupied state, or

$$c_{\nu\mu}'=(t_{\nu\mu}+t_{\nu\mu}'+t_{\nu\mu}\,t_{\nu\mu}'/t_{\nu,\,2\nu-\mu})^{-1}\,.\,(e^2/\pi L)$$

when $2\boldsymbol{\nu}-\boldsymbol{\mu}$ is an unoccupied state. We now sum all the coefficients $c_{\nu\mu}$ and $c_{\nu\mu}'$ for which $\boldsymbol{\mu}-\boldsymbol{\nu}$ is equal to a fixed value $\boldsymbol{\lambda}$. The vector $\boldsymbol{\lambda}$ can take all values which are smaller than or equal to $2k_0$, where k_0 is the

absolute value of a wave vector at the top of the Fermi-distribution. Without giving here full details of the rather lengthy, though elementary calculations, the summing of the $c_{\nu\mu}$ and $c_{\nu\mu}'$ for constant $\boldsymbol{\lambda}=\boldsymbol{\mu}-\boldsymbol{\nu}$ turns out to give in a good approximation

$$\sum_{\lambda=\mu-\nu} c_{\nu\mu}+\sum_{\lambda=\mu-\nu} c_{\nu\mu}'=\boldsymbol{\lambda}^2 \cdot c_\lambda=\frac{1-(\frac{3}{4})\cdot(|\boldsymbol{\lambda}|/k_0)+(\frac{1}{16})\cdot(|\boldsymbol{\lambda}|/k_0)^3}{A\cdot|\boldsymbol{\lambda}|^n k_0{}^3+\epsilon(\sigma)}\cdot\lambda^2 \quad (16)$$

where $\epsilon(\sigma)$ has been written for $\sigma^2\cdot\epsilon'(\sigma)$, $\epsilon'(\sigma)$ being the function defined in § 4, where $\sigma=|\boldsymbol{\lambda}|/k_0$ and the quantity A is given by

$$A=(3\pi/4)\cdot(2\cdot3^2\cdot\pi)^{1/3}\cdot(k_0r_s)^{-1}=9{\cdot}05/k_{0s}.$$

Introducing numerical values we get from (16)

$$c_\lambda=\frac{1-(\frac{3}{4})\cdot(|\boldsymbol{\lambda}|/k_0)+(\frac{1}{16})\cdot(|\boldsymbol{\lambda}|/k_0)^3}{(9{\cdot}05/r_s)\cdot(|\boldsymbol{\lambda}|/k_0)^4+\epsilon(\sigma)}\cdot \quad \ldots \quad (17)$$

Returning now to (15) we obtain for the average $h_{\text{av.}}(\mathbf{y}-\mathbf{x})$ of the function $h_\nu(\mathbf{y}-\mathbf{x})$, averaged over all $\boldsymbol{\nu}$

$$h_{\text{av.}}(\mathbf{y}-\mathbf{x})=\sum_\lambda c_\lambda\cdot\exp(2\pi i\boldsymbol{\lambda}(\mathbf{y}-\mathbf{x})/L) \quad \ldots \quad (18)$$

where the summation runs over all vectors $\boldsymbol{\lambda}$ for which $|\boldsymbol{\lambda}|$ is smaller than or equal to $2k_0$.

The calculation of the coefficients c_λ has been carried out for different values of the interelectronic spacing r_s. As an example the coefficients for the case $r_s=4$ which is very close to the actual interelectronic spacing in Na have been written down in table 2 and have been plotted against λ in fig. 4.

Table 2. Coefficients c_λ for $r_s=4$

$\lambda=$	$0{\cdot}125k_0$	$0{\cdot}25k_0$	$0{\cdot}375k_0$	$0{\cdot}5k_0$	$0{\cdot}6k_0$	$0{\cdot}7k_0$
$c_\lambda=$	0·94	0·93	0·93	0·99	0·8	0·6
$\lambda=$	$0{\cdot}75k_0$	$0{\cdot}8k_0$	$0{\cdot}9k_0$	$1{\cdot}0k_0$	$1{\cdot}5k_0$	$2{\cdot}0k_0$
$c_\lambda=$	0·5	0·4	0·24	0·14	0·01	0

From these data and formula (17) it is obvious that the coefficients c_λ are nearly equal to unity up to a certain wave vector and then tend towards zero with increasing $\boldsymbol{\lambda}$. This means that up to a certain wave vector the perturbation measured by the c_λ's remains constant and decreases rapidly for larger wave vectors. This behaviour of the coefficients c_λ suggests that the summation in (18) should be cut off at a fixed wave vector $\boldsymbol{\lambda}=\boldsymbol{\lambda}_c$ and the coefficients c_λ replaced by unity. This yields

$$h_{\text{av.}}(\mathbf{y}-\mathbf{x})=\sum_{|\lambda|\leq|\lambda_c|}\exp(2\pi i\boldsymbol{\lambda}(\mathbf{y}-\mathbf{x})/L) \quad \ldots \quad (19)$$

where the ' cut-off ' wavelength $\boldsymbol{\lambda}_c$ will be expressed as a fraction of the absolute value k_0 of a wave vector at the top of the Fermi-distribution.

We denote this fraction β':

$$|\boldsymbol{\lambda}_c| = \beta' \cdot k_0.$$

In this approximation we have now to determine the cut-off wavelength as a function of r_s. We have chosen for $\boldsymbol{\lambda}_c$ that value of $\boldsymbol{\lambda}$ for which the coefficients c_λ have decreased to the value 0·5 which obviously is a satisfactory assumption. This calculation has been carried out in the range of actual metallic densities and has given the values of β' plotted against r_s in fig. 5. This figure also contains the values of β in the Bohm and Pines treatment and it can be seen that the quantities β and β' which determine the 'cut-off' wavelength in both treatments have nearly the same numerical values.

Fig. 4

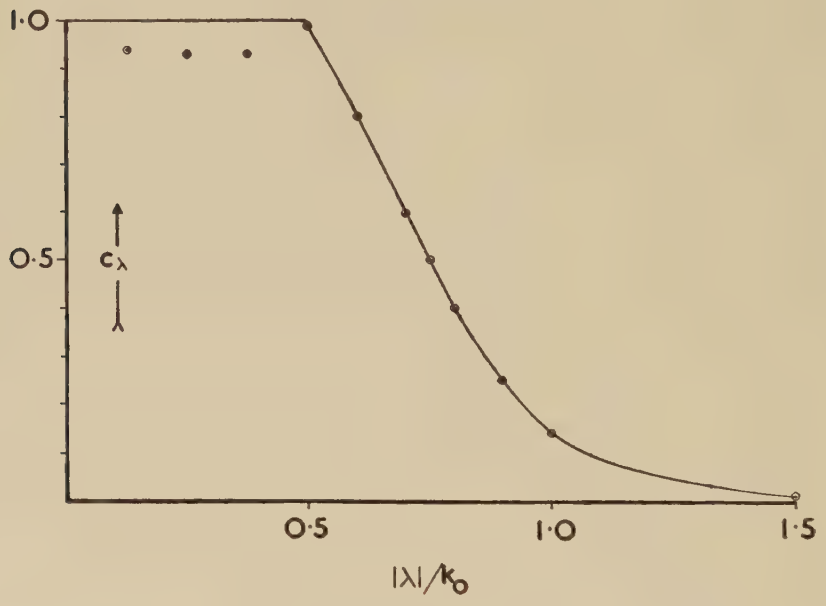

The coefficients c_λ.

§ 6. The Modulating Function

Using the approximation (19) for $h_{\text{av.}}(\mathbf{y}-\mathbf{x})$ it is now easy to perform the summation on the right side of (19). Measuring $|\mathbf{y}-\mathbf{x}|$ in multiples r of the Bohr radius a_0, $|\mathbf{y}-\mathbf{x}| = r \cdot a_0$ and by setting $r/r_s = z$ we obtain

$$h_{\text{av.}}(\mathbf{y}-\mathbf{x}) = (4/3\pi) \cdot z^{-2}\{z^{-1} \cdot \sin(2\pi \cdot 0{\cdot}306 \cdot \beta' \cdot z) - 2\pi \cdot 0{\cdot}306 \cdot \beta' \times \cos(2\pi \cdot 0{\cdot}306 \cdot \beta' \cdot z)\} \quad . \quad . \quad . \quad . \quad . \quad . \quad (20)$$

and this result immediately follows from (19) without further approximation. This function is positive everywhere, has its largest value for $r=0$ and decreases with increasing r. Remembering now formula (14) and the method of our averaging procedure, the modulating function which has to be multiplied with the starting wave function (12) and which

represents the inclusion of correlation between electrons of opposite spin is found to be

$$F(\mathbf{x}_i,\mathbf{y}_j)=\prod_{i=1}^{n}(1-h_{\text{av.}}(\mathbf{y}_1-\mathbf{x}_i)-h_{\text{av.}}(\mathbf{y}_2-\mathbf{x}_i)-\ \ldots\ -h_{\text{av.}}(\mathbf{y}_n-\mathbf{x}_i)). \quad (21)$$

In this form the modulating factor cannot be compared immediately with (6) or the Bohm and Pines result (8) ; moreover the perturbation method applied by Wigner breaks down when for one $\mathbf{x}_i$ several of the $h_{\text{av.}}(\mathbf{y}_j-\mathbf{x}_i)$ become large, i.e. when several of the differences $|\mathbf{y}_j-\mathbf{x}_i|$ become simultaneously very small for one (or several) $\mathbf{x}_i$. We therefore confine ourselves to the case when for a fixed $\mathbf{x}_i$ only one of the coordinates $\mathbf{y}_j$, let us say $\mathbf{y}_1$, comes very close to $\mathbf{x}_i$ while all the others $|\mathbf{y}_2-\mathbf{x}_i|$, . . . , $|\mathbf{y}_n-\mathbf{x}_i|$ are sufficiently large so that the corresponding $h_{\text{av.}}$ can be neglected. Taking out of the product (21) the term which contains $\mathbf{x}_i$, it can be written under the restriction just stated (which can be partly removed afterwards)

$$f(\mathbf{y}_1-\mathbf{x}_i)=1-h_{\text{av.}}(\mathbf{y}_1-\mathbf{x}_i). \quad . \quad . \quad . \quad . \quad . \quad . \quad . \quad (22)$$

This expression has to be compared with $f(r_{ij})$ given in formula (10) which has been derived from the result of Bohm and Pines.

Fig. 5

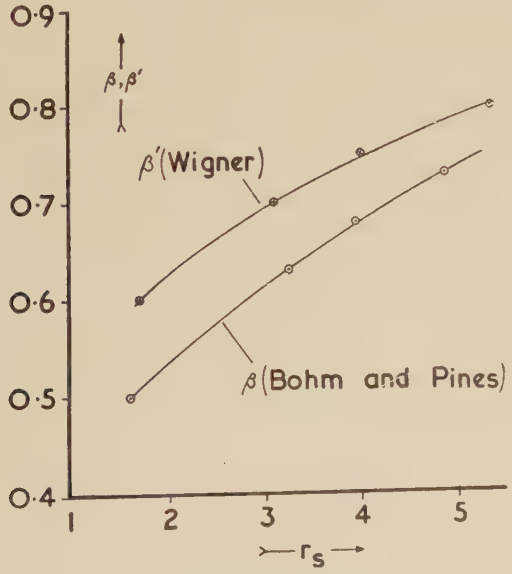

The quantities β and β'.

In the limit $|\mathbf{y}_1-\mathbf{x}_i|\to 0$ it can be easily deduced from (20) that $f(\mathbf{y}_1-\mathbf{x}_i)$ tends to

$$f(0)=\beta'^3 \quad . \quad . \quad . \quad . \quad . \quad . \quad . \quad . \quad . \quad . \quad (23)$$

and this has to be compared with the corresponding result of Bohm and

Pines given in formula (11) and table 1. Both results have been plotted against the interelectronic spacing r_s in fig. 3 and it can be seen that they nearly coincide in the range of actual metallic densities.

To complete the comparison in the case where for a fixed $\mathbf{x}_i$ just one of the differences $|\mathbf{y}_j-\mathbf{x}_i|$ becomes small while all the others are large we have plotted the complete function (22) $f(\mathbf{y}_1-\mathbf{x}_i)=f(r)$ in figs. 1 and 2 for the cases $r_s=2$ and $r_s=4$. These figures also contain the function (10) $f(r_{ij})$ derived from Bohm and Pines' work. In the range from $r=0$ to $r\approx 2$ ($r=r_{ij}$) both theories give nearly the same values for the modulating function, while for larger values of r the Wigner treatment gives higher values.

As we have already mentioned above, the Wigner treatment breaks down when for one (or several) $\mathbf{x}_i$ several of the $\mathbf{y}_j-\mathbf{x}_i$ become simultaneously very small and therefore the $h_{\text{av.}}(\mathbf{y}_j-\mathbf{x}_i)$ large, i.e. when

$$\sum_{j=1}^{n} h_{\text{av.}}(\mathbf{y}_j-\mathbf{x}_i) \quad . \quad . \quad . \quad . \quad . \quad . \quad . \quad . \quad (24)$$

becomes large. But this difficulty can be overcome to a certain extent. From the case looked at above in which just one of the $h_{\text{av.}}$ became large while all the others were negligibly small, it can be seen that the Wigner treatment represents a good approximation when

$$\sum_{j=1}^{n} h_{\text{av.}}(\mathbf{y}_j-\mathbf{x}_i)<0{\cdot}5. \quad . \quad . \quad . \quad . \quad . \quad . \quad . \quad (25)$$

The numerical value depends, of course, on the degree of approximation desired. We have therefore to deal with the case when this inequality is no longer fulfilled, i.e. when one electron comes close together with m electrons, $m>1$, of opposite spin. We have to find the modulating factor brought about by this configuration. Obviously there are two possible cases. Either the single electron has an $\mathbf{x}$-coordinate and the m electrons have $\mathbf{y}$-coordinates or *vice versa*. According to (21) the corresponding factor in the modulating function in the first case is given by

$$1-\sum_{j=1}^{m} h_{\text{av.}}(\mathbf{y}_j-\mathbf{x}_i) \quad . \quad . \quad . \quad . \quad . \quad . \quad . \quad (26)$$

and in the second case by

$$\prod_{i=1}^{m} [1-h_{\text{av.}}(\mathbf{y}_j-\mathbf{x}_i)]. \quad . \quad . \quad . \quad . \quad . \quad . \quad (27)$$

We have assumed that (25) is not fulfilled so that (26) no longer represents a good approximation. But in the range of actual metallic densities $h_{\text{av.}}$ is always $<0{\cdot}5$. Therefore (27) still represents a reasonable approximation, while (26) is no longer valid. It was just the lack of symmetry in the positional coordinates $\mathbf{x}_i$ and $\mathbf{y}_j$ of formula (21) which has enabled us to avoid the breakdown of the Wigner treatment when (24) becomes large. However, when the $h_{\text{av.}}$ involved in (26) and (27) are small, both formulae give nearly the same numerical value.

§ 7. A Classical Analogue

Although it does not mean very much we would like to mention here a relation of the modulating function with a classically defined quantity. In the case of two electrons which are the distance r apart, the corresponding term in the modulating function for $r \to 0$ is given by

$$f(0) - \beta'^3$$

in the Wigner treatment [see formula (23)] and by

$$f(0) = \exp(-0{\cdot}352 \,.\, r_s^{1/2} \,.\, \beta)$$

in the work of Bohm and Pines [see formula (11)]. The quantity $f(0)$ is related to a classically defined quantity in the following way. The mean kinetic energy of an electron in a Fermi gas is given in atomic units by

$$\epsilon_{kin} = 2{\cdot}21/r_s^2.$$

If we look at an electron of this kinetic energy as a classical particle and let it run against an electron at rest, it comes to rest at a distance r_0 (measured in multiples of the Bohr radius a_0) where the whole of its kinetic energy has been transformed into potential energy. Then the relation

$$r_0/r_s = r_s/2{\cdot}21$$

holds. If we now plot r_0/r_s against $f(0)$ for different values of the inter-electronic spacing we see that a linear relation exists between both quantities. The result has been illustrated in fig. 6.

Fig. 6

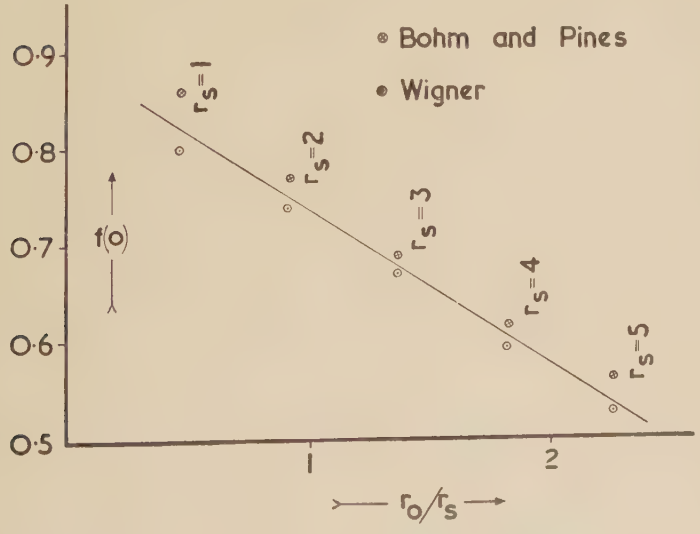

The quantity $f(0)$ and the 'hole'—radius r_0.

Acknowledgments

The author wishes to express his warmest thanks to Professor N. F Mott for kind hospitality and stimulating discussions, and to the British Council for a fellowship enabling him to carry out this work.

References

Bohm, D., and Pines, D., 1951, *Phys. Rev.*, **82,** 625 ; 1953, *Ibid.*, **92,** 609.
Dellbrück, M., 1930, *Proc. Roy. Soc.* A, **129,** 686.
Mayer, J. E., 1955, *Phys. Rev.*, **100,** 1579.
Pines, D., 1953, *Phys. Rev.*, **92,** 626 ; 1955, *Solid State Physics* (New York : Academic Press), Vol. 1.
Pines, D., and Bohm, D., 1952, *Phys. Rev.*, **85,** 338.
Wigner, E., 1934, *Phys. Rev.*, **46,** 1002.
Wigner, E., and Seitz, F., 1934, *Phys. Rev.*, **46,** 509.

Liquid Immiscibility in Metal Systems

By B. W. Mott
Atomic Energy Research Establishment, Harwell

[Received March 17, 1956 ; and in revised form June 13, 1956]

Abstract

An analysis is made of liquid immiscibility in metal systems. It is shown that the simple Hildebrand rule, which holds for non-polar liquids, can be modified to apply to metal systems, by the introduction of a new term which allows for the increased energy due to a difference in electronegativity of the components. The electronegativity term involves the maximum number of bonds which can form between two given metals, and is considered to be a function of their relative atomic sizes. On the theory suggested, out of a total of 529 alloy systems considered, 426 can be accounted for compared with 312 on the simple Hildebrand rule. Of the exceptions, several can be explained on the basis of errors in the calculation of the energy factors involved, and others can be brought into agreement on the assumption that the electronegativities of some specified elements vary with the elements with which they are alloyed. The application of the modified hypothesis to ternary systems is discussed.

§ 1. Introduction

The factors affecting the alloying behaviour of the commoner metals and metalloids have been considered in great detail in the last two decades, and for many binary metallic systems, it is possible to make reasonable estimates of the extent of the solid solubilities and likelihood of compound formation. Much of the pioneer work in this field has been carried out by Hume-Rothery, Raynor and their collaborators and their conclusions have been recently summarized (Hume-Rothery and Raynor 1954). The principal factors which govern the extent of the solid solubility of one metal in another are the difference in their atomic diameters, their relative valencies and the difference in their electro-chemical nature. If the difference in atomic size between two elements is greater than about 14%, then the strain in the lattice produced by substitution of one type of atom for the other becomes so large that the solubility range is restricted. The extent of the solubility also depends on the lattice structures of the two elements, since a marked difference in the type of bond formed in the pure metals can lead to restricted solubilities ; other conditions being satisfied,

complete mutual solubility can only occur when the components have similar crystal structures. Hume-Rothery also postulated that other conditions being equal, a metal of lower valency is more likely to dissolve one of higher valency than vice versa. This generalization is not always followed, especially in the case of polyvalent elements, and attention has to be paid to the Brillouin-zone characteristics of the solvent element. If there is a large difference in electrochemical nature between the two elements, then a strong tendency to form stable compounds can be expected and this will decrease the extent of solid solubility, even if the size factor is favourable. Compounds or stable intermediate phases are also formed in systems for which the relative atomic sizes are such that a certain type of packing is easily achieved ; the structure of the new phase may be either completely different from those of the parent lattices or based on them as in a superlattice.

In general, it can be assumed that for a system showing marked solubility in the solid state, there is no *a priori* reason for restricted solubility in the liquid condition, so that if the characteristics of two elements are such that solid solution is predicted, then no liquid immiscibility would be expected. There are many binary systems which show restricted solid solution but are miscible in all proportions in the liquid phase. This is due to two main differences between the liquid and solid states. The distribution of atoms in a liquid is less restricted than in the solid so that the liquid can accommodate atoms of different sizes more easily and hence the range of relative atomic size for complete liquid miscibility is much wider than that for solid solution. Secondly, although a high electrochemical factor can restrict solid solution, it may help to attract two elements together in the liquid state to give liquid miscibility.

The object of the present work was (*a*) to establish the requirements for complete liquid miscibility of two elements and (*b*) to suggest a working basis for the prediction of the effect of a third element on the range of immiscibility of two given elements.

§ 2. Review of Previous Work on Miscibility of Liquid Metals

Only two serious attempts to obtain a general theory of liquid metal immiscibility have been reported. Axon (1948) based his work on the relation between the size factor and the difference between the melting points of the two metals, while Hildebrand and Scott (1950) applied the relationships for immiscibility in non-polar liquids to liquid metal systems.

Axon attempted to systematize the knowledge of the factors influencing the form of binary equilibrium diagrams, and considered systems in which no intermediate phases are found, neglecting those that give complete solid solubility. The systems were of two types, viz. : those showing liquid immiscibility and a eutectic respectively. A diagram was constructed in which each system was represented by a point having co-ordinates representing a size factor and a temperature factor. These were defined as follows.

$$\text{Size factor} = \frac{(L-S)}{S} \times 100,$$

where L and S are the closest distances of approach of the larger and smaller atoms respectively in the pure elements.

$$\text{Temperature factor} = \frac{2\Delta\theta}{(\theta_1+\theta_2)}$$

where θ_1 and θ_2 are the melting points of the two metals on the absolute scale and $\Delta\theta$ is the difference between them.

The diagram obtained could be divided into three regions as illustrated in fig. 1. Region A was limited to a size factor of 30% and a temperature factor of 0·175, and only included systems of a simple eutectic type in which the eutectic composition did not vary much from 50 atm. %. For region B, representing systems having a size factor greater than 30%, all but one gave a miscibility gap. Systems in region C were approximately equally divided between the two types. For region C it was noted that the eutectic composition moved progressively away from 50 atm. % as the temperature factor increased beyond 0·175.

Fig. 1

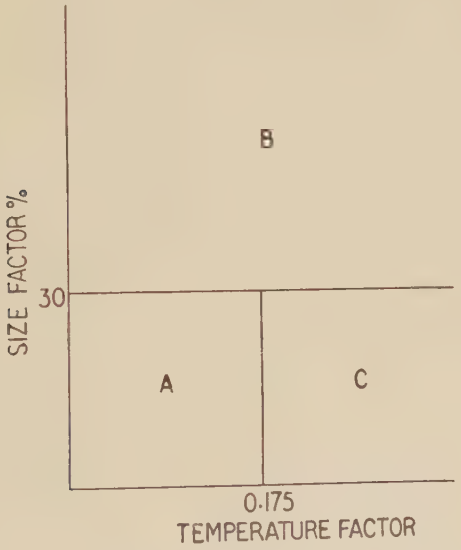

Axon's diagram for immiscible and eutectic-type metallic systems.

This approach is of interest but has been limited to about 80 binary systems of a relatively simple type, and does not include those in which liquid immiscibility has been reported over a limited region of composition. Further, no account is taken of the electrochemical nature of the elements forming the alloy and no suggestions were made of extending the analysis to ternary systems. It could be surmized from Axon's hypothesis that the range of miscibility of two metals could be increased by the addition of a third element for which both the atomic size and the melting point were

intermediate between the corresponding properties for the other two. The validity of this has not been examined.

The other general approach to the problem was that of Hildebrand and Scott (1950) who calculated that the excess free energy of formation of a liquid solution was very similar to the theoretical expression for the energy of mixing of a regular solution. The energy of mixing ΔE^M is given by

$$\Delta E^M = V\left[\left(\frac{\Delta E_A{}^V}{V_A}\right)^{1/2} - \left(\frac{\Delta E_B{}^V}{V_B}\right)^{1/2}\right]^2 \cdot \phi_A \phi_B$$

where V is the average atomic volume of the solution, V_A and V_B the atomic volumes of components A and B, $\Delta E_A{}^V$ and $\Delta E_B{}^V$ their heats of vapourization, and ϕ_A and ϕ_B the volume fractions of the two components. Hildebrand postulated that when the heat of mixing is sufficiently great, separation into two liquid phases will occur and the condition for complete miscibility was deduced as

$$\tfrac{1}{2}(V_A + V_B)\left[\left(\frac{\Delta E_A{}^V}{V_A}\right)^{1/2} - \left(\frac{\Delta E_B{}^V}{V_B}\right)^{1/2}\right]^2 < 2RT.$$

The term $(\Delta E_A{}^V/V_A)^{1/2}$ was considered to be a measure of the binding energy of component A and was called the 'solubility parameter' δ.

The condition for immiscibility therefore becomes

$$\tfrac{1}{2}(V_A + V_B)\,(\delta_A - \delta_B)^2 > 2RT.$$

This relationship proved to be a most useful guide to the behaviour of non-polar liquids. When applied to liquid metal systems, Hildebrand and Scott (1950) found that of 47 immiscible binary systems, 40 obeyed the relationship, 2 were borderline cases and 5 showed marked disagreement. On the other hand, nearly 50% of the alloys which are known to be miscible in the liquid state, would be immiscible according to Hildebrand's rule. These include many technologically important systems such as Cu–Sn, Cu–Zn, Mg–Al, Al–Zn, Al–Ni, etc. for which the nature of the equilibrium diagrams is in little doubt. Many of these exceptions to the immiscibility rule show compound formation, suggesting that there may be a relatively high electrochemical attraction between the elements which is not taken into account by the Hildebrand relationship. If a factor could be introduced into the expression to allow for the electrochemical factor, the exceptions to the simple rule might be removed. This possibility is discussed in the following sections.

§ 3. Electronegativity Concepts

There are numerous possible ways of defining the chemical affinity between two elements; the main difficulty is to find which is appropriate to the atoms in the liquid metal state. One simple method of classifying the elements is from their relative position in a table of electrode potentials but, since the potentials refer to the ions in aqueous solution, it is unlikely that these apply to liquid metals. In fact a study of various binary systems quickly revealed that the difference in electrode potential between

two metals could not be simply correlated with the behaviour of their molten alloys. Other methods of expressing electronegativities were therefore considered and included the following.

(*a*) Mulliken (1934 a, 1934 b, 1935, 1949) defined the electronegativity (X) for an univalent atom as the mean of the ionization potential I and the electron affinity E.

i.e. $X=\frac{1}{2}(I+E)$ electron volts.

There is a lack of knowledge of the values of E for various elements and Mulliken's electronegativity concept has received little application.

(*b*) From consideration of the heats of formation of halides of various elements, Pauling (1932) developed an electronegativity or X scale such that the square of the difference in the numbers assigned to any two elements $(X_A-X_B)^2$ is roughly proportional to the heat Δ accompanying the formation of a bond between them. If $D(AB)$ represents the dissociation energy of a bond between A and B, then according to Pauling:

$$D(AB)=\tfrac{1}{2}[D(AA)-D(BB)]+\Delta.$$

$\sqrt{\Delta}$ is found empirically to be additive, and X_A and X_B are chosen so that their difference is proportional to $\sqrt{\Delta}$.

(*c*) Gordy (1946) examined the electronegativity of some thirty elements as given by Pauling, and found that X could be expressed in terms of the number of valency electrons n', and the single covalent radius of the atom r according to the expression

$$X=\frac{0{\cdot}31}{r}(n'+1)+0{\cdot}50.$$

This expression can be derived by defining the electronegativity of a neutral atom as the potential Ze/r, where Ze is the effective nuclear charge of the atom acting on a valency electron at a distance r from the nucleus equal to the single-bond covalent radius of the atom. Assuming that the electrons in the closed shells exert their full screening power and those in the valency shell have a screening constant of 0·5, Z is found to be equal to 0·5 $(n'+1)$. On this basis, the electronegativity can be expressed as $[K_1(n'+1)/r+K_2]$, where both K_1 and K_2 are constants, the electronegativity scale being arbitrary. The most marked deviations from Gordy's rule were the values for copper, silver and gold when n' was taken as unity, although if the Pauling valencies for these elements are substituted in the Gordy equation, the X values agree closely with those estimated by Pauling.

When the electronegativities are recalculated from Gordy's equation using the Pauling valencies throughout, there are many marked differences with the experimental values as given by Pauling. There is no doubt that the electronegativity of a given element depends on the valency it assumes in a particular system, but there are no obvious grounds for considering the Pauling valency for some elements and not for others.

Altshuller (1954) has considered the electronegativity values for the copper, zinc and gallium series of sub-group elements as calculated by

Gordy. He suggests that the values for copper, silver and gold are too high, and those for zinc, mercury and cadmium are too low. Recalculation of the electronegativities from the dissociation energies of the homopolar halides and hydrides give the following values compared with those quoted by Gordy.

Element	Cu	Ag	Au	Zn	Cd	Hg	Ga	In	Tl
Altshuller	1·6	1·6	1·8	1·7	1·9	1·9	1·2	1·2	1·3
Gordy	2·0	1·9	3·1	1·2	1·1	1·0	1·4	1·4	1·3

(*d*) Walsh (1948) found that the force constant controlling the vibration of a diatomic hydride is roughly proportional to the square of the first ionization potential of the element, and suggested that the strength of the bond between hydrogen and a given element should be taken as a measure of electronegativity. In general, there is a reasonable relationship between the values given by Walsh and Pauling but there are differences which are most marked for elements such as Be, Mg, Hg, Si, etc. Walsh associated these exceptions with a ns^2 pair of electrons in the outer shell of the normal state of the atom, and postulated that the bond strength with hydrogen for these elements should be related, not to the ionization energy of the ground state, but to the lower energy required to ionize an electron from an excited valency state. Some support for this is obtained from a plot of the force constants of diatomic *A–O* molecules against the ionization potential of *A*. Instead of a single curve as for the *A–H* bonds, the points for each group of the Periodic Table lie on a characteristic curve. Therefore, although the hydride bond strength is a useful guide to electronegativity in some cases, it does not provide a general basis for comparison of various elements.

(*e*) Haissinsky (1946) recognized that the electronegativity of a given element will vary to some extent with the element with which it is combined; this can be appreciated from the difference in the electronegativity values derived from the oxides and bromides as compared with values obtained from the fluorides and chlorides. There will also be a tendency for the electronegativity to increase with the valency and Haissinsky deduced that this would be less marked for the metalloid elements and noble metals. From a consideration of the heats of formation of the chlorides, bromides and iodides, Haissinsky developed a series of electronegativities for a number of elements, which was extended by a process of extrapolation and interpolation from group to group and period to period of the Periodic Table. The electronegativity values are generally in good agreement with those of Pauling, the most notable exception being gold and mercury.

§ 4. Choice of Electronegativity Values

The chosen values of electronegativity for 56 elements are given in table 1 together with the source and the valency state where appropriate. For many elements, the values given by Pauling and Haissinsky are in reasonable agreement and have therefore been adopted for the present work. With few exceptions, the Haissinsky values have only been used where a Pauling figure is not available. In cases in which Haissinsky differentiates the electronegativity for various valency states of a given element, the value selected is that giving the best agreement with the data available, e.g., Mn^{II}, Mo^{VI}, Tl^{II}, V^{V} and W^{IV}; in the case of Mn, Mo and V, this corresponds to the most probable valency in alloys but the Tl^{III} and W^{VI} states are more likely than Tl^{II} and W^{IV}. The choice of electronegativity value is discussed further in later sections.

§ 5. Procedure

Data on alloy systems have been taken from various sources including Smithell's Metals Reference Book, A.S.M. Metals Handbook, Metal Abstracts and the books by Hansen (1936) and Janecke (1940) on alloy constitution. The systems have been divided into two main categories, viz. elements miscible in all concentrations in the liquid state and those in which some liquid immiscibility has been reported, whether extensive or limited to a narrow range of composition. For some immiscible systems, there is little doubt as to their authenticity but for others, either the data is contradictory or the work was carried out many years ago with relatively impure materials and inadequate techniques. Systems which may have been reported incorrectly as immiscible are therefore listed separately. For ease of classification, the systems have been tabulated according to their group in the Periodic Table.

The Hildebrand factor $\frac{1}{2}(V_A + V_B)(\delta_A - \delta_B)^2$ was estimated for each binary system from the solubility parameters of Hildebrand and Scott where available (see table 1) otherwise the parameter of a given element was calculated from the most probable heat of vapourization. The solubility parameter of the element of lower melting point was extrapolated to the temperature at which the second element melts, assuming the variation of the solubility parameter with temperature to be linear and approximately the same for elements in a given group. As a guide to the temperature variation of the solubility parameters of elements in a given group, the data given by Hildebrand and Scott (1950) were plotted and extended.

Although at normal pressure it is difficult to assign liquid immiscibility to a system in which one metal boils before the other melts, such systems have been included in the analysis, since increasing the pressure to sufficiently raise the boiling point of one element should have little effect on its solubility parameter as defined by Hildebrand. For convenience, the difference between the Hildebrand factor and the energy

Table 1. Chosen Electronegativities and Solubility Parameters (at 25°C) for Metals and Metalloids

Element valency state given where appropriate	Electro-negativity value chosen	Solubility parameter $(cal/cm^3)^{1/2}$	Element valency state given where appropriate	Electro-negativity value chosen	Solubility parameter $(cal/cm^3)^{1/2}$	Element valency state given where appropriate	Electro-negativity value chosen	Solubility parameter $(cal/cm^3)^{1/2}$
Ag	1·9P	82	In	1·4P	60	Ru	2·1H	139
Al	1·5PH	86	Ir	2·1H	139	Sb^{V}	2·1H	59
As	2·0PH	66	K	0·8PH	21	Sc	1·3H	80
Au	3·1PW	93	La	1·2P	63	Se	2·4P	35†
Ba	0·9PH	33	Li	1·0PWH	54	Si	1·8PH	88
Be	1·5PH	129	Mg	1·2PH	50	Sn^{II}	1·7PH	65
Bi	1·8PH	48	Mn	1·4H	95	Sr	1·0PH	34
Ca	1·0PWH	40	Mo	2·1PH	128	Ta	1·4H	136
Cd	1·1P	45	Na	0·9PH	33	Te	2·1PH	31†
Ce	1·1H	66†	Nb	1·8P	127	Th	1·1H	85†
Co	1·7H	126	Ni	1·7H	124	Ti	1·6PH	94
Cr^{II}	1·5H	108	Os	2·1H	144	Tl^{III}	1·9H	49
Cs	0·7H	16	Pb	1·5P	51	U	1·3H	100
Cu^{II}	2·2PW	107	Pd	2·0H	102	V^{V}	1·8H	119
Fe	1·7H	117	Pr	1·1H	64†	W^{IV}	1·6H	145
Ga	1·4P	74	Pt	2·1H	121	Y	1·3P	72
Ge	1·7PH	76	Rb	0·8PH	19	Zn	1·2P	58
Hf	1·3H	—	Re	2·2H	146	Zr	1·6P	94
Hg	1·0P	31	Rh	2·1H	129			

P, Pauling (1932); W, Walsh (1946); H, Haissinsky (1946).

† Except for those marked †, all solubility parameters taken from Hildebrand and Scott (1950).

Table 2. Data for Systems with Authentic Immiscibility

System	Hildebrand excess (cal/g mol)	Electronegativity factor (electron volts)	k
Li–Na	6,300	0·01	27·3
Li–K	24,500	0·04	26·6
Li–Rb	35,800	0·04	38·8
Li–Cs	49,000	0·09	23·6
Li–Fe	34,200	0·49	3·0
Na–Mg	1,100	0·09	0·53
Na–Ca	—(1,500)	0·01	—
Na–Zn	6,700	0·09	3·2
Na–Cd	300	0·04	0·33
Na–Al	42,000	0·36	5·1
Na–La	19,800	0·09	9·2
Na–Fe	96,400	0·64	6·5
K–Mg	17,900	0·16	4·9
K–Zn	30,600	0·16	8·3
K–Cd	11,700	0·09	5·6
K–Al	107,800	0·49	9·54
K–Pb	25,800	0·49	2·3
K–Fe	215,200	0·81	11·5
Rb–Fe	272,000	0·81	14·6
Cs–Fe	320,000	1·00	13·9
Cu–Tl	20,200	0·09	14·1
Cu–Pb	28,000	0·49	2·5
Cu–Cr	—(8,800)	0·49	—
Cu–U	—(5,100)	0·81	—
Cu–Se	50,800	0·04	55·1
Cu–Te	65,600	0·01	284·4
Cu–Co	—(2,300)	0·25	—
Ag–Ta	37,700	0·25	6·5
Ag–V	7,100	0·01	30·8
Ag–Cr	—(3,300)	0·16	—
Ag–W	66,400	0·09	32·0
Ag–U	—(1,700)	0·36	—
Ag–Se	24,700	0·25	4·3
Ag–Fe	4,700	0·04	5·1
Ag–Co	15,100	0·04	16·4
Ag–Ni	9,600	0·04	10·4
Ag–Ir	36,700	0·04	39·8
Au–Mo	7,600	1·00	0·33
Au–W	21,400	2·25	0·41
Au–Se	41,300	0·49	3·7
Be–Mg	72,400	0·09	349·0
Be–Sn	34,500	0·04	374·0
Mg–Fe	41,600	0·25	7·2
Mg–W	98,800	0·16	26·8
Ca–Cd	—(4,500)	0·01	—
Ca–W	163,400	0·36	19·7
Ca–Fe	74,400	0·49	6·6

Table 2—(*continued*)

System	Hildebrand excess (cal/g mol)	Electronegativity factor (electron volts)	k
Ba–Fe	131,000	0·64	8·9
Sr–Fe	124,000	0·49	11·0
Zn–Tl	—(2,300)	0·49	—
Zn–Pb	—(2,600)	0·09	—
Zn–Bi	—(2,000)	0·36	—
Zn–W	105,400	0·16	28·6
Cd–Al	15,600	0·16	4·2
Cd–Ga	8,800	0·09	4·2
Cd–Cr	28,000	0·16	7·6
Cd–Fe	48,100	0·36	5·8
Hg–Ga	23,400	0·16	6·3
Hg–Si	29,100	0·64	1·97
Hg–Nb	123,000	0·64	8·33
Al–In	5,700	0·01	24·7
Al–Tl	12,100	0·16	3·3
Al–Pb	10,900	0·00	∞
Al–Bi	15,500	0·09	7·5
La–Ti	18,000	0·16	4·9
La–Mn	15,500	0·04	16·8
Ga–Tl	6,200	0·25	1·1
Ga–Pb	4,900	0·01	21·2
Ga–Bi	8,200	0·16	2·2
Ga–Te	28,900	0·49	2·6
In–Te	14,700	0·49	1·3
Tl–Si	10,900	0·01	43·4
Tl–Ge	7,300	0·04	7·9
Tl–As	2,300	0·01	10·0
Tl–Se	3,900	0·25	0·68
Tl–Te	4,700	0·04	5·1
Tl–Mn	22,700	0·25	3·9
Tl–Fe	41,300	0·04	44·8
Tl–Co	62,400	0·04	67·6
Tl–Ni	50,300	0·04	54·5
Th–U	—(4,500)	0·04	—
Si–Pb	10,500	0·09	5·1
Si–Bi	15,700	0·00	∞
Sn–Cr	3,300	0·04	3·6
Sn–W	72,800	0·01	3156·0
Sn–Fe	18,600	0·00	∞
Pb–Zr	21,500	0·01	93·2
Pb–Cr	19,500	0·00	∞
Pb–Se	5,300	0·81	0·28
Pb–Mn	20,200	0·01	87·6
Pb–Fe	40,100	0·04	43·5
Pb–Co	63,300	0·04	68·6
Pb–Ni	50,900	0·04	55·2
Bi–Cr	26,900	0·09	13·0

Table 2—(*continued*)

System	Hildebrand excess (cal/g mol)	Electronegativity factor (electron volts)	k
Bi–Se	1,500	0·36	0·18
Bi–Mn	27,300	0·16	7·4
Bi–Fe	51,000	0·01	221·2
Bi–Co	78,200	0·01	349·1
U–Ce	8,500	0·04	9·2

Table 3. Data for Miscible Systems

Alloy system	Hildebrand excess (cal/g mol)	Electronegativity factor (electron volts)	k
Li–Cu	24,100	1·44	0·73
Li–Ag	30,500	0·81	1·6
Li–Hg	4,300	0·00	∞
Li–Al	8,100	0·25	1·4
Li–Sn	900	0·49	0·08
Na–K	2,700	0·01	11·7
Na–Rb	6,300	0·01	27·3
Na–Cs	12,100	0·04	13·1
Na–Au	60,100	4·84	0·52
Na–Ga	28,400	0·25	4·9
Na–Tl	3,700	1·00	0·16
Na–Ge	28,100	0·64	1·9
Na–Sn	19,800	0·64	1·3
Na–Pb	6,000	0·36	0·72
Na–Sb	12,900	1·44	0·39
Na–Bi	4,300	0·81	0·23
K–Tl	22,400	1·21	0·80
K–Sn	58,000	0·81	3·1
K–Sb	42,400	1·69	1·1
K–Bi	22,100	1·00	0·96
Rb–Hg	3,800	0·04	4·1
Cs–Hg	8,400	0·09	4·0
Cu–Mg	31,500	1·00	1·37
Cu–Ca	60,600	1·44	1·8
Cu–Zn	11,200	1·00	0·49
Cu–Cd	34,600	1·21	1·2
Cu–Hg	54,800	1·44	1·7
Cu–La	17,100	1·00	0·74
Cu–Ca	4,300	0·64	0·29
Cu–In	20,000	0·64	1·4
Cu–Ge	4,100	0·25	0·71
Cu–Sn	10,600	0·25	1·8
Cu–As	8,600	0·04	9·3

Table 3—(*continued*)

Alloy system	Hildebrand excess (cal/g mol)	Electronegativity factor (electron volts)	k
Cu–Sb	17,000	0·01	73·7
Cu–Bi	34,800	0·16	9·4
Cu–Ce	13,600	1·21	0·49
Cu–Pr	17,300	1·21	0·62
Ag–Be	13,500	0·16	3·7
Ag–Mg	10,000	0·49	0·9
Ag–Ca	22,800	0·81	1·2
Ag–Sr	47,000	0·81	2·5
Ag–Zn	3,900	0·49	0·35
Ag–Cd	13,800	0·64	0·93
Ag–Hg	27,900	0·81	1·5
Ag–In	800	0·25	0·14
Ag–Tl	9,200	0·00	∞
Ag–Pb	7,100	0·16	1·9
Ag–Sb	800	0·04	0·87
Ag–Bi	10,300	0·01	44·7
Ag–Pt	16,100	0·04	17·5
Au–Be	4,100	2·56	0·069
Au–Mg	22,700	3·61	0·27
Au–Ca	44,000	4·41	0·43
Au–Zn	6,000	3·61	0·07
Au–Cd	26,300	4·00	0·29
Au–Hg	44,700	4·41	0·44
Au–La	7,600	3·61	0·09
Au–In	6,400	2·89	0·10
Au–Tl	21,400	1·44	0·64
Au–Sn	3,800	1·96	0·08
Au–Pb	19,900	2·56	0·34
Au–As	2,600	1·21	0·09
Au–Sb	12,200	1·00	0·53
Au–Bi	26,700	1·69	0·68
Au–Te	52,700	1·00	2·3
Au–Co	3,400	1·96	0·08
Au–Ni	2,400	1·96	0·05
Au–Rh	6,600	1·00	0·29
Au–Pt	4,400	1·00	0·19
Au–Ce	5,200	4·00	0·06
Au–Pr	7,600	4·00	0·08
Be–Al	11,700	0·00	∞
Be–Si	8,400	0·09	4·0
Mg–Sr	1,200	0·04	1·3
Mg–Ba	2,600	0·09	1·3
Mg–Hg	500	0·04	0·54
Mg–Al	11,000	0·09	5·3
Mg–Ga	5,700	0·04	6·2
Mg–Si	15,900	0·36	1·9
Mg–Ge	6,800	0·25	1·2

Table 3—(*continued*)

Alloy system	Hildebrand excess (cal/g mol)	Electronegativity factor (electron volts)	k
Mg–Mn	24,200	0·04	26·3
Mg–Co	62,200	0·25	10·8
Ca–Al	24,300	0·25	4·2
Ca–Si	33,900	0·64	2·3
Ca–Sn	6,700	0·49	0·59
Sr–Al	49,700	0·25	8·6
Sr–Sn	22,700	0·49	2·0
Sr–Pb	5,200	0·25	0·9
Ba–Al	59,600	0·36	7·2
Ba–Sn	28,800	0·64	2·0
Ba–Pb	8,300	0·36	1·0
Zn–Hg	6,600	0·04	7·2
Zn–Al	4,400	0·09	2·1
Zn–Ti	7,400	0·16	2·0
Zn–Zr	14,100	0·16	3·8
Zn–Ge	6,900	0·25	1·2
Zn–Cr	12,800	0·09	6·2
Zn–Te	8,900	0·81	0·48
Zn–Mn	10,200	0·04	11·0
Zn–Fe	23,600	0·25	4·1
Zn–Co	34,000	0·25	5·9
Zn–Ni	31,900	0·25	5·5
Zn–Pt	39,500	0·81	2·1
Cd–Hg	300	0·01	1·3
Cd–In	1,300	0·09	0·63
Cd–Sn	4,700	0·36	0·57
Cd–As	3,900	0·81	0·21
Cd–Ni	62,600	0·36	7·5
Cd–Pt	77,800	1·00	3·37
Hg–Al	31,100	0·25	5·4
Hg–Tl	6,200	0·81	0·33
Hg–Sn	18,500	0·49	1·6
Hg–Pb	8,000	0·25	1·4
Hg–Bi	6,600	0·64	0·45
Hg–Fe	68,500	0·49	6·1
Hg–Ce	24,600	0·01	106·7
Al–La	1,500	0·09	0·72
Al–Sn	600	0·04	0·65
Al–V	4,200	0·09	2·0
Al–Sb	5,100	0·36	0·61
Al–Mo	25,700	0·36	3·1
Al–W	45,000	0·01	195·0
Al–Se	28,000	0·81	1·5
Al–Te	38,200	0·36	4·6
Al–Fe	2,200	0·04	2·4
Al–Co	9,100	0·04	9·9
Al–Ni	7,700	0·04	8·3

Table 3—(*continued*)

Alloy system	Hildebrand excess (cal/g mol)	Electronegativity factor (electron volts)	k
Al–Pt	11,300	0·36	1·4
Al–Ce	1,800	0·16	0·49
Al–Pr	400	0·16	0·11
La–Ni	37,000	0·25	6·4
Ga–Ni	12,600	0·09	6·1
In–Zr	2,500	0·04	2·7
Tl–Pt	64,100	0·04	69·5
Ti–Nb	3,700	0·04	4·0
Ti–Ta	20,200	0·04	21·9
Ti–Mo	8,000	0·25	1·4
Ti–W	22,200	0·00	∞
Ti–Co	900	0·01	3·9
Zr–Sn	2,700	0·01	11·7
Zr–Nb	4,100	0·04	4·4
Zr–Mo	9,000	0·25	1·6
Zr–Sb	17,400	0·25	3·0
Zr–Ru	19,600	0·25	3·4
Th–V	2,600	0·49	0·23
Th–Nb	27,700	0·49	2·5
Th–Bi	27,300	0·49	2·4
Th–Se	36,200	1·69	0·93
Th–Te	43·800	1·00	1·9
Th–Fe	2,300	0·36	0·28
Th–Co	10,600	0·36	1·3
Th–Ni	8,700	0·36	1·0
Si–Ta	29,500	0·16	8·0
Si–Sb	4,900	0·09	2·4
Si–Mo	16,000	0·09	7·7
Si–Co	7,700	0·01	33·4
Si–Ni	5,000	0·01	21·7
Si–Ce	900	0·49	0·08
Ge–Bi	3,200	0·01	13·9
Ge–Te	28,600	0·16	7·8
Ge–Fe	3,600	0·00	∞
Ge–Co	9,600	0·00	∞
Ge–Ni	7,600	0·00	∞
Sn–Pb	1,000	0·04	1·1
Sn–Bi	3,200	0·01	13·9
Sn–U	7,400	0·16	2·0
Sn–Te	19,900	0·16	5·4
Sn–Mn	4,700	0·09	2·3
Sn–Co	31,700	0·00	∞
Sn–Ni	29,100	0·00	∞
Sn–Pt	33,100	0·16	9·0
Pb–Te	5,700	0·36	0·69
Pb–Pd	24,100	0·25	4·2
Pb–Pt	66,800	0·36	8·0

Table 3—(*continued*)

Alloy system	Hildebrand excess (cal/g mol)	Electronegativity factor (electron volts)	k
V–W	2,700	0·04	2·9
Nb–U	3,400	0·25	0·59
Ta–U	12,500	0·01	54·2
As–Mn	2,600	0·36	0·31
As–Fe	14,200	0·09	6·8
As–Co	12,200	0·09	5·9
As–Ni	19,900	0·09	9·6
As–Pt	29,100	0·01	126·0
Sb–Cr	18,300	0·36	2·2
Sb–Se	10,000	0·09	4·8
Sb–Te	10,700	0·00	∞
Sb–Mn	13,500	0·49	1·2
Sb–Fe	32,600	0·16	8·8
Sb–Co	48,600	0·16	13·2
Sb–Ni	45,600	0·16	12·4
Sb–Pd	16,700	0·01	72·4
Sb–Pt	57,000	0·00	∞
Bi–U	28,800	0·25	5·0
Bi–Ni	65,600	0·01	284·0
Bi–Rh	81,000	0·09	39·0
Bi–Pd	21,900	0·04	23·7
Cr–W	6,700	0·01	29·1
Cr–Re	7,300	0·49	0·65
Cr–Ir	8,800	0·36	0·82
Mo–U	8,000	0·64	0·54
W–U	23,100	0·09	11·1
W–Pd	5,100	0·16	1·4
Se–Fe	57,400	0·49	5·1
Fe–Ce	27,600	0·36	3·3
Co–Ce	38,800	0·36	4·7
Ni–Ce	35,700	0·36	4·3
Ni–Pr	38,900	0·36	4·7

Table 4. Data for Systems of Doubtful Immiscibility

Alloy system	Hildebrand excess (cal/g mol)	Electronegativity factor (electron volts)	k
Na–Ag	35,900	1·00	1·6
Cu–V	−(6,900)	0·16	—
Cu–Mo	−(800)	0·01	—
Cu–W	3,200	0·36	0·39
Cu–Fe	−(6,200)	0·25	—
Ag–Ba	52,000	1·00	22·5

Table 4—(*continued*)

Alloy system	Hildebrand excess (cal/g mol)	Electronegativity factor (electron volts)	k
Ag–Ti	—(5,900)	0·09	—
Ag–Mo	39,800	0·04	43·1
Ag–Te	37,300	0·04	40·4
Ag–Mn	—(3,200)	0·25	—
Be–U	3,300	0·04	3·6
Mg–La	400	0·00	∞
Mg–U	29,200	0·01	126·6
Mg–Ni	52,600	0·25	9·1
Zn–Se	5,200	1·44	0·16
Cd–Si	11,900	0·49	1·1
Cd–Se	100	1·21	0·004
In–Si	3,900	0·16	1·1
Sn–Se	13,800	0·49	1·2
Pb–W	131,000	0·01	56·8
Pb–U	25,800	0·04	28·0
As–Te	21,400	0·01	92·8

term $2RT$ (where T^0 absolute is the melting point of the more refractory component) for each system will be termed the 'excess Hildebrand factor' and this quantity has been listed for immiscible, miscible and doubtful systems in tables 2, 3 and 4. Miscible systems for which the Hildebrand rule holds, i.e., where excess Hildebrand factor is considered to be negative, have not been included in the tables. There are a few immiscible metal systems in which the excess Hildebrand factor is negative; these have been listed for completeness in table 2.

§ 6. Results of Plotting the Excess Hildebrand Factor against Electronegativity

If it is assumed that the failure of the Hildebrand rule when applied to metal systems is due to an electronegativity factor, then immiscibility would only be expected for a high excess Hildebrand factor with a low electronegativity. Conversely, if the electronegativity were high, then in general, this would counteract a high excess Hildebrand factor, and miscibility would be obtained. To test this hypothesis, the electronegativity against excess Hildebrand factor has been plotted in fig. 2 for low values of these parameters and in fig. 3 for the remaining ranges.

Undoubtedly, although there are several exceptions, the dots representing immiscible systems tend to lie above the crosses representing miscible alloys. An arbitrary line has been drawn through the origin in figs. 2 and 3, which divides each diagram so that there is a greater number of dots in the top left-hand portion and a greater number of crosses in the

bottom right-hand corner. The slope of the dividing line in each diagram could vary over a fairly wide range without markedly affecting the relative distribution of miscible and immiscible systems. Accepting that the assumptions are correct, it is profitable to examine the significance of the slope of this line.

Fig. 2

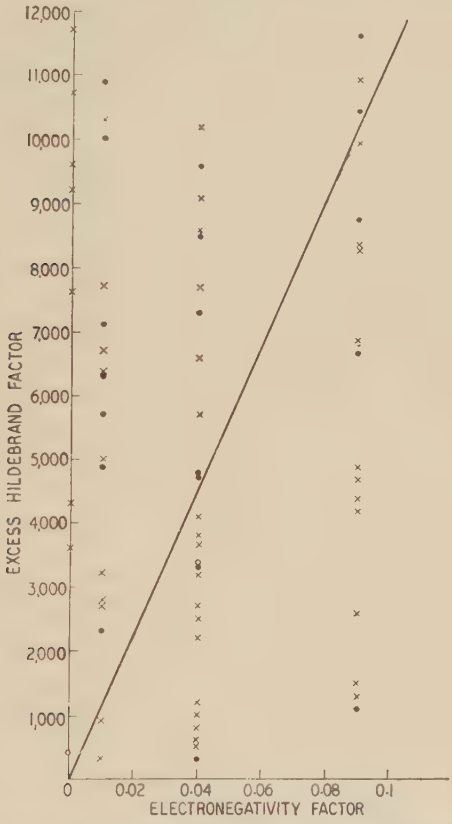

Plot of excess Hildebrand factor against electronegativity factor (low values).

§ 7. Suggested Modification to Hildebrand's Hypothesis

According to Hildebrand, immiscibility in non-polar liquids should occur if

$$\tfrac{1}{2}(V_A+V_B)\,(\delta_A-\delta_B)^2>2RT.$$

On the present theory, for metallic systems in which there is an electronegativity factor, it is necessary to introduce a new term E_B, which represents the binding energy, so that the condition for immiscibility becomes

$$\tfrac{1}{2}(V_A+V_B)\,(\delta_A-\delta_B)^2-E_B>2RT.$$

The binding energy, E_B which is required for the above expression is the combined energy of all the bonds which can form between the two elements. A simple picture of a bond is not possible as resonance always occurs to

some extent between the various types which include ionic, covalent and metallic. If however the mean fraction of each type of bond is represented by f_I, f_C and f_M respectively and E_I, E_C and E_M are the energies associated with one bond if wholly of one type, then the binding energy for n bonds is given by

$$n(f_I E_I + f_C E_C + f_M E_M).$$

Fig. 3

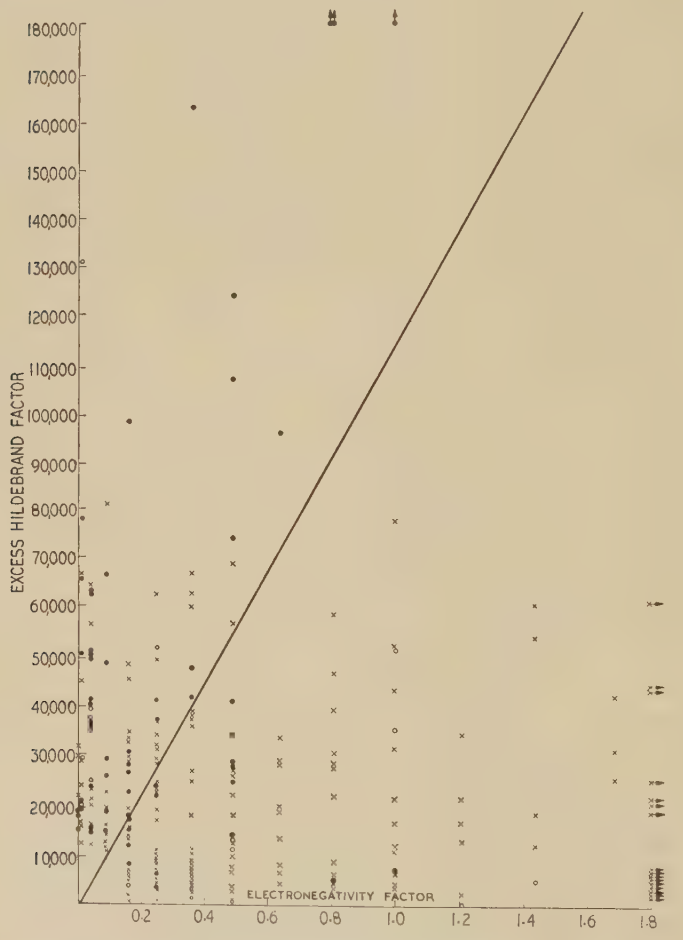

Plot of excess Hildebrand factor against electronegativity factor (high values)

At the moment, there appears to be no accurate method of assessing the energy E_M, associated with a metallic bond but it is generally considered that it is more closely related to the covalent than the ionic bond. If, as a first approximation, we can assume $E_C = E_M$ then the expression for the binding energy becomes

$$E_B = n[E_C(f_C + f_M) + f_I E_I].$$

By definition, $f_I+f_M+f_C=1$, so that the above expression can be rewritten

$$E_B=n[E_C(1-f_I)+f_IE_I].$$

If this represents the covalent-ionic resonance energy of n bonds then by definition (see Pauling), it is approximately equal to $(X_A-X_B)^2$; so that

$$E_B\approx n(X_A-X_B)^2 \text{ electron volts}$$

or 23 060 n $(X_A-X_B)^2$ calories/g.

Thus to a first approximation, the condition for immiscibility becomes

$$\tfrac{1}{2}(V_A+V_B)(\delta_A-\delta_B)^2-23\,060\,n(X_A-X_B)^2>2\,RT.$$

Rearranging this expression, immiscibility may be expected if

$$\frac{\tfrac{1}{2}(V_A+V_B)(\delta_A-\delta_B)^2-2\,RT}{23\,060(X_A-X_B)^2}>n.$$

The above relationship states that if two elements can form a sufficient number of A–B type bonds, then the energy associated with bonding will counter-balance the binding energy associated with the elements as expressed by Hildebrand's solubility parameter, and liquid miscibility will occur. If two elements cannot form at least k A–B type bonds, where k is given by the expression

$$\frac{\tfrac{1}{2}(V_A+V_B)(\delta_A-\delta_B)^2-2\,RT}{23\,060(X_A-X_B)^2}$$

then the two liquids will be immiscible.

In addition to assigning a precise energy to a given bond, there is also the problem of deciding the maximum number of bonds per atom which two metals can form: i.e. the maximum value of n. Presumably the maximum number of bonds formed by a given metal is directly related to the number of electrons available for bonding, i.e. to its maximum valency. The valencies of the elements considered vary from 1 to 6 so that, as a first approximation, we can assume that if the ratio of the excess Hildebrand factor to the electronegativity factor is greater than 6, then immiscibility could be expected. On the other hand, if this ratio is less than 1, the metals should be miscible. (The arbitrary dividing lines in figs. 2 and 3 correspond to a k of about 5 which is reasonable on the above basis.) If the ratio is between 1 and 6, the type of system obtained may be affected not only by the valencies of the two elements, but also by their relative atomic sizes which will determine the possible types of packing and hence the coordination number. The upper limit for the average number of nearest neighbours for both solids and liquids is 12 (although this number may be exceeded locally) so that on the average, the maximum number of near neighbours of unlike atoms is 6, which appears to be an additional reason for choosing this as the maximum number of bonds.

The possible types of packing and hence the maximum number of bonds that can form in a given system will depend on the relative sizes of

the atoms or ions. To see if any general guide could be obtained on the effect of relative atomic size on the critical k value (which will determine whether immiscibility occurs or not), the calculated k values in the range 1 to 6 for both miscible and immiscible systems were plotted against the percentage difference in the Goldschmidt atomic diameter (based on the smaller atom). As for figs. 2 and 3, miscible systems were represented by crosses and immiscible systems by dots, and the plot is shown in fig. 4. A curve has been drawn which encloses the maximum ratio of dots to

Fig. 4

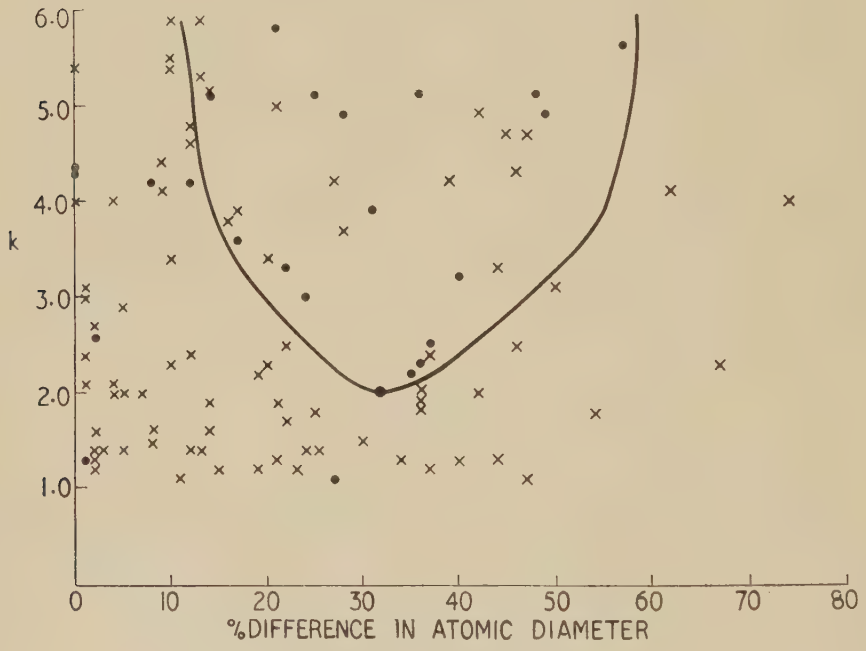

Plot of k value against difference in atomic size.

crosses, i.e. of immiscible to miscible systems. Only 7 of the 24 immiscible systems are outside and 16 out of 80 miscible systems are inside the area enclosed by the curve. Little reliance can be placed on the shape of the dividing curve since errors in both the excess Hildebrand and electronegativity factors can appreciably affect the calculated value of k. In addition, the percentage difference in atomic size has been calculated from the Goldschmidt diameters, which are estimated from the distance apart of the atoms in the pure crystalline solid. At the best, therefore, this size difference will only approximate to that appertaining to alloys in the liquid state, although the error in calculating the atomic ratio is not likely to be significant compared with other errors. The type of packing may also be affected by the relative compressibility of the atoms.

Two conclusions may be drawn from fig. 4. The critical k value appears to reach a minimum of two for a percentage difference in size of

about 33% implying that the coordination number is lowest for such systems, which is not unreasonable. It is noteworthy that only two immiscible systems have a k value between 1 and 2 whereas there are 38 miscible systems which fall into this range. Figure 4 suggests that the critical k value is 6 for systems where the difference in atomic size of the two elements is less than 10% but a size difference of from 10 to 60% appears to reduce the number of bonds that can be formed. The situation is restored again when the atomic sizes differ by more than about 60%, which is reasonable as this is the limit at which interstitial packing may occur. As discussed by Barrer (1948), the coordination number for unlike atoms in interstitial solutions can be six which could permit six bonds.

§ 8. Consideration of Exceptions

From the above discussion, a useful working basis for assessing the type of liquid equilibrium between two metals is a calculated k value of less than 2 for complete miscibility and greater than 6 for some immiscibility. If the k value is between 2 and 6, then the incidence of immiscibility also depends on the relative atomic sizes and although no rigid relationship can be given at this stage, the curve of fig. 4 can be taken as a guide. On this basis, out of a total of 529 alloy systems considered, 426 can be accounted for compared with 312 on the simple Hildebrand rule.

Detailed comparison is as follows :—

	Immiscible systems	Miscible systems
(i) Total number considered.	99	430
(ii) Number conforming to simple Hildebrand rule.	88	224
(iii) Number conforming to simple modified rule. i.e. $k>6$ for immiscibility, $k<2$ for miscibility.	57	328
(iv) Number with k from 2 to 6.	22	42
(v) Number of type (iv) conforming to size rule (fig. 4).	15	26
(vi) Total conforming to modified rule, i.e. sum of types (iii) and (v).	72	354

In addition to the above 529 systems, there were 22 for which the experimental evidence was either conflicting or insufficient to draw any definite conclusions as to the existence of liquid immiscibility (see table 4). The present theory suggests that immiscibility could be expected in the following 8 systems, Ag–Ba, Ag–Mo, Be–U, Mg–U, Pb–W, Pb–U, As–Te, and Mg–Ni. For the remaining 14 systems, the analysis indicates no immiscibility, which is in general agreement with more recent investigations.

A question to be decided is whether the exceptions to the modified rule are real or explicable by errors involved in the calculation of k. In view of the uncertainties in the experimental determination of the latent heat of vapourization of a metal and in the extrapolation of the solubility parameter to high temperatures, for many systems the value of $(\delta_A - \delta_B)$ could reasonably be in error by ± 5. The effect of this on the excess Hildebrand factor increases with increase in the difference between the solubility parameters and has been calculated for various values of $(\delta_A - \delta_B)$. Table 5 gives the maximum and minimum errors for the excess Hildebrand factor assuming a combined error of 5 in the solubility parameters.

Table 5. Errors in the Hildebrand Factor for an error of 5 in $(\delta_A - \delta_B)$

$(\delta_A - \delta_B)$	Maximum errors in Hildebrand factor (cal/g atom)	
15	+1,750	−1,250
30	+3,250	−2,750
50	+5,250	−4,750
65	+6,750	−6,250
80	+8,250	−7,750
100	+10,250	−9,750

When possible errors of this magnitude are taken into consideration, the k value of many miscible systems which appear to be exceptions can be brought into agreement although there are still some which cannot be explained on this basis. The electronegativity values are generally expressed to the nearest 0·1 electron volt so that the possible error in $(X_A - X_B)$ is $\pm 0{\cdot}1$. The effect of this error on k decreases with increase in the electronegativity factor but can be very important for small differences in electronegativity. Further, as previously discussed, the electronegativity of a given element depends on the valency it assumes and can therefore vary with the nature of the alloying element. For example, the electronic behaviour of the transitional elements is dependent on their environment and on this basis, their electronegativities cannot be represented by single numbers. Other elements whose electronegativities may change with environment include mercury, thallium, tin, lead, arsenic, antimony, and bismuth ; at the moment no satisfactory basis exists for assessing the probable variation. An additional complication which may arise, especially in the case of the transitional elements, is that when the metallic component of the bonding is large, the error introduced by assuming that the energy of a metallic bond is similar to that of a covalent bond may become significant. This may be a further reason for the large number of exceptions among the transitional elements.

§ 9. Extension of Hypothesis to Ternary Systems

It is often of technological importance to decrease the range of liquid immiscibility of a given pair of metals by alloying with a third element. There are few rules which enable one to choose the third element to any degree of certainty, but it is suggested that the modified Hildebrand hypothesis elaborated above can be used to advantage. To extend the range of miscibility of two metals A and B, the choice of the third element C should be such that its solubility parameter δ_C should preferably be in the range of δ_A - δ_B or not greatly different from δ_A or δ_B, and the electronegativity X_C should be as different as possible to X_A and X_B. Little data is available on the effect of a third element on the immiscibility range of two metals, but the following three examples from published data may be given as not inconsistent with the above hypothesis :—cadmium additions to bismuth–zinc alloys, tin to lead–zinc alloys and zirconium to uranium–thorium alloys, all of which give increased miscibility. The electronegativity values and solubility parameters at room temperature, given below for the three systems:

(*a*)		Cd	Bi	Zn
	δ	45	48	58
	X	1·1	1·8	1·2
(*b*)		Sn	Pb	Zn
	δ	65	51	58
	X	1·7	1·5	1·2
(*c*)		Zr	U	Th
	δ	94	128	85
	X	1·6	1·3	1·1

§ 10. Discussion

This theoretical analysis was made primarily to determine whether the simple Hildebrand immiscibility rule based on the concept of the solubility parameter, could be applied to metal systems, provided that due attention is paid to the decreased energy of the system arising from the difference in electronegativity of its components. Restrictions on the accuracy of the calculations were imposed by the lack of precise information on the properties which determine the solubility parameter and its variation with temperature, and by the difficulty of providing a precise figure for the electronegativity factor for a given system. Despite this, it has been shown that the idea of solubility parameter can be applied to liquid metal systems when combined with Pauling's electronegativity concept based on the binding energy of two elements. Briefly, of 88 immiscible systems which obey the simple Hildebrand rule, 72 agree with the modified hypothesis ; of 206 immiscible systems chosen because they do not agree with

Hildebrand's rule, 130 can be brought into line by allowing for electrochemical differences. Several exceptions can be explained allowing for reasonable errors in the physical constants used in the calculations or by assuming that the electronegativities of certain elements depend on the metal with which they are alloyed. The dependence of the valency on the alloying element is not new to alloy theory but at the moment, it is difficult to see on what basis one chooses the electronegativity in a given case.

A general picture of the liquid alloy state can be deduced from the above analysis. For non-polar liquids, the solubility parameter as defined by Hildebrand appears to be a satisfactory method of calculating the type of equilibrium between constituents. If two such liquids are mixed, then provided that their solubility parameters are not too different, the liquids will be mutually soluble in all proportions ; when the solubility parameters differ appreciably, a miscibility gap will be observed. Similar basic principles apply to liquid metal systems but the situation is complicated by an attraction between unlike atoms due to differences in their ionization potentials and electron affinities. Thus although the solubility parameters of two elements may be sufficiently different to give immiscibility in the absence of an electronegativity factor, if they can form enough bonds of sufficient strength, miscibility will occur. The major problem associated with this hypothesis is to determine the maximum number of bonds which can form between two given elements. If the metals have the same size, they can be packed in the same way as the pure metals and the maximum number of bonds would appear to be six. As the size difference increases, simple packing becomes more difficult, the number of close atoms of each type decreases and the number of possible bonds will decrease to two when one element is about a third as large again as the other. With further increase in the size difference to about 60%, the atoms can be packed into the interstices between the other type of atoms and the number of possible bonds is about six.

Unfortunately, in the present state of knowledge, it is not possible to predict with absolute certainty whether two metals will be miscible or immiscible in the liquid state. For a given system, the possibility of miscibility depends on the estimated value for k and the accuracy to which this can be done. If the solubility parameters and their variation with temperature, and the electronegativity values were accurately known, it would be possible to get a reliable value for k. A knowledge of the bond formation between two elements with variation in their relative size proportions would enable one, not only to predict immiscibility, but to calculate the ranges of composition and temperature over which it occurs. It is considered, however, that the above type of analysis forms the best basis available on which to estimate the possibility of immiscibility. Further, it can be used as a guide to the best choice of element to add to a given system showing immiscibility to increase the range of miscibility.

The hypothesis as suggested above obviously requires further development. No distinction has been made between systems in which the elements are virtually completely immiscible and those giving immiscibility over a narrow range only. An analysis of elements which give both limited liquid immiscibility and compounds would also be of interest. The value of the modified Hildebrand rule lies mainly in the success that can be obtained in predicting immiscibility in systems which have not been investigated experimentally.

References

Altshuller, A. P., 1954, *J. Chem. Phys.*, **22**, 765.

Axon, H. J., 1948, *Nature, Lond.*, **162**, 997.

Barrer, R. M., 1948, *Disc. Faraday Soc.*, **4**, 68.

Gordy, J., 1946, *Phys. Rev.*, **69**, 130, 604.

Haissinsky, M., 1946, *J. Phys. Rad.*, **7**, 12.

Hansen, M., 1936, *Der Aufbau der Zweistofflegierungen* (Berlin : Julius Springer).

Hildebrand, J. H., and Scott, R. L., 1950, *The Solubility of Non-Electrolytes* (New York : Rheinhold Publishing Corporation).

Hume-Rothery, W., and Raynor, G. V., 1954, *The Structure of Metals and Alloys* (London : The Institute of Metals).

Janecke, E., 1940, *Kurzgefasstes Handbuch aller Legierungen* (Berlin : Otto Spamer Verlag).

Mulliken, R. S., 1934 a, *Phys. Rev.*, **46**, 549 ; 1934 b, *J. Chem. Phys.*, **2**, 782 ; 1935, *Ibid.*, **3**, 573 ; 1949, *Ibid.*, **46**, 497.

Pauling, L., 1932, *J. Amer. Chem. Soc.*, **54**, 3570.

Walsh, A. D., 1948, *J. Chem. Soc.*, Part I, 398.

CORRESPONDENCE

On the Naor Relations between Madelung Constants for Cubic Ionic Lattices

By F. G. Fumi and M. P. Tosi
Cattedra di Fisica Teorica dell'Università, Palermo, Italy

[Received August 10, 1956]

Bertaut (1954) has proved by the use of the Patterson function that linear relations exist between the Madelung constants for some cubic ionic lattices. He mentions that these relations were first found by Naor through an extension of the Frank method of lattice summation (Frank 1950), but Naor's proof does not appear to have been published (Bertaut, private communication). Here we give two simple proofs of Naor's relations.

The Madelung constant α_a of a cubic ionic lattice referred to the lattice parameter a is defined as

$$z\alpha_a = -\tfrac{1}{2}a \sum_p \epsilon_p \phi(\mathbf{r}_p) \quad . \quad . \quad . \quad . \quad . \quad . \quad . \quad (1)$$

where $\phi(\mathbf{r}_p)$ is the electrostatic lattice potential at the position of the pth ion of the unit cell†, ϵ_p is the charge of this ion in units of the smallest ionic charge in the lattice, and z is the number of molecules in the unit cell.

To prove the Naor relations we write $\phi(\mathbf{r}_p)$ as a sum of the electrostatic potentials in $\mathbf{r}_p$ due to the simple cubic lattices which compose the crystal (Hund 1935): following Hund, we denote by $\psi(xyz)$ the electrostatic potential in the point xa, ya, za (a, lattice constant) due to a simple cubic lattice of positive unit charges, neutralized by a uniform distribution of negative charge. For the CsCl-type of lattice one has, with obvious notations,

$$\alpha_a(\mathrm{CsCl}) = -\tfrac{1}{2}a[\phi_{\mathrm{CsCl}}(M^+) - \phi_{\mathrm{CsCl}}(X^-)] = -a\phi_{\mathrm{CsCl}}(M^+). \quad . \quad . \quad (2)$$

However,

$$\phi_{\mathrm{CsCl}}(M^+) = \bar{\psi}(000) - \psi(\tfrac{1}{2}\tfrac{1}{2}\tfrac{1}{2}) \quad . \quad . \quad . \quad . \quad . \quad . \quad . \quad (3)$$

where $\bar{\psi}(000)$ is the self-potential of the 'neutralized' simple cubic lattice of metal ions M^+ and $-\psi(\frac{1}{2}\frac{1}{2}\frac{1}{2})$ is the potential due to the 'neutralized' simple cubic lattice of halogen ions X^-. So, using the Hund identity (Birman 1955, Fumi and Tosi, to appear) $\bar{\psi}(000) = 3\psi(\frac{1}{2}00) + 3\psi(\frac{1}{2}\frac{1}{2}0) + \psi(\frac{1}{2}\frac{1}{2}\frac{1}{2})$, one obtains

$$\alpha_a(\mathrm{CsCl}) = -3a[\psi(\tfrac{1}{2}00) + \psi(\tfrac{1}{2}\tfrac{1}{2}0)]. \quad . \quad . \quad . \quad . \quad . \quad (4)$$

† We call *unit cell* the cell which contains an ion for each Bravais sub-lattice of the structure, namely the smallest lattice cell.

Similarly, if one uses the cubic symmetry of $\psi(xyz)$, the Hund identity for $\bar{\psi}(000)$ and the identity $\psi(\frac{1}{4}\frac{1}{4}\frac{1}{4})=\frac{1}{4}\psi(\frac{1}{2}\frac{1}{2}\frac{1}{2})$, one finds

$$\alpha_a(\mathrm{NaCl})=-\tfrac{1}{2}a[\phi_{\mathrm{NaCl}}(M^+)-\phi_{\mathrm{NaCl}}(X^-)]=-6a\psi(\tfrac{1}{2}\tfrac{1}{2}0) \quad . \quad . \quad (5)$$

$$\alpha_a(\text{zincblende})=-\tfrac{1}{2}a[\phi_{\mathrm{ZnS}}(M^+)-\phi_{\mathrm{ZnS}}(X^-)]=-3a[\psi(\tfrac{1}{2}00)+2\psi(\tfrac{1}{2}\tfrac{1}{2}0)] \quad (6)$$

$$\alpha_a(\mathrm{CaF_2})=-\tfrac{1}{2}a[2\phi_{\mathrm{CaF_2}}(M^{++})-2\phi_{\mathrm{CaF_2}}(X^-)]=-6a[2\psi(\tfrac{1}{2}00)+3\psi(\tfrac{1}{2}\tfrac{1}{2}0)] \quad (7)$$

$$\begin{aligned}2\alpha_a(\mathrm{Cu_2O})&=-\tfrac{1}{2}a[4\phi_{\mathrm{Cu_2O}}(M^+)-4\phi_{\mathrm{Cu_2O}}(X^{--})]\\&=-6a[3\psi(\tfrac{1}{2}00)+4\psi(\tfrac{1}{2}\tfrac{1}{2}0)+\psi(\tfrac{1}{2}\tfrac{1}{2}\tfrac{1}{2})]\dagger. \quad . \quad . \quad . \quad (8)\end{aligned}$$

These expressions for the α_a's lead at once to the Naor relations

$$\alpha_a(\mathrm{CaF_2})=4\alpha_a(\mathrm{CsCl})+\alpha_a(\mathrm{NaCl}) \quad . \quad . \quad . \quad . \quad . \quad . \quad (9)$$

$$\alpha_a(\mathrm{CaF_2})=-\alpha_a(\mathrm{NaCl})+4\alpha_a(\text{zincblende}). \quad . \quad . \quad . \quad (10)$$

From eqns. (4)–(8) it is also clear that no other independent, linear relation exists between the Madelung constants of the structures that we have considered.

The Naor relations can also be derived very simply by considering the CaF_2-type of lattice with lattice constant a alternatively as a superposition of a CsCl lattice of lattice constant $\frac{1}{2}a$ and of a NaCl lattice with lattice constant a or as a superposition of a zincblende lattice with double charges and of a NaCl lattice, both with lattice constant a. In the first case one has

$$\phi_{\mathrm{CaF_2}}(M^{++})=2\phi_{\mathrm{CsCl}}(M^+)+\phi_{\mathrm{NaCl}}(M^+) \quad . \quad . \quad . \quad . \quad . \quad . \quad . \quad (11)$$

$$\phi_{\mathrm{CaF_2}}(X^-)=2\phi_{\mathrm{CsCl}}(X^-)+\phi_{\mathrm{NaCl}}(\tfrac{1}{4}\tfrac{1}{4}\tfrac{1}{4})=2\phi_{\mathrm{CsCl}}(X^-) \quad . \quad . \quad . \quad (12)$$

from which eqn. (9) follows directly. Similarly in the second case

$$\phi_{\mathrm{CaF_2}}(M^{++})=2\phi_{\mathrm{ZnS}}(M^+)+\phi_{\mathrm{NaCl}}(\tfrac{1}{4}\tfrac{1}{4}\tfrac{1}{4})=2\phi_{\mathrm{ZnS}}(M^+) \quad . \quad . \quad (13)$$

$$\phi_{\mathrm{CaF_2}}(X^-)=2\phi_{\mathrm{ZnS}}(X^-)+\phi_{\mathrm{NaCl}}(M^+) \quad . \quad . \quad . \quad . \quad . \quad . \quad . \quad (14)$$

which give directly eqn. (10).

References

Bertaut, F., 1954, *C.R. Acad. Sci.*, **239**, 234.

Birman, J., 1955, *Phys. Rev.*, **97**, 897.

Frank, F. C., 1950, *Phil. Mag.*, **41**, 1287.

Fumi, F. G., and Tosi, M. P., *The Theory of Ionic Crystals*, to appear in *Solid State Physics* (New York: Academic Press).

Hund, F., 1935, *Z. f. Phys.*, **94**, 11.

† This equation is given explicitly in Hund's paper, and lead Hund to discover the incorrectness of Emersleben's value for $\alpha_a(Cu_2O)$. However, the incorrect value $[\alpha_a(Cu_2O)=9{\cdot}5044]$ is still quoted in the standard literature (e.g. M. Born and K. Huang, *Dynamical Theory of Crystal Lattices* (Oxford 1954), p. 387) in place of the correct value $\alpha_a(Cu_2O)=10{\cdot}2594$.

Isotopic Spin Impurities

By F. C. Barker
Research School of Physical Sciences, Australian National University, Canberra

[Received July 17, 1956]

It has usually been assumed that the isotopic spin impurities in highly excited states of a light nucleus will be much larger than those in the low lying states, due to the proximity of states of different isotopic spin (Gell-Mann and Telegdi 1953, Wilkinson 1953, MacDonald 1956). This is valid only if the matrix elements of the Coulomb interaction connecting these nearby states to the highly excited states are as large as are the matrix elements involved for the low lying states.

It appears, however, that the large matrix elements of the Coulomb interaction are those coupling states belonging to different configurations. For an infinitely long range potential, all matrix elements connecting states of different isotopic spin would vanish, due to the orthogonality of the states. For the Coulomb interaction, the orthogonality shows up more for states of the same configuration, where there is cancellation amongst the different two-particle matrix elements, than for states belonging to different configurations, where the two-particle matrix elements are smaller but do not tend to cancel. As an example, we give

Ψ_0	Ψ_1	$(\Psi_0 H^c \Psi_1)$ (Mev)
$\Psi(1s^4 1p^8[44]000)$	$\Psi((1s^4 1p^7[43]\frac{1}{2}\frac{1}{2}1, 2p)100)$	−0·48
,,	$\Psi((1s^3[3]\frac{1}{2}\frac{1}{2}0, 1p^8[44]000, 2s)100)$	−0·36
$\Psi((1s^4 1p^7[43]\frac{1}{2}\frac{1}{2}1, 1d)001)$	$\Psi((1s^4 1p^7[43]\frac{1}{2}\frac{1}{2}1, 1d)101)$	−0·02
,,	$\Psi((1s^4 1p^7[421]\frac{1}{2}\frac{1}{2}1, 1d)101)$	0·01
,,	$\Psi((1s^4 1p^7[43]\frac{1}{2}\frac{1}{2}1, 2s)101)$	0·02
,,	$\Psi((1s^4 1p^7[43]\frac{1}{2}\frac{1}{2}1, 2d)101)$	0·11
,,	$\Psi(((1s^4 1p^6[42]010, 2p)\frac{1}{2}\frac{1}{2}1, 1d)101)$	−0·23
,,	$\Psi(((1s^4 1p^6[42]012_{II}, 2p)\frac{1}{2}\frac{1}{2}1, 1d)101)$	−0·35
,,	$\Psi(((1s^4 1p^6[33]111, 2p)\frac{1}{2}\frac{1}{2}1, 1d)101)$	0·15

in the table some matrix elements connecting $T=0$ and $T=1$ states of ^{12}C in L–S coupling ; the triads of numbers are values of TSL, and the states Ψ_0 are appropriate to the ground state of ^{12}C and to a $T=0$ state of about 20 Mev excitation.

We have used

$$H^c = \frac{e^2}{4} \sum_{i<j} (1-\tau_{zi})(1-\tau_{zj}) \frac{1}{r_{ij}}$$

and radial wave functions for an oscillator potential well, with parameter $a = 2{\cdot}2 \times 10^{-13}$ cm. The matrix elements connecting states differing in

the excitation of two particles are small compared with those connecting states differing in only one particle, as was pointed out by MacDonald (1956).

On the basis of these matrix elements and those similarly calculated for other nuclei, it would seem that in general the main isotopic spin admixtures to a state are states of different configurations, with the amount of admixture independent of the excitation of the state. Thus isotopic spin may remain a useful quantum number up to quite high excitation energies.

The experimental evidence on isotopic spin impurities is mainly in accordance with this view. To the extent that (d, d′) and (d, α) reactions proceed through a compound nucleus, the observed absence of transitions to final states with T values different from that of the initial nucleus indicates absence of isotopic spin mixing in the states of the compound nucleus, which are at high excitation. Goward and Wilkins (1955) have interpreted their ^{12}C(γ, α) results in terms of very small isotopic spin impurities in the excited states of ^{12}C. The impurities of various states of light nuclei as obtained from electric dipole transitions and competing reactions have been given by Wilkinson and collaborators (see Wilkinson 1953, Wilkinson and Clegg 1956). Some apparently large impurities were found, the largest being about 20% intensity of $T=1$ impurity in the mainly $T=0$ state at 6·88 MeV in ^{10}B. It is also probable that there is a large impurity in the 12·69 MeV state of ^{14}N (Barker and Mann 1957). Some large impurities are to be expected in a few cases when two combining states lie unusually close together, however, in view of what has been said above, the explanation of Wilkinson and Clegg (1956) for the large mixing in the ^{10}B state is not tenable.

Acknowledgment

The calculations outlined here arose from discussions which the author had with Dr. A. K. Mann, University of Pennsylvania.

References

Barker, F. C., and Mann, A. K., 1957, *Phil. Mag.* **2,** 5.
Gell-Mann, M., and Telegdi, V. L., 1953, *Phys. Rev.*, **91,** 169.
Goward, F. K., and Wilkins, J. J., 1955, *Proc. Roy. Soc.* A, **228,** 376.
MacDonald, W. M., 1956, *Phys. Rev.*, **101,** 271.
Wilkinson, D. H., 1953, *Nature, Lond.*, **172,** 576.
Wilkinson, D. H., and Clegg, A. B., 1956, *Phil. Mag.*, **1,** 291.

REVIEWS OF BOOKS

Relativity : The Special Theory. By J. L. Synge. (Amsterdam : North-Holland Publishing Company, 1956.) [Pp. xiv+450.] Price 38 guilders.

The keynote of this admirable treatise on the special theory of relativity is sounded in the preface where Professor Synge says "To understand a subject, one must tear it apart and reconstruct it in a form intellectually satisfying to oneself". It is in this spirit of constructive criticism that the author gives a most complete account of the theory in which he discusses not only the familiar topics of the Lorentz transformation and its application to mechanics and electromagnetic theory but also investigates a number of interesting and important and puzzling questions which must also have come into the minds of students but which are not discussed in any of the standard works. Among these special topics which Professor Synge has investigated *ab initio* we may mention in particular the relativistic form of a discrete Newtonian system with action and interaction between its particles, the elastic collision of particles, the conservation of angular momentum, and models of uncharged 'particles' of finite energy constructed out of non-singular solutions of Maxwell's equations *in vacuo*, together with model photons constructed according to the same plan. No difficulty is shirked in this work and detailed proofs are given of all the important theorems. In particular we may mention the particularly useful analysis of the Michelson–Morley experiment with special reference to the concept of the rigidity of the framework supporting the interferometer. The book is beautifully printed and will take its place as a standard treatise on the subject.

G. T.

Physical Mathematics. By Chester H. Page. (Princeton, New Jersey : D. van Nostrand Co. Inc. 1955.) [Pp. x+329.]

There is, among university students of physics and engineering, an increasing need for an understanding of advanced mathematical techniques. If they have been trained mainly in the experimental side of their subject, they often lack practice in mathematical discipline, and consequently find some of the standard mathematical text-books difficult to follow. Dr. Page's book gives a very careful treatment of some selected topics, and could usefully be recommended to good graduate or advanced students who have such limited mathematical experience. The arguments are clearly presented, and illustrated with physical examples.

Several chapters are devoted to the general theory of eigenfunctions and eigenvalues of differential equations, treated by variational methods and by separation of the variables, and illustrated by the properties of the Helmholtz equation. The detailed formulae are given for the transformations between the main coordinate systems in three dimensions, and the differential equations in the separated variables are classified in terms of their singularities. There is, however, very little mention of the special functions which satisfy these differential equations, and no mention of asymptotic approximations, the W.K.B. method, or the Airy Integral function. Green's functions and integral equations are fully dealt with, and this is perhaps the most useful feature of the book. The last two-fifths of the book are devoted mainly to Fourier integrals and Laplace transforms. The illustrations are almost entirely from electrical circuit theory. The basic theory of the complex variable is treated only briefly in an appendix in one of the chapters. There is a full discussion of the relations between the resistive and reactive parts of an impedance or

admittance function, and between the amplitude and phase, known to communication engineers as Bode's theorem.

The book will be of most use in the fields of circuit theory and wave propagation, but students of other branches of physics will find much to interest them, especially in the earlier chapters. K. G. B.

Science and Information Theory. By L. Brillouin. (New York: Academic Press Inc.; London: Academic Books Ltd., 1956.) [Pp. xii+320.] Price $6.80.

In recent years Information Theory must have been a source of uneasiness for many physicists, as one of the subjects "on which one hears so much and on which one ought to read up". Here at last is a book which one can wholeheartedly recommend to all physicists and scientists of an advanced level.

The central theme of the book is the relation of the process of collecting information on physical systems to the 2d principle of thermodynamics.

More than half of Brillouin's book is devoted to the elucidation of the by no means quite simple connection between information and entropy, which he has widely generalized and brilliantly illustrated. It can now be said that the principle of indeterminacy and the 'negentropy' principle are the two fundamental limitations of all physical measurements, but while the importance of the first is long recognized, the second has not so far received all the attention which it deserves. I regret only that (apart from a few brief remarks on p. 233) the author has not emphasized that the exorcism of the Maxwell Demon 'incidentally' proves also the inconsistency of classical physics with thermodynamics, that is to say that the 2d Principle, like the 3d, derives its validity from quantum physics. This is a contention first put forward by Max Born, and not yet universally accepted.

It is as yet hard to say what influence information theory will have on the future development of physics. Of all scientists the physicists are most reluctant to adopt statistical methods. The structural simplicity of their subject enables them to consider parameters one by one, and to reject conclusions obtained by elaborate statistical methods from complex material which does not show a clear result on inspection. But information theory, though it is in essence a statistical science, does not suggest giving up this noble prejudice. It suggests merely that in many cases a set of parameters can be more accurately obtained from complex experiments than from one-by-one tests. Moreover the theory gives upper bounds for the legitimate number of questions which a given experiment can be expected to answer.

Though the book will be most enjoyed by advanced physicists, it can be equally recommended to all scientists who had no previous contact with information theory, and to electrical engineers who had no intimate knowledge of statistical physics or with thermodynamics. The main results of communication theory are all derived from first principles, with just that level of mathematics which theoretical physicists have long accepted as their standard, that is to say with careful, even painstaking discussions of consequences, but without digging down into the foundations as deep as set theory. D. G.

Vacuum Deposition of Thin Films. By L. Holland. (London: Chapman & Hall Ltd., 1956.) [Pp. xx+541.] Price 70*s*.

The author is the Head of the Vacuum Coating Research Laboratory of Edwards High Vacuum Ltd., and his experience of the technology of his subject is reflected in the practical approach throughout the book and the range of topics chosen. A preliminary chapter on vacuum equipment is rigorously selective, and does not attempt to take the place of a text on vacuum practice, though some very useful advice is given. Chapters follow on the degassing of plastics *in vacuo*, various methods of cleaning surfaces, three on the evaporation

of various materials and one on the growth, structure and properties of vacuum-deposited films. Then the preparation of films for particular applications is described : Chapter 8 on metal films for electrical purposes such as metallized resistors (this section might have been expanded with advantage), zinc coating of tissue for condensers and the deposition of electrodes on to crystal vibrators ; 9 and 10 on optical interference films ; 11 on evaporated aluminium films, especially for mirrors ; 12 on evaporated coatings on plastics and lacquered surfaces ; 13 on shadow-casting and the production of surface replicas for electron microscopes ; 14 on cathodic sputtering ; 15 and 16 on oxide films, including electrically-conducting oxides. There is a valuable appendix collecting together much information on deposition characteristics and refractive indices of inorganic compounds.

Throughout the book the treatment is selective and critical in the light of the author's own experience. It is up-to-date and well documented. The list of 557 references at the end is numbered in the order of citation in the text, but the author index refers to this list and enables particular papers to be traced. A short bibliography of relevant books is included in the author's preface. Where needed the fundamental physics of the processes involved is discussed, usually with a sound grasp of the main principles. It would have been outside the scope of the book to have delved deeply into theory, but it would have added considerably to the value of some sections to have been more quantitative and precise, for example when discussing adsorption, re-evaporation and life-times of surface atoms. As Professor Tolansky rightly remarks in his appreciative foreword, the subject of vacuum deposition is still as much an art as a science and anyone taking up experimental work in it needs an experienced guide. Mr. Holland through this book supplies that need. Other workers in this and neighbouring fields will be able to add information from their own experience, e.g. the effects of chlorine liberated from some glasses when baked, but they will be grateful to the author for providing so much practical advice, so many data and such a good selection of references to other work. F. A. V.

The Atomic Nucleus. By R. D. Evans. (London : McGraw-Hill.) [Pp. xv + 972.] Price 109*s*.

This massive book is based on the graduate course in nuclear physics which the author has given at the Massachusetts Institute of Technology for the past twenty years ; there can be indeed little in it that has survived those two decades apart from the quotation from Lucretius with which it begins. Despite its origin it does not give the impression of patchwork. In this country it will be read with profit by beginners in research but its other large potential market among honours undergraduates will, alas !, be closed by its forbidding price.

The writing is brisk although frequently rather loose. Thus while we are merely startled to learn from the caption to the figure on p. 246 that " Data are a composite of several authors in various energy ranges ", we are seriously misled on the facing page by " The incident photon can be absorbed either as an electric dipole or as a magnetic dipole . . . . ".

The balance in a book of this kind must always be to some degree a personal matter. For example to the present reviewer there is much too little material on nuclear reactions relative to the space devoted to static nuclear properties. Again it seems that twenty pages may be a rather generous allocation of print for discussing the stopping of electrons by thick absorbers when all that we are told about the photo-disintegration of nuclei other than the deuteron is that most of it takes place above 8 Mev and that the cross sections are negligible compared with those for the Compton effect and for pair production (which is false). These examples of unbalance lead to a more serious general criticism which is that the book consciously or unconsciously tries to be a text-book containing only what is unquestionably right—while pretending to give an account

of present-day nuclear physics. The two are incompatible. As a result the author usually stops short of any novel, unconsolidated or controversial work and the reader gets little feeling for the way in which nuclear physics is in fact developing today. Despite these remarks this is by far the best book on experimental nuclear physics presently available.

The references are indexed into the main text—a most useful feature—and the index itself is very good (indeed on the Lamb shift it is more informative than the text). For a first edition the book is remarkably free from misprints and trivial errors and it is a monument to the care of the author. The large number of problems set in the text is a useful feature.

We finally note that a book which figures in a series whose title contains the word " International " should not date scientific events from local history. Mendeleev's establishment of the periodic table is dated by Dr. Evans as " About the time of the American Civil War ". Enquiries by the present reviewer among a statistically significant number of his colleagues have enabled him to fix this event in the year 1842 ± 30. However lest the reviewer appear ungrateful he must record his thanks for the very precise information gleaned from p. 755 that " on June 5, 1951, Dom DiMaggio had a batting average of 0·359, had been at bat 189 times in 44 games and had hit safely at least once in each of his last 25 consecutive games ". Whatever that means. D. H. W.

Recent Advances in Science. By M. H. Shamos and G. M. Murphy. (New York: Interscience Publishers, Inc.; London: Interscience Publishers Ltd.) (Published jointly with the New York University Press.) [Pp. xi+384.] Price $7.50.

This is an interesting volume containing articles on recent advances in physics and applied mathematics written at a level which is meant to be acceptable to all scientists and engineers in whatever field they work. Most of the authors are extremely eminent and leaders of their subjects; for instance Bethe writes on nuclear structure, Morse on operations research and Shockley on transistors. On the whole the authors seem to the present reviewer to have been successful in writing at the right level though of course there are the usual anomalies, such as a discussion in one article of what is meant by a wave and the use of Maxwell's equations in another. None the less the book can be recommended to those for whom it is meant, namely anyone with a general knowledge of science who wishes to know what is happening in certain branches of pure and applied physics. N. F. M.

Introduction to Solid State Physics. Second Edition. By C. Kittel. (London: Chapman & Hall.) [Pp. xvii+617.] Price 96*s*.

A second edition of Kittel's well known " Introduction to Solid State Physics " is welcome. It is about two hundred pages longer than the first edition and contains a fuller account of the theory of energy bands and new material on alloys, semiconductors and imperfections in solids. N. F. M.

Photoconductivity Conference held at Atlantic City, November 4–6, 1954. By R. G. Breckenridge, B. R. Russell and E. E. Hahn. (New York: John Wiley & Sons Inc.; London: Chapman & Hall Ltd.) [Pp. xiii+653.] Price 108*s*.

This volume contains the papers presented at a conference in Atlantic City in November 1954 sponsored by the University of Pennsylvania, the Radio Corporation of America and the U.S. Office of Naval Research. It contains papers on a very wide range of subjects, theoretical and applied, and will be of considerable value to workers in this field. N. F. M.

CORRIGENDUM

The Effect of Free Electrons on Lattice Conduction

By J. M. Ziman
Cavendish Laboratory, Cambridge

In a recent paper (Ziman 1956), the mean free path of phonons scattered by electrons was calculated, but the phonon creation processes, which tend to balance out the annihilation processes to some extent, were neglected. Their effect is to increase the relaxation time by an amount which, as may be shown by standard methods (Wilson 1953), corresponds to the deletion of the factor $(1-e^{-z})^{-1}$ in eqns. (9) and (19) of my paper. The curves for $\bar{\phi}$ have been recalculated, but turn out to be very similar to those drawn in fig. 1. The low temperature asymptote is almost unchanged, having the form

$$(a) \qquad T_F > T_S\,; \quad \text{as } T \to 0, \quad \bar{\phi} \to 0{\cdot}2088\, T_S/T. \quad . \quad . \quad . \quad . \quad (21)$$

The minimum values of $\bar{\phi}$ are a few per cent larger, but come at the same values of T/T_S. Only at high temperatures is there a significant difference, with

$$(c) \text{ as } T \to \infty, \quad \bar{\phi} \to \frac{\pi^4\sqrt{\pi}}{640}\left(\frac{T}{T_F}\right)^{3/2}\left(\frac{T}{T_S}\right)\exp\left(\frac{T_S}{T}\right) \times \left\{1-\frac{4}{3}\frac{T_S}{T}-\frac{1}{3\sqrt{\pi}}\left(\frac{T_F}{T}\right)^{3/2}+\frac{4}{9\sqrt{\pi}}\left(\frac{T_F}{T}\right)^{3/2}\frac{T_S}{T}\right\}^{-1} \quad . \quad . \quad (23)$$

The mean free path thus rises as $T^{5/2}$ which is much steeper than any observed effect.

I am indebted to Dr. R. Stratton for pointing out this error.

References

Wilson, A. H., 1953, *The Theory of Metals*, 2nd Ed. (Cambridge: University Press), p. 292.
Ziman, J. M., 1956, *Phil. Mag.*, **1**, 191.

Fig. 2

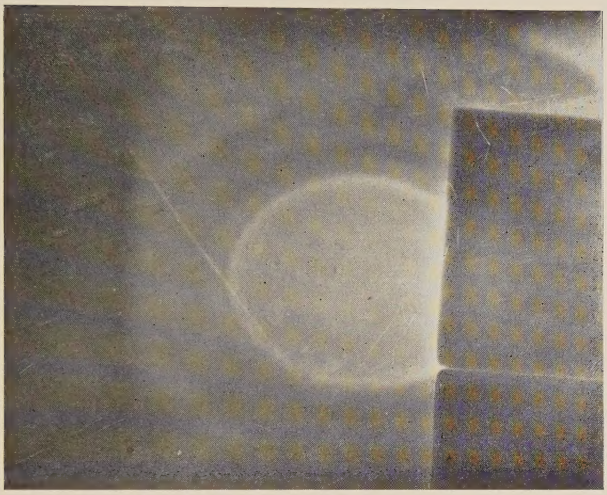

(*a*)

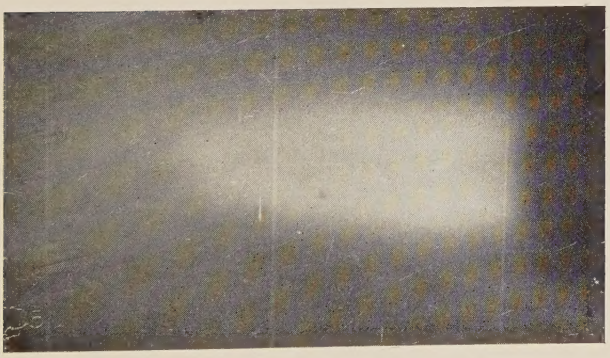

(*b*)

X-ray film reproductions ; (*a*) exposed behind absorbing block at A, (*b*) exposed in front of exposure position at P in fig. 1.